

Spring 2023

Molecular Devices for Measuring Weak Solvophobic Interactions and the Development of Pedagogical Tools for Organic Chemistry Students

Alexander N. Manzewitsch

Follow this and additional works at: <https://scholarcommons.sc.edu/etd>



Recommended Citation

Manzewitsch, A. N.(2023). *Molecular Devices for Measuring Weak Solvophobic Interactions and the Development of Pedagogical Tools for Organic Chemistry Students*. (Doctoral dissertation). Retrieved from <https://scholarcommons.sc.edu/etd/7359>

This Open Access Dissertation is brought to you by Scholar Commons. It has been accepted for inclusion in Theses and Dissertations by an authorized administrator of Scholar Commons. For more information, please contact digres@mailbox.sc.edu.

MOLECULAR DEVICES FOR MEASURING WEAK SOLVOPHOBIC
INTERACTIONS AND THE DEVELOPMENT OF PEDAGOGICAL TOOLS FOR
ORGANIC CHEMISTRY STUDENTS

by

Alexander N. Manzewitsch

Bachelor of Science
Wingate University, 2017

Submitted in Partial Fulfillment of the Requirements

For the Degree of Doctor of Philosophy in

Chemistry

College of Arts and Sciences

University of South Carolina

2023

Accepted by:

Ken D. Shimizu, Major Professor

Linda S. Shimizu, Committee Member

Vitaly Rassolov, Committee Member

Andreas Hayden, Committee Member

Dr. Cherryl Addy, Interim Vice Provost and Dean of the Graduate School

© Copyright by Alexander N. Manzewitsch, 2023
All Rights Reserved.

DEDICATION

To the Creator of all things Jesus Christ.

“All things were made through Him and for Him... and in Him all things hold together”.

Also to Alisha and our children.

ACKNOWLEDGEMENTS

My thanks is first and foremost to the Creator and Sustainer of all things, Jesus Christ, for mercifully bringing me safely to the end of this chapter of my life. All things were made for Your glory; may all my endeavors go towards that end.

Thanks to Dr. Shimizu for all the insight, encouragement, and astonishing patience you have shown during my time at the University of South Carolina. I am grateful for all the work you put into my studies here, as well as me as a person. I hope my career hereafter will make you proud.

Thanks to Dr. Sheri Strickland for all the guidance and mentorship you provided over the years. I always admired your passion for science and your genuine care for your students and colleagues. I hope to be half the professor you are someday.

Thanks to all my labmates: Ping, Joe, Chris, Erik, Ishwor, Daniel, Binzhou, and Hao, and Oluebube. You made coming to the lab a joy. I wish you all the best.

Thanks to Alisha for supporting me through all my bumbling misadventures in grad school, and for being such a loving mother to our children. I would have undoubtedly crumbled without your unwavering and undeserved affirmation. I love you beyond what human words can express.

Thanks to Elizabeth, Elizabeth's little sibling, Joe, Grace, mom, dad, Mr. NK, Mrs. Tammy, Nathan, Aaron, Stacey, and Micah. I am happy that I had such an amaing family to accompany me through this program. I love you one and all.

Thanks to Mr. “Doc” Worly for never accepting any of my whiny excuses, pushing to be a better man, to finish what I started. Oorah!

Thanks to Sandy Allen for your Christian mentorship and helping me navigate life.

ABSTRACT

The main topics of this dissertation are: 1) the development and discussion of a new molecular balance for measuring alkyl-alkyl interactions in a wide array of organic solvents, 2) the development of linear solvation energy relationships between solvent interaction parameters and solvent accessible surface area (SASA) in CH-arene interactions, and 3) the development of online resources for helping undergraduate students perform organic chemistry mechanisms problems well.

The solvophobic effect, that is the forced association between two solutes due to intermolecular attraction of the solvent molecules, is ubiquitous in organic chemistry and responsible for many significant phenomena thereof. However, there is a lack of experimental data on the effect due to its weak nature. Therefore, an intermolecular torsional balance system was developed specifically to isolate and measure the solvophobic effect across a wide range of organic solvents. The SASAs of the balances were altered to gauge how the solvophobic effect changes with the size of the solvent-solute interface. From the data collected, a predictive model correlating solvent cohesion, solute association energy, and solvent-solute interface area was developed which accurately predicted the association energy of the hydrophobic effect from previous literature.

Like solvent cohesion, the Kamlet-Taft, Catalán, and Laurence solvent parameters have been closely related with various solute-solvent association properties. Using a set of molecular torsional balances, we correlated the relationships between solvent parameters,

solute-solvent interface area, and solvent-solute association energy of different CH-arene interactions. Results demonstrated a similar solvophobic effect between both CH- π interactions and CH- aromatic edge interactions, and that similar solvent parameters dominate the interactions.

College level organic chemistry presents itself as a major difficulty to many undergraduate students. In response, we surveyed a sample of underperforming exams to assess which areas were the most troublesome in writing electron-pushing formalisms (EPF). Online tutorial modules were then developed which instructs students in a step-by-step procedure on how to accomplish EPF problems with specific focus on the most prevalent problem areas. Furthermore, additional notes linking to problem to fundamental concepts of organic chemistry were added within the example problems in order to facilitate the transition of students from understanding organic chemistry from rote memorization to a relational understanding of the principles.

TABLE OF CONTENTS

DEDICATION	iii
ACKNOWLEDGEMENTS.....	iv
ABSTRACT	vi
LIST OF TABLES	xi
LIST OF FIGURES	xv
LIST OF EQUATIONS	xx
LIST OF ABBREVIATIONS.....	xxi
CHAPTER 1 MOLECULAR DEVICES FOR MEASURING SOLVOPHOBIC EFFECTS AND DEVELOPING SCAFFOLDING TOOLS FOR TEACHING ORGANIC CHEMISTRY	1
1.1 ABSTRACT.....	2
1.2 HYDROPHOBIC AND SOLVOPHOBIC EFFECTS	2
1.3 MEASURING SOLVOPHOBIC EFFECTS WITH UNIMOLECULAR DEVICES	4
1.4 PREDICTING HYDROPHOBIC AND SOLVOPHOBIC EFFECTS	6
1.5 IDENTIFYING AND ADDRESSING DIFFICULTIES IN LEARNING ORGANIC CHEMISTRY	8
1.6 REFERENCES	10
CHAPTER 2 AN EMPIRICAL MODEL FOR SOLVOPHOBIC INTERACTIONS IN ORGANIC SOLVENTS	14
2.1 ABSTRACT.....	15
2.2 INTRODUCTION	16
2.3 EXPERIMENTAL DESIGN	16

2.4 RESULTS AND DISCUSSION.....	21
2.5 CONCLUSIONS.....	34
2.6 SUPPLEMENTAL INFORMATION.....	34
2.7 REFERENCES	75
CHAPTER 3 PROBING SOLVENT EFFECTS IN CH-ARENE INTERACTIONS WITH MOLECULAR TORSIONAL BALANCES AND MULTIPARAMETER LINEAR SOLVATION ENERGY RELATIONSHIPS	78
3.1 ABSTRACT.....	79
3.2 INTRODUCTION	79
3.3 DESCRIPTION OF SOLVENT LSER MODELS.....	81
3.4 EXPERIMENTAL DESIGN	82
3.5 RESULTS AND DISCUSSION.....	85
3.6 CONCLUSIONS.....	90
3.7 SPECIAL ACKNOWLEDGEMENTS	90
3.8 SUPPLEMENTAL INFORMATION.....	90
3.9 REFERENCES	120
CHAPTER 4 DEVELOPING SCAFFOLDING MODULES FOR TEACHING ELECTRON PUSHING FORMALISMS IN UNDERGRADUATE ORGANIC CHEMISTRY	123
4.1 ABSTRACT.....	124
4.2 INTRODUCTION	124
4.3 DATA COLLECTION	126
4.4 STRUCTURE OF STEP-BY-STEP PROCEDURE FOR MECHANISMS	129
4.5 CONCLUSIONS.....	132
4.6 REFERENCES	132

CHAPTER 5 FUTURE RESEARCH	133
5.1 ABSTRACT.....	134
5.2 SOLVOPHOBIC EFFECT CATALYSIS AND SELECTIVITY IN DIELS-ALDER REACTIONS.....	134
5.3 MODULATING REACTIONS USING SOLVOPHOBIC EFFECTS TO FORM STERICALLY STRAINED GROUPS.....	135
5.4 FUTURE OF ALKYL-ALKYL INTERACTIONS WITH FOCUS ON PAST EXPERIMENTS	140
5.5 CONCLUSIONS.....	144
5.6 COMPUTATIONAL MODEL COORDINATES.....	145
5.7 REFERENCES	153

LIST OF TABLES

Table 1.1 Unimolecular devices used to observe solvent effects in which parameters were correlated with increased solute-solute interactions.	5
Table 2.1 The 46 solvent systems used to measure the solvophobic effects of the balances along with their cohesive energy density values and solvent functional groups.	19
Table 2.2 General information about calculated crystal structure for compound 1a. These data can be obtained free of charge from The Cambridge Crystallographic Data Centre via www.ccdc.cam.ac.uk/data_request/cif	41
Table 2.3 General information about calculated crystal structure for compound 1b. These data can be obtained free of charge from The Cambridge Crystallographic Data Centre via www.ccdc.cam.ac.uk/data_request/cif	42
Table 2.4 Redundant folding energy measurements of 1a, 1b, and 1c in chloroform-d ₃	57
Table 2.5 Solvents used for decoupled ¹⁹ F NMR experiments and the measure energy difference between the <i>folded</i> and <i>unfolded</i> conformers (folding energy).	58
Table 2.6 Calculated solvent accessible surface area (SASA) of <i>folded</i> and <i>unfolded</i> conformers balances 1a, 1b, and 1c from this study, as well as 5 and 6 from Cockroft et al. and Schreiner et al. *measurements taken with a 2.63 Å probe to match the molecular radius of benzene.	62
Table 2.7 Xyz coordinates of the <i>folded</i> conformer structure of 1a.	63
Table 2.8 Xyz coordinates of the <i>unfolded</i> conformer structure of 1a.	64
Table 2.9 Xyz coordinates of the <i>folded</i> conformer structure of 1b.	65
Table 2.10 Xyz coordinates of the <i>unfolded</i> conformer structure of 1b.	66
Table 2.11 Xyz coordinates of the <i>folded</i> conformer structure of 1c.	67
Table 2.12 Xyz coordinates of the <i>unfolded</i> conformer structure of 1c.	68

Table 2.13 Xyz coordinates of the <i>folded</i> conformer structure of 5a.	69
Table 2.14 Xyz coordinates of the <i>unfolded</i> conformer structure of 5a.	70
Table 2.15 Xyz coordinates of the <i>folded</i> conformer structure of 5b.	71
Table 2.16 Xyz coordinates of the <i>unfolded</i> conformer structure of 5b.	72
Table 2.17 Xyz coordinates of the <i>folded</i> conformer structure of 6.	73
Table 2.18 Xyz coordinates of the <i>unfolded</i> conformer structure of 6.	74
Table 3.1 Calculated SASA and Δ SASA of alkyl-aryl balances, calculated using a 1 Å surface probe.	84
Table 3.2 Kamlet-Taft parameters' correlation to Δ G. Parameters taken from literature.	87
Table 3.3 Catalán parameters' correlation to Δ G. Parameters taken from literature.....	88
Table 3.4 Laurence parameters' correlation to Δ G. Parameters taken from literature.	89
Table 3.5 References for synthesis procedures of molecular torsional balances.....	91
Table 3.6 General information about calculated crystal structure for balance 1. These data can be obtained free of charge from The Cambridge Crystallographic Data Centre via www.ccdc.cam.ac.uk/data_request/cif	95
Table 3.7 General information about calculated crystal structure for balance 2. These data can be obtained free of charge from The Cambridge Crystallographic Data Centre via www.ccdc.cam.ac.uk/data_request/cif	97
Table 3.8 General information about calculated crystal structure for balance 3. These data can be obtained free of charge from The Cambridge Crystallographic Data Centre via www.ccdc.cam.ac.uk/data_request/cif	98
Table 3.9 Xyz coordinates of the <i>anti</i> - conformer structure of 1.....	104
Table 3.10 Xyz coordinates of the <i>syn</i> - conformer structure of 1.	105
Table 3.11 Xyz coordinates of the <i>anti</i> - conformer structure of 2.....	106
Table 3.12 Xyz coordinates of the <i>syn</i> - conformer structure of 2.	107
Table 3.13 Xyz coordinates of the <i>anti</i> - conformer structure of 3.....	108

Table 3.14 Xyz coordinates of the <i>syn</i> - conformer structure of 3.	109
Table 3.15 Xyz coordinates of the <i>anti</i> - conformer structure of 4.....	110
Table 3.16 Xyz coordinates of the <i>syn</i> - conformer structure of 4.	111
Table 3.17 Xyz coordinates of the <i>anti</i> - conformer structure of 5.....	112
Table 3.18 Xyz coordinates of the <i>syn</i> - conformer structure of 5.	113
Table 3.19 Xyz coordinates of the <i>anti</i> - conformer structure of 6.....	114
Table 3.20 Xyz coordinates of the <i>syn</i> - conformer structure of 6.	115
Table 3.21 Xyz coordinates of the <i>anti</i> - conformer structure of 7.....	116
Table 3.22 Xyz coordinates of the <i>syn</i> - conformer structure of 7.	117
Table 3.23 Folding energies of CH-arene molecular balances in various solvents upon equilibrium (kcal/mol).	118
Table 4.1 Types of errors in the mechanism section of 34 failing grade final exams.	127
Table 5.1 Calculated SASA and Δ SASA of proposed molecule series 2 and 3 (equilibrium geometry optimized by density functional theory, B3LYP- D3, 6-311+G**).	137
Table 5.2 Calculated SASA and Δ SASA of proposed molecule series 5 and 6 (equilibrium geometry optimized by density functional theory, B3LYP- D3, 6-311+G**).	139
Table 5.3 Folding energies of unpublished molecular balances in chloroform-d and acetonitrile-d3 relative to balance 1a from Chapter 2.	143
Table 5.4 Xyz coordinates of the structure of 2a.	145
Table 5.5 Xyz coordinates of the structure of 3a.	146
Table 5.6 Xyz coordinates of the structure of 2b.....	147
Table 5.7 Xyz coordinates of the structure of 3b.....	148
Table 5.8 Xyz coordinates of the structure of 2c.	149
Table 5.9 Xyz coordinates of the structure of 3c.	150

Table 5.10 Xyz coordinates of the structure of 5b.....	151
Table 5.11 Xyz coordinates of the structure of 6b.....	151
Table 5.12 Xyz coordinates of the structure of 5c.....	152
Table 5.13 Xyz coordinates of the structure of 6b.....	152

LIST OF FIGURES

Figure 1.1 Equilibrium between solvated organic compounds (left) stabilized by solvent-solute attractions, and the desolvated state (right) stabilized by solute-solute and solvent-solvent attractions.	3
Figure 2.1 Schematic representation of the <i>folded-unfolded</i> equilibria of molecular balances 1a-c with short, medium, and long alkyl thioether groups.....	18
Figure 2.2 General synthetic route for balances 1a, 1b, and 1c, with long, medium, and short alkyl thioether groups.....	19
Figure 2.3 Examples of the proton decoupled ^{19}F NMR spectra (376 MHz) highlighting the region with the <i>folded</i> (<i>f</i>) and <i>unfolded</i> (<i>u</i>) conformer singlets for balance a) 1a in <i>n</i> -hexane at 23 °C after equilibration, b) 1a in DMSO- d_6 at 23 °C after equilibration, c) crystals of 1a dissolved in cold CDCl_3 (-50°C) prior to equilibration, d) 1a in deuterated chloroform at 23 °C after equilibration.	21
Figure 2.4 X-ray crystallography structures of 1a (left) and 1b (right). Both structures crystalized in the <i>folded</i> conformers with the alkyl groups of the ether and thioethers forming intramolecular alkyl-alkyl interactions.....	23
Figure 2.5 Correlation plots for the folding energies versus solvent <i>ced</i> (ΔG) for balances a) 1a, b) 1b, and c) 1c. Separate trendlines were drawn for the aprotic (black) and protic (red) solvents. b) Solvent <i>ced</i> vs. ΔG between folded and unfolded conformers of balances a) 1a, b) 1b, and c) 1c.	25
Figure 2.6 a) The $\Delta\Delta G$ versus solvent <i>ced</i> correlation plot for 1a with the different solvent types highlighted based on their functional groups: alkanes (black solid circles), amines (black empty circle), ethers (red solid square), aromatics (orange empty square), carboxylic acids (yellow solid squares), alcohols (green hollow diamonds) ketones, aldehydes, and carboxylic esters (light blue solid triangles), alkyl halides (dark blue hollow triangles), DMSO and mixtures with DMSO(purple +), mixtures with water (brown -), and other groups (gray *). b) The $\Delta\Delta G$ versus solvent <i>ced</i> correlation plots for balances 1a, 1b, and 5a.	27
Figure 2.7 Molecular balances designed to measure the organic solvophobic effects from a) Cockroft (a)and Schreiner (b and c) that were compared with balances 1.....	28

Figure 2.8 The correlation plot of slope $\Delta\Delta G_{ced}$ versus $\Delta\Delta SASA$ for balances 1a, 1b, 1c, and 5a (black circles). Data points for balances 6 and 7 (red squares) were plotted for comparison but use unnormalized surface area values ($\Delta SASA$).	30
Figure 2.9 A contour plot of the solvophobic interaction energies in kcal/mol calculated for the differences surface area on the formation of complexes of non-polar surfaces in solvent systems with <i>ced</i> values from 0 to 600 cal/cm ³	33
Figure 2.10 Synthesis of nitrobenzene 2.....	35
Figure 2.11 Synthesis of aniline 3.....	36
Figure 2.12 Synthesis of maleimide 4.....	36
Figure 2.13 Synthesis of balance 1a.....	37
Figure 2.14 Synthesis of balance 1b.	38
Figure 2.15 Synthesis of balance 1c.....	39
Figure 2.16 X-ray structure of compound 1a. Compound 1a was crystallized in methanol for 2 days in 2 mL dram.....	41
Figure 2.17 X-ray structure of compound 1a. Compound 1b was crystallized in methanol for 2 days in 2 mL dram.....	42
Figure 2.18 ¹ H NMR spectrum of nitrobenzene 2 (400 MHz, chloroform-d).....	44
Figure 2.19 ¹³ C NMR spectrum of nitrobenzene 2 (100 MHz, chloroform-d).....	45
Figure 2.20 ¹⁹ F NMR spectrum of nitrobenzene 2 (376 MHz, chloroform-d).	45
Figure 2.21 ¹ H NMR spectrum of aniline 3 (400 MHz, chloroform-d).....	46
Figure 2.22 ¹³ C NMR spectrum of aniline 3 (100 MHz, chloroform-d).....	46
Figure 2.23 ¹⁹ F NMR spectrum of aniline 3 (376 MHz, chloroform-d).	47
Figure 2.24 ¹ H NMR spectrum of maleimide 4 (400 MHz, chloroform-d).....	47
Figure 2.25 ¹³ C NMR spectrum of maleimide 4 (100 MHz, chloroform-d).....	48
Figure 2.26 ¹⁹ F NMR spectrum of maleimide 4 (376 MHz, chloroform-d).	48

Figure 2.27 ^1H NMR spectrum of balance 1a (400 MHz, chloroform-d).....	49
Figure 2.28 ^{13}C NMR spectrum of balance 1a (100 MHz, chloroform-d).	49
Figure 2.29 ^{19}F NMR spectrum of balance 1a (376 MHz, chloroform-d).....	50
Figure 2.30 ^1H NMR spectrum of balance 1b (400 MHz, chloroform-d).	50
Figure 2.31 ^{13}C NMR spectrum of balance 1b (100 MHz, chloroform-d).	51
Figure 2.32 ^{19}F NMR spectrum of balance 1b (376 MHz, chloroform-d).....	51
Figure 2.33 ^1H NMR spectrum of balance 1c (400 MHz, chloroform-d).....	52
Figure 2.34 ^{13}C NMR spectrum of balance 1c (100 MHz, chloroform-d).	52
Figure 2.35 ^{19}F NMR spectrum of balance 1c (376 MHz, chloroform-d).....	53
Figure 2.36 Decoupled ^{19}F NMR spectrum of crystalline compound 1a, taken immediately after sample was introduced to solution at -50 °C.	55
Figure 2.37 Decoupled ^{19}F NMR spectrum of crystalline compound 1b, taken immediately after sample was introduced to solution at -50 °C.	55
Figure 3.1 a) Equilibrium of torsional molecular balances between the <i>anti</i> - and <i>syn</i> - conformers, with the total SASA varying between conformers. While X could form CH- π interactions in the <i>syn</i> - conformer, while Y could form solvophobic interactions in the <i>anti</i> - conformer, b) balance 2 with measured distances from the Y group to the arene edge in the <i>anti</i> - conformer and the X group to the arene center in the <i>syn</i> - conformer.	83
Figure 3.2 ΔG between <i>syn</i> - and <i>anti</i> - conformers compared against ΔSASA in chloroform-d, demonstrating similar solvent effects between balances which could only form CH- π interactions and those which could also form CH-arene edge interactions.....	85
Figure 3.3 Synthesis of balance 1.	92
Figure 3.4 Synthesis of balance 2.	93
Figure 3.5 Synthesis of balance 3.	94
Figure 3.6 X-ray structure of balance 1. Balance 1 was crystallized in a mixture of methanol and chloroform for 30 days in 2 mL dram.	95

Figure 3.7 X-ray structure of balance 2. Balance 2 was crystallized in a mixture of methanol and chloroform for 30 days in 2 mL dram.	96
Figure 3.8 X-ray structure of balance 3. Balance 3 was crystallized in a mixture of methanol and chloroform for 30 days in 2 mL dram.	98
Figure 3.9 ^1H NMR spectrum of balance 1 (400 MHz, chloroform-d).	100
Figure 3.10 ^{13}C NMR spectrum of balance 1 (100 MHz, chloroform-d).	100
Figure 3.11 ^1H NMR spectrum of balance 2 (400 MHz, chloroform-d).	101
Figure 3.12 ^{13}C NMR spectrum of balance 2 (100 MHz, chloroform-d).	101
Figure 3.13 ^1H NMR spectrum of balance 2 (400 MHz, chloroform-d).	102
Figure 3.14 ^{13}C NMR spectrum of balance 2 (100 MHz, chloroform-d).	102
Figure 3.15 ΔSASA between <i>syn</i> - and <i>anti</i> - conformers compared against ΔG . The study was conducted in 7 different solvent environments: chloroform-d ₃ (red), benzene-6d (orange), dichloromethane-d ₂ (yellow), acetonitrile-d ₃ (green), dimethyl sulfoxide-d ₆ (blue), 91% dimethyl sulfoxide-d ₆ /water mixture (purple), 78% dimethyl sulfoxide-d ₆ /water mixture (black), and 67% dimethyl sulfoxide-d ₆ /water mixture (gray). The ced values of mixed solvents were calculated based on the assumption that ced scales linearly with the v/v % solvent composition.	119
Figure 4.1 Example of mechanism problem where students are asked to draw in formalism arrows.	130
Figure 4.2 Example of mechanism problem where students are asked to draw in the products of a mechanism step.	131
Figure 5.1 Relative Diels-Alder reaction rates in non-polar and polar solvents. Data from Otto et al.	135
Figure 5.2 Controlling diastereoselectivity to favor <i>syn</i> - or <i>anti</i> - addition of sterically bulky maleimide substrates by altering solvent environment and solvophobicity.	136
Figure 5.3 Controlling the regioselectivity of Diels-Alder reactions between 1,3-cyclohexadiene and <i>p</i> -benzoquinone derivatives using solvophobic effects. Symmetrical compound 4a is a control designed to form little to no product due to steric strain.	139

Figure 5.4 Synthesis of aromatic linker balances contain design elements that maybe useful in future systems: a) synthesis of aryl-aryl linker balance, b) formation of alkyl-aryl linker balance starting from maleimide intermediate, c) list of the reaction reagents.	142
---	-----

LIST OF EQUATIONS

Equation 1.1 $\Delta G = (XYZ)^{\circ} + a\alpha + b\beta + s \cdot (\pi^{*} + d\delta)$	8
Equation 2.1 $\Delta G_{\text{solvophobic}} = ced \cdot \Delta \text{SASA} \cdot -5.26 \times 10^{-2} \text{ cal}^{-1} \text{ cm}^3 \text{ \AA}^{-2} \text{ kcal mol}^{-1}$	17
Equation 2.2 $\text{Error}\left(\frac{\text{folded}}{\text{unfolded}}\right) = \sqrt{(\text{Error}_{(\text{folded})})^2 + (\text{Error}_{(\text{unfolded})})^2}$	56
Equation 2.3 $\text{Error}_{\Delta G} = -RT\text{Error}([\text{folded}]/[\text{unfolded}])$	56
Equation 2.4 $\text{Error}_{\Delta \Delta G} = \sqrt{(\text{Error}_{(\Delta G)})^2 + (\text{Error}_{(\Delta G)})^2}$	56
Equation 3.1 $\Delta G = \Delta G^{\circ} + a\alpha + b\beta + s(\pi^{*} + d\delta)$	81
Equation 3.2 $\Delta G = \Delta G^{\circ} + b\text{SA} + c\text{SB} + d\text{SP} + e\text{SdP}$	82
Equation 3.3 $\Delta G = \Delta G^{\circ} + \text{di}(\text{DI}) + e\text{ES} + a\alpha 1 + b\beta 1$	82
Equation 3.4 $\text{Error}\left(\frac{\text{syn}}{\text{anti}}\right) = \sqrt{(\text{Error}_{(\text{syn})})^2 + (\text{Error}_{(\text{anti})})^2}$	120
Equation 3.5 $\text{Error}_{\Delta G} = -RT\text{Error}([\text{syn}]/[\text{anti}])$	120

LIST OF ABBREVIATIONS

<i>ced</i>	Cohesive energy density
EPF	Electron pushing formalism
SASA	Solvent accessible surface area

CHAPTER 1

MOLECULAR DEVICES FOR MEASURING SOLVOPHOBIC EFFECTS AND DEVELOPING SCAFFOLDING TOOLS FOR TEACHING ORGANIC CHEMISTRY

1.1 Abstract

The first chapter of this dissertation provides an introduction to solvent induced non-covalent interactions, the practical implication thereof, and challenges in studying such. Likewise, the importance of weak non-covalent interactions which are composed of electrostatic as well as dispersion components will be discussed, including the topic of multiparameter linear solvation energy relationships (LSER). Next, a brief overview will be given on how molecular devices have been used to collect measurements of weak noncovalent interactions. Finally, a discussion will be given on the modes of learning organic chemistry undergraduate students employ as the prolegomena for designing online learning tools for them.

1.2 Hydrophobic and Solvophobic Effects

Solvent environments profoundly affect how solutes interact with one another, influencing reaction rates and self-assembly stability trends. The most notable example of this is the hydrophobic effect, which drives the segregation of organic substrates in aqueous media. An example of the hydrophobic effect is in the emulsification of oil droplets in water. The hydrophobic effect also plays a role in key biological functions, such as protein folding,¹ lipid aggregation,² and enzymatic functions.^{3,4} The hydrophobic effect can also accelerate the rate of reactions in water, such as in Diels-Alder cycloadditions and Claisen rearrangements.⁵ The ability to catalyze certain organic reactions without the use of expensive or harsh catalysis makes hydrophobicity important in synthesis and green chemistry.

The hydrophobic effect consists of several competing and synergistic forces. Counterintuitively, the hydrophobic effect is not driven by repulsive forces between the aqueous media and the organic solutes. In many instances, particularly for hydrogen bonding organic solutes, there is very good attraction between the organic solute and the water molecules. However, this solute-solute attraction is in competition with two attractive interactions: the solvent-solvent and solute-solute interactions (**Figure 1.1**). In aqueous media, the solute-solvent association is dominant due to the ability of water molecules to form multiple strong solvent-solvent hydrogen bonds. This creates an extremely strong attraction between water molecules. Finally, the solvent-solute competes against the hydrophobic effect, which is why hydrogen bonding and ionic solutes form weaker hydrophobic interactions. The interplay between these three forces manifests in what is observed to be the hydrophobic effect.

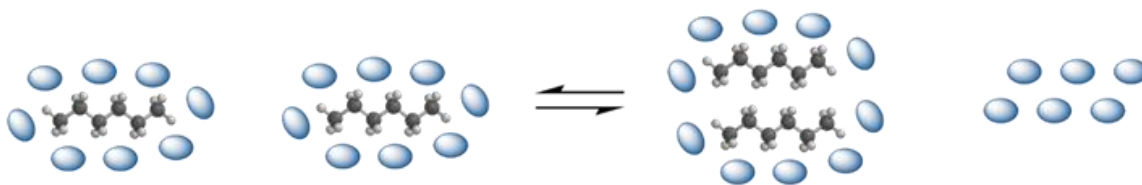


Figure 1.1 Equilibrium between solvated organic compounds (left) stabilized by solvent-solute attractions, and the desolvated state (right) stabilized by solute-solute and solvent-solvent attractions.

Organic solvents lack the strong cohesive hydrogen and dipole-dipole bonding of water, thus making the organic solvophobic effect significantly weaker than the hydrophobic effect. This obstacle has made the study of the solvophobic effect challenging. Despite its weak nature, the organic solvophobic effect is still of interest due to its influence in reaction rates and selectivity, molecular recognition, and self-assembly.

1.3 Measuring Solvophobic Effects with Molecular Devices in Organic Solvents

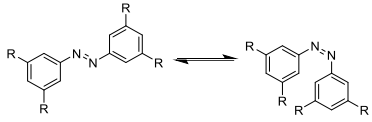
Unimolecular devices have been effectively employed for observing weak non-covalent interactions.⁶ Molecular torsional balances assume multiple conformations, which are observable on an NMR timescale by a transitional barrier. Upon equilibrium, the differences in the population of the two conformers reflects their thermodynamic stability, which can then be converted into energy values using the Gibbs free energy relationship. The benefits of using unimolecular systems include the ability to obtain desired interactions without the need for high concentrations of analyte, good control of interaction distances and geometry, and the independence from using supporting interactions to enable weaker interactions to occur. Furthermore, the use of alkyl-alkyl interactions has been found to be efficient in measuring solvophobic effects.^{7,8} Due to the minimal masking of the actual solvophobic effects, non-polar saturated hydrocarbons exhibit weak VDW intermolecular attractions which can be measured. Thus, incorporating alkyl-alkyl interactions into molecular devices is an effective tool for isolating weak solvophobic interactions.

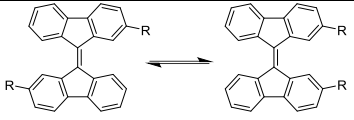
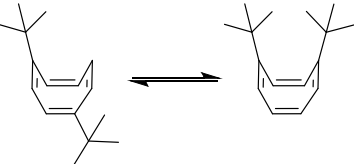
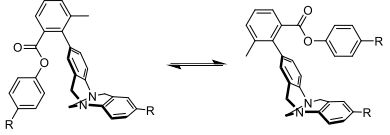
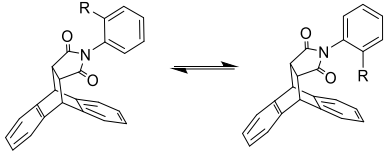
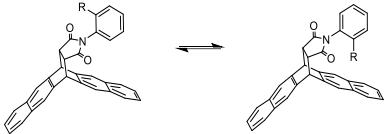
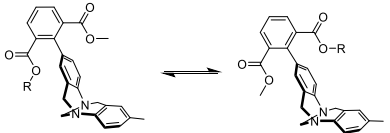
Several variations of unimolecular devices have been developed for measuring weak VDW forces (**Table 1.1**). Classic examples are cycloocta-1,3,5,7-tetraene derivatives which can assume a chair-like *unfolded* conformations or a puckered *folded* conformations.⁹ The *folded* conformations become more favorable with larger alkyl substituents and more polar solvents.¹⁰ An azide molecular switch, developed by Wegner et al., which transitions from a *syn*-conformation to an *anti*-conformation upon ultraviolet radiation excitation, has been utilized to show that increasing the length of pendant alkyl chains increases the half-life of the *syn*-conformations.⁸ The system was also responsive to different solvents, where in a more cohesive solvent (i.e. DMSO), the half-life of the *syn*-

conformation increased dramatically compared to low cohesion solvents like *n*-decane. Similar results were obtained by Schweighauser et al. using non-linear alkyl groups¹¹ and by Wilming using a bifluorenylidene balance¹². Cockroft et al. used Wilcox's Troger base torsional balance model to develop a molecular torsional balance where an alkyl chain pendant rotates with a phenyl axis.^{13,14} Weak alkyl-alkyl interactions were measured in a wide range of solvents, including organic-aqueous mixtures and perfluorinated solvents. Moreover the measurements taken were very accurate with errors of less than 0.03 kcal/mol.

Even in alkyl-aryl molecular device systems where solvophobic interactions could not be isolated, solvophobic effects could still be recognized and characterized. Using the Troger base molecular balance, Bhayana and coworkers saw the promotion of the *folded* conformer across several alkyl-aryl interactions from measuring in water from chloroform.¹⁵ Maier and coworkers, using a succinimide alkyl-aryl balance, observed that high polarity non-protic solvents promoted the *folded* conformation in their balance system.¹⁶ Lastly, Emenike and coworkers were able to correlate folding trends in their succinimide balance system to solvent polarity and hydrogen bonding trends.¹⁷

Table 1.1: Unimolecular devices used to observe solvent effects in which parameters were correlated with increased solute-solute interactions.

Author	Molecular device	Interaction measured	Solvents used	Solvent/solute parameters used
Wegner 2015 and 2019		Linear and non-linear alkyl-alkyl	2	Number of carbons in solute

Schreiner 2022		Linear and non-linear alkyl-alkyl	7	Δ SASA of solute
Schreiner 2020		Non-linear alkyl-alkyl	16	Catalán polarizability of solvent
Cockroft 2013 and 2015		Linear alkyl- alkyl and perfluorinated alkyl-alkyl	24	<i>ced</i> of solvent
Shimizu 2017		Alkyl-aryl	21	<i>ced</i> of solvent
Emenike 2018		Alkyl-aryl	7	Kamlet-Taft parameters of solvent
Wilcox 2007		Alkyl-aryl	2	Δ SASA of solute

1.4 Predicting Hydrophobic and Solvophobic Effects

Solvent and solute parameters can be individually or collectively employed to model and characterize solvophobic interactions. The strength of the hydrophobic and solvophobic effects correlates to the change in solvent accessible surface area (Δ SASA) of the solutes in the interaction equilibrium, which provides an estimate of the number of solvent molecules released by the formation of solute-solute complexes as outlined by the Lum-Chandler-Weeks theory.¹⁸ The SASA calculations can be adjusted to incorporate the molecular radius of the solvent, with SASA solvent probes typically being 1.4 Å to reflect

the molecular radius of water.^{19,20} The correlation between SASA and the strength of the hydrophobic and solvophobic effects have been demonstrated by melting and boiling point experiments.^{21,22}

Solvent cohesion, a measure of attractive interactions between solvent molecules, is another key component. Cohesive energy density (*ced*) is experimentally derived from the heat of evaporation of a solvent from the solution to the gas phase. The correlation between *ced* and both hydrophobic and solvophobic interactions has been demonstrated.^{14,23} For instance, *ced* is a good predictor of the solvophobic effect of hydrocarbons where special interactions are minimized. Organic solvents generally fall within the *ced* range of 50 to 210 cal/cm³, while water has a *ced* of 550 cal/cm³, making extrapolation of cohesion trends from one to the other difficult.

Another experimental parameter, ET(30), which describes a solvent's polarity using the wavelength of a dissolved solvatochromatic dye, has also been correlated with the strength of hydrophobic and solvophobic effects.^{23,24} It provides a measure of how well solvent molecules can form dipole-dipole interactions with solvent and solute molecules.²⁵

The Kamlet-Taft solvent parameters, which describe specific polarized interaction events in which solvent molecules participate, account for the hydrogen donor (α), hydrogen acceptor (β), polarizability and dipolarizability (π) abilities of a solvent with a correction in energetics (δ) for aromatics and alkyl halides.²⁶ The combination of these terms enables the prediction of solvent-solvent attractions as well as solute-solvent interactions. Solvation energy can be mathematically represented (**Equation 1.1**), where a, b, s, and d are fitting coefficients and (XYZ)[°] represents unaccounted factors.

Equation 1.1: $\Delta G = (XYZ)^{\circ} + a\alpha + b\beta + s(\pi^{*} + d\delta)$

There are also lesser-known Laurence and Catalán parameters used in characterizing solvent polarity and hydrogen bonding effects.²⁷⁻²⁹ Multiparameter relationships are beneficial for studying alkyl-aryl systems as demonstrated by Emenike and coworkers, due to their ability to describe multiple solvent and solute interactions simultaneously.¹⁷

Using this background, the goal of the research was to use unimolecular devices which could measure weak solvophobic effects and develop simple models based on known solvent and solute parameters which could be used to analyze the data to accurately predict the solvophobic energies for different systems. In particular, alkyl-alkyl and CH-arene interactions were analyzed using a combination of solute SASA data and solvent parameter data to predict interaction energies. The projects utilize succinimide balances as they have proven to be a versatile measuring tool throughout many solvents and interaction types.⁶

1.5 Identifying and Addressing Difficulties in Learning Organic Chemistry

Organic chemistry is a required course for many undergraduate students, particularly those pursuing degrees in medicine and biology related sciences, offered by nearly every institution of higher education. However, many students find passing the course challenging, leading to high attrition rates, often cited to be between 30-50% for pre-medical majors as of 2008.³⁰ Even students who have excelled in previous mathematics and chemistry courses have been known to struggle with the subject, leading to as much as 40% of students to changing majors.³¹ This high attrition rate is detrimental to students,

causing delays in graduation, additional tuition and student loan costs, and increased anxiety which can lead to further underperformance.³²

Educational scientists have been studying the work and thought processes of students to identify areas of difficulty and inform educators on optimal approaches to teaching organic chemistry. Studies have been conducted to understand how students conceptualize both organic chemistry as a whole, and specific concepts within it, from which practical suggestions are made. One useful distinction made by Skemp is the categorization of instrumental learning and relational learning.³³ Instrumental learning is based on students learning a set procedure or rule for solving a specific type of problem. Relational learning is based on students learning the special connections concepts have with one another. As summarized by Skemp, instrumental learning involves knowing what to do, while relational learning involves knowing what to do and for what reason.³³

Advantages of relational learning include a need for fewer rules and procedures to memorize, greater adaptability to new topics, and a better foundation for addressing problems that deviate from the norms of the field. For organic chemistry, which has a wide range of topics students must learn, relational learning is optimal and should be encouraged. However, while often dismissed as "rote memorization", instrumental learning has practical benefits for an exam-based course. Instrumental learning is a faster method to become proficient in performing in a specific topic. This is beneficial in an organic chemistry course as students are required to become proficient in the class topics by their exam dates. Even though students acknowledge that instrumental learning is inferior to relational learning for understanding the topics, it is often resorted to as it is a more intuitive and expedient way to study for examinations. Furthermore, seeing immediate results from

this method gives students a confidence boost to continue applying themselves to their studies.

Educational scaffolding is a pedagogical methodology where a complex task is divided into smaller, feasible tasks for the students to complete.³⁴ The benefit to this approach is that students are not overwhelmed in having to understand difficult concepts or perform difficult tasks all at once. However, once the tasks are completed correctly, the student will have achieved a goal they otherwise would not be able to complete on their own without assistance from the system. It also leads to students experiencing small achievements which keeps them motivated to continue learning the concept at hand. Importantly, scaffolding is to be used as a temporary means of helping the student until they are comfortable and proficient in the concept being taught. Otherwise, it tends to promote a shallower instrumental understanding of the subject instead of relational understanding.³⁵ Scaffolding is widely implemented in the field of mathematics education,³⁶ but is fairly limited in organic chemistry education.

An online resource was developed to provide a scaffolding framework for students to learn electron pushing formalisms (EPF) in reaction mechanisms. The purpose was to assist struggling students in gaining proficiency in the topic and to provide them with the tools for transitioning from an instrumental to a relational mode of learning.

1.6 References

- (1) Kauzmann, W. Some Factors in the Interpretation of Protein Denaturation. *Adv. in Protein Chem.*; Elsevier, **1959**; Vol. 14, pp 1–63.
- (2) Feng, S.; Kong, L.; Gee, S.; Im, W. Molecular Condensate in a Membrane: A Tugging Game between Hydrophobicity and Polarity with Its Biological Significance. *Langmuir* **2022**, 38 (19), 5955–5962.

- (3) Rodrigues, R. C.; Ortiz, C.; Berenguer-Murcia, Á.; Torres, R.; Fernández-Lafuente, R. Modifying Enzyme Activity and Selectivity by Immobilization. *Chem. Soc. Rev.* **2013**, 42 (15), 6290–6307.
- (4) Bert, J.; van Tol, A.; Odenthal, J. B.; Jongejan, J. A.; Duine, J. A. Relation of Enzymatic Reaction Rate and Hydrophobicity of the Solvent. In *Prog. in Biotechnol.*; Elsevier, **1992**; Vol. 8, pp 229–235.
- (5) Narayan, S.; Muldoon, J.; Finn, M.G.; Fokin, V.V.; Kolb, H.C.; Sharpless, K.B. “On Water”: Unique Reactivity of Organic Compounds in Aqueous Suspension. *Angew. Chem., Int. Ed.* **2005**, 44: 3275–3279.
- (6) Li, P. Vik, E. Shimizu, K.D. Arylimide Molecular Balances: A Comprehensive Platform for Studying Aromatic Interactions in Solution. *Acc. Chem. Res.* **2020** 53 (11), 2705–2714.
- (7) Schümann, J. M.; Wagner, J. P.; Eckhardt, A. K.; Quanz, H.; Schreiner, P. R. Intramolecular London Dispersion Interactions Do Not Cancel in Solution. *J. Am. Chem. Soc.* **2021**, 143 (1), 41–45.
- (8) Strauss, M. A.; Wegner, H. A. Exploring London Dispersion and Solvent Interactions at Alkyl–Alkyl Interfaces Using Azobenzene Switches. *Angew. Chem. Int. Ed.* **2019**, 58 (51), 18552–18556.
- (9) Lyttle, M. Streitwieser, A. Kluttz, R. Unusual Equilibrium Between 1,4- and 1,6-di-tert-butylcyclooctatetraenes, *J. Am. Chem. Soc.* **1981** 103 (11), 3232–3233.
- (10) Schümann, J. M.; Wagner, J. P.; Eckhardt, A. K.; Quanz, H.; Schreiner, P. R. Intramolecular London Dispersion Interactions Do Not Cancel in Solution. *J. Am. Chem. Soc.* **2021**, 143 (1), 41–45.
- (11) Schweighauser, L.; Strauss, M. A.; Bellotto, S.; Wegner, H. A. Attraction or Repulsion? London Dispersion Forces Control Azobenzene Switches. *Angew. Chem. Int. Ed.* **2015**, 54 (45), 13436–13439.
- (12) Wilming, F. M.; Marazzi, B.; Debes, P. P.; Becker, J.; Schreiner, P. R. Probing the Size Limit of Dispersion Energy Donors with a Bifluorenylidene Balance: Magic Cyclohexyl. *J. Org. Chem.* **2023**, 88 (2), 1024–1035.
- (13) Yang, L.; Adam, C.; Nichol, G. S.; Cockroft, S. L. How Much Do van Der Waals Dispersion Forces Contribute to Molecular Recognition in Solution? *Nat. Chem.* **2013**, 5, 1006–1010.
- (14) Adam, C.; Yang, L.; Cockroft, S. L. Partitioning Solvophobic and Dispersion Forces in Alkyl and Perfluoroalkyl Cohesion. *Angew. Chem. Int. Ed.* **2015**, 54 (4), 1164–1167.
- (15) Bhayana, B.; Wilcox, C. S. A Minimal Protein Folding Model To Measure Hydrophobic and CH– π Effects on Interactions between Nonpolar Surfaces in Water. *Angew. Chem. Int. Ed.* **2007**, 119 (36), 6957–6960.
- (16) Maier, J. Li, Erik C. Vik, Christopher J. Yehl, Sharon M. S. Strickland, and Ken D. *J. Am. Chem. Soc.* **2017**, 139 (19), 6550–6553.
- (17) Emenike, B. U.; Spinelle, R. A.; Rosario, A.; Shinn, D. W.; Yoo, B. Solvent Modulation of Aromatic Substituent Effects in Molecular Balances Controlled by CH– π Interactions. *J. Phys. Chem. A* **2018**, 122 (4), 909–915.
- (18) Lum, K.; Chandler, D.; Weeks, J.D. Hydrophobicity at small and large length scales. *J. Phys. Chem. B* **1999**, 103 (22), 4570–4577.

- (19) Pauling, L. *The Nature of the Chemical Bond: An Introduction to Modern Structural Chemistry*, 3rd ed.; Cornell University Press: Ithaca, NY, **1960**.
- (20) Hasel, W.; Hendrickson, T.; Still, W.C. A rapid approximation to the solvent accessible surface areas of atoms, *Tetrahedron Comput. Methodol.* **1988**, *1* (2), 103–116.
- (21) Yoshiro, O; Tsuchida, M. Linear boiling point relationships. *Ind. Eng. Chem.* 1957, *49* (3) 415-417.
- (22) Yalkowsky; Samuel H.; and Valvani, S. Solubilities and Partitioning Relationships Between Aqueous Solubilities, Partition Coefficients, and Molecular Surface Areas of Rigid Aromatic Hydrocarbons." *J. Chem. Eng. Data* **1979**, *24* (2), 127-129.
- (23) Yang, L.; Adam, C.; Cockroft, S. L. Quantifying Solvophobic Effects in Nonpolar Cohesive Interactions. *J. Am. Chem. Soc.* **2015**, *137* (32), 10084–10087.
- (24) Würthner, F. Solvent Effects in Supramolecular Chemistry: Linear Free Energy Relationships for Common Intermolecular Interactions *J. Org. Chem.* **2022** *87* (3), 1602-1615.
- (25) Smithrud, D.; Diederich, F. Strength of molecular complexation of apolar solutes in water and in organic solvents is predictable by linear free energy relationships: a general model for solvation effects on apolar binding *J. Am. Chem. Soc.* **1990** *112* (1), 339-343.
- (26) Reichardt, C. Strength of molecular complexation of apolar solutes in water and in organic solvents is predictable by linear free energy relationships: a general model for solvation effects on apolar binding *J. Org. Chem.* **2022** *87* (3), 1616-1629.
- (27) Laurence, C.; Legros, J.; Chantzis, A.; Planchat, A.; Jacquemin. D. A Database of Dispersion-Induction DI, Electrostatic ES, and Hydrogen Bonding α 1 and β 1 Solvent Parameters and Some Applications to the Multiparameter Correlation Analysis of Solvent Effects *J. Phys. Chem. B* **2015** *119* (7), 3174-3184.
- (28) Catalán, J. Solvatochromic Correlation Analysis of Monomolecular $S_N1/E1$ Heterolysis Reactions of Tertiary Haloalkanes. *J. Mol. Liq.* **2021**, *324*, 114699.
- (29) Catalán, J. Toward a Generalized Treatment of the Solvent Effect Based on Four Empirical Scales: Dipolarity (SdP, a New Scale), Polarizability (SP), Acidity (SA), and Basicity (SB) of the Medium *J Phys. Chem. B* **2009**, *113* (17), 5951-5960.
- (30) Grove, N. P.; Hershberger, J. W.; Bretz, S. L. Impact of a Spiral Organic Curriculum on Student Attrition and Learning. *Chem. Educ. Res. Pract.* **2008**, *9* (2), 157–162.
- (31) Poole, M.; Glaser, R. Organic Chemistry Online: Building Collaborative Learning Communities through Electronic Communication Tools *J. Chem. Ed.* **1999**, *76* (5), 699.
- (32) Gibbons, R. E.; Xu, X.; Villafañe, S. M.; Raker, J. R. Testing a Reciprocal Causation Model between Anxiety, Enjoyment and Academic Performance in Postsecondary Organic Chemistry. *Educ. Psychol.* **2018**, *38* (6), 838–856.
- (33) Skemp, R. R. Relational Understanding and Instrumental Understanding. *Arith. Teach.* **1978**, *26* (3), 9–15.
- (34) Burns, A.; De, H.; For, C. Teachers' Voices. 8: *Explicitly Supporting Reading and Writing in the Classroom*; Nceltr: Sydney, **2005**.
- (35) Zwetzschler, L. Adaptivity Challenges for Relational Scaffolding. *CERME 9* **2015**; pp 1531–1532.

- (36) Bakker, A.; Smit, J.; Wegerif, R. Scaffolding and Dialogic Teaching in Mathematics Education: Introduction and Review. *ZDM* **2015**, *47* (7), 1047–1065.

CHAPTER 2

AN EMPIRICAL MODEL FOR SOLVOPHOBIC INTERACTIONS IN ORGANIC
SOLVENTS

2.1 Abstract

An empirical model was developed to predict organic solvophobic effects based on the measurements of a series of molecular balances. The balances have an *N*-phenylimide framework and were designed to measure the weak solvophobic interactions between non-polar alkyl surfaces. Solution studies and X-ray crystallography confirmed that the balances formed intramolecular alkyl-alkyl interactions in the *folded* conformers. The structural modularity of the balances enabled systematic variation of the lengths of the interacting alkyl surfaces. Control balances which could not form strong intramolecular interactions were critical in isolating the weak solvophobic effect by removing framework and specific solvent-solute contributions to the folding equilibria. The folding ratios were measured in 46 deuterated and non-deuterated solvent systems via integration of the ^{19}F NMR spectra. Consistent with previous studies, a strong correlation was observed between the interaction energies and the solvent cohesive energy density (*ced*) and with the change in solvent accessible surface areas (SASA). An empirical model was developed from the combination of the SASA and *ced* parameters along with the incorporation of the solvent data from Cockroft's alkyl-alkyl balance. The model predicts the solvophobic interaction energy per unit area for any solvent with known *ced* values. The interaction energies predicted by the model were consistent with recent organic solvophobic measurements and

with the literature values for the hydrophobic effect for non-polar surfaces, demonstrating the accuracy and value of the model.

2.2 Introduction

The solvophobic effects of water have been extensively studied due to their strength and central role in many important processes such as protein folding,¹⁻³ micelle and membrane stability,^{4,5} enzyme selectivity,^{6,7} and synthetic reaction rates and stereoselectivity.⁸⁻¹⁰ While the origins of solvophobic interactions are complex, a common rationalization is the exchange of weak solvent-solute interactions for stronger solvent-solvent interactions, which drives the formation of the solute-solute complex (**Figure 2.1**). Thus, the strength of the hydrophobic effect can be attributed to the high cohesive energy of water molecules. The solvophobic effects for organic solvents are considerably weaker due to the low cohesive energy of organic solvents. Accordingly, the solvophobic effect of organic solvents has been less studied.¹¹⁻¹³ However, organic solvents are widely used for many applications and processes, and even weak organic solvophobic effects can influence catalyst selectivities,¹⁴ crystal packing patterns,^{15,16} and assembly stabilities.^{17,18} Therefore, the goal of this study was to develop an empirical model which could predict the strength of the solvophobic effects for alkyl-alkyl interactions in any organic solvent.

2.3 Experimental Design

Our approach to developing a predictive model builds on previous organic solvophobic effect studies.^{12,13} Cohesive energy density (*ced*) is a solvent parameter that has been shown to have a strong correlation with solvophobic interaction energies.^{12,13,19-21} The solvophobic effects are strongest in high cohesion solvents, with water having the highest *ced* value of 550 cal/cm³. The *ced* values of common organic solvents such as benzene, chloroform, and THF are significantly lower (84.7 to 86.9 cal/cm³), which is consistent with the weak solvophobic effects in organic solvents. The solvophobic effect has also been correlated with the change in solvent accessible

surface area (Δ SASA).^{22,23} This parameter provides a measure of the number of solvent molecules or the surface area of the solvent molecules displaced from the solvent-solute complexes upon formation of the solute-solute complex.^{24,25} In this work, an empirical expression was developed for the solvophobic interaction energies from the solvent *ced* and the Δ SASA of the interaction. The equation was derived in two stages. First, the normalized folding energies ($\Delta\Delta G$) for a series of molecular balances that formed intramolecular alkyl-alkyl interactions were measured over a wide range of solvent environments. The slopes of the $\Delta\Delta G$ versus *ced* plot ($\text{slope}_{\Delta\Delta G/ced}$) for each balance provided a measure of the magnitude of the solvophobic effects for each balance. Second, the $\text{slope}_{\Delta\Delta G/ced}$ values were correlated with the Δ SASA for the intramolecular alkyl-alkyl interactions. The trendline for this second plot provided an expression for the solvophobic interaction energy (**Equation 2.1**) with respect to *ced* and Δ SASA, which was tested by comparing the predicted solvophobic interaction energies against previous measures of the solvophobic effects in organic¹⁹ and aqueous solvent systems.²⁶

Equation 2.1 $\Delta G_{\text{solvophobic}} = ced \cdot \Delta\text{SASA} \cdot -5.26 \times 10^{-2} \text{ cal}^{-1} \text{ cm}^3 \text{ \AA}^{-2} \text{ kcal mol}^{-1}$

Accurate measures of the weak organic solvophobic effects were provided by molecular torsional balances (**Figure 2.1**), which were designed to measure the intramolecular interaction of two alkyl surfaces (R_1 and R_2) via their influence on a conformational equilibria.²⁷⁻²⁹ The central $C_{\text{phenyl}}-N_{\text{imide}}$ single bond has restricted rotation, generating distinct *folded* and *unfolded* conformers.³⁰⁻³³ In the *folded* conformer, the alkyl groups are held close together in an aligned geometry which favors the formation of an intramolecular alkyl-alkyl interaction. In the *unfolded* conformer, the alkyl groups are held apart, preventing the formation of alkyl-alkyl interactions. In the ^1H and ^{19}F NMR spectra, the peaks for the *folded* and *unfolded* conformers were in slow exchange at room

temperature. Thus, the *folded/unfolded* ratio could be measured by integration of the area under the corresponding peaks.

Saturated hydrocarbon R_1 and R_2 groups were chosen as the interacting surfaces to help isolate the solvophobic effects. Alkyl groups are non-polar and do not form strong solvent-solute interactions such as hydrogen bonds or electrostatic interactions. Thus, the primary solvent effects would be solvophobic effects.

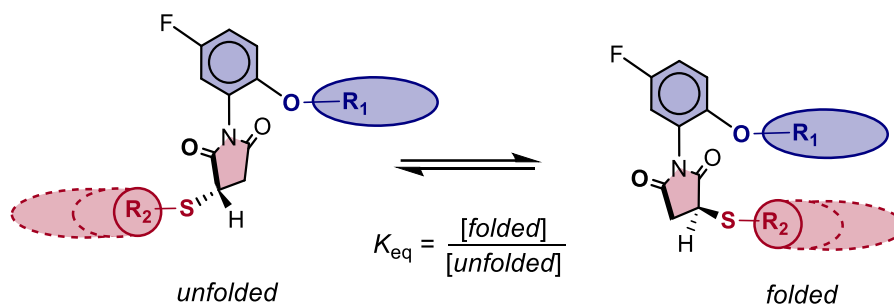


Figure 2.1 Schematic representation of the *folded-unfolded* equilibria of molecular balances **1a-c** with short, medium, and long alkyl thioether groups.

The modular design of the balances enabled efficient synthesis and variation of the contact surface areas of the interactions (**Figure 2.2**). Balances **1a**, **1b**, and **1c** with the same length R_1 groups (decyl) but with varying length R_2 groups were assembled in 4 steps. First, the *n*-decyl ether (OR_1) was installed on the phenyl rotor via nucleophilic aromatic substitution on 2,5-difluoronitrobenzene to yield phenyl ether **2**. The nitro group of **2** was reduced with H_2 and Pd/C to give aniline **3**, which was condensed with maleic anhydride to give maleimide **4**. In the final step, the Michael addition of alkyl thiols of varying lengths

to maleimide **4** yielded long (**1a**), medium (**1b**), and short (**1c**) balances with $R_2 = (CH_2)_9CH_3$, $(CH_2)_5CH_3$, and CH_2CH_3 , respectively.

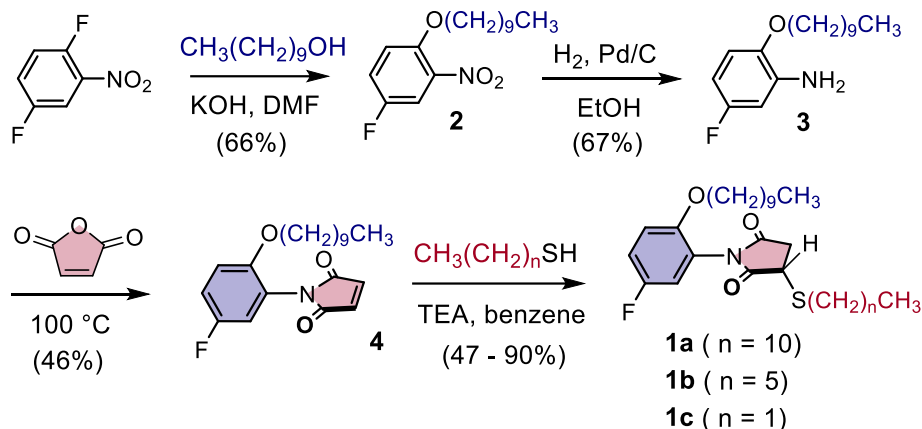


Figure 2.2 General synthetic route for balances **1a**, **1b**, and **1c**, with long, medium, and short alkyl thioether groups.

To facilitate measurement in a wider range of organic solvent systems, a ^{19}F NMR label was inserted into the 5-position of the *N*-phenyl rotor. Thus, the NMR measurements of the folding ratios were not limited to deuterated solvents (**Table 2.1**). Of the 46 solvent systems, 28 were non-deuterated solvents with an additional 5 mixed solvent systems. Monitoring the folding equilibria using proton decoupled ^{19}F NMR was critical to provide the needed accuracy to measure the weak organic solvophobic effects. Fluorine NMR has a sensitivity similar to proton NMR but with greater integration accuracy.³⁴ Due to the large ^{19}F NMR spectral window and absence of interfering peaks from the solvent or balance, the peaks for the *folded* and *unfolded* conformers of balances **1a-c** were baseline separated singlets in all solvent systems (**Figure 2.3**).

Table 2.1 The 46 solvent systems used to measure the solvophobic effects of the balances along with their cohesive energy density values and solvent functional groups.

solvent ^a	ced (cal/cm ³) ^b	solvent functional group classification
<i>n</i> -pentane	50.27	alkane
<i>n</i> -hexane	52.4	alkane

triethylamine	57	amine
diethyl ether	60	ether
cyclohexane	66.9	alkane
<i>N,N</i> -diethylamine	67.24	amine
1,2-dimethoxyethane	74.88	ether
<i>p</i> -xylene	78.3	aromatic
toluene	79.4	aromatic
ethyl acetate	81.7	carboxylic ester
methyl acetate	83.61	carboxylic ester
benzene-d ₆	84.7	aromatic
chloroform-d	85.4	alkyl halide
THF	86.9	ether
furan	88.36	ether
cyclohexanone	91.86	ketone
methylene chloride	93.7	alkyl halide
acetone-d ₆	94.3	ketone
propanoic acid	95.15	carboxylic acid
1,1,2,2-tetrachloroethane	98.01	alkyl halide
1-decanol	99.5	alcohol
1,2-dichloroethane	103.4	alkyl halide
1,4-dioxane	105.06	ether
25% DMSO-d ₆ /chloroform-d	105.52	DMSO mixture
acetic acid	109.5	carboxylic acid
<i>t</i> -butanol	110.3	alcohol
pyridine	112.4	aromatic
acetophenone	113.63	ketone, aromatic
40% DMSO-d ₆ /chloroform-d	118.02	DMSO mixture
50% DMSO-d ₆ /chloroform-d	126.55	DMSO mixture
<i>i</i> -propanol	132.3	alcohol
acetonitrile-d ₃	138.9	Nitrile
<i>N,N</i> -dimethylformamide	138.9	amide
75% ethanol/benzene-d ₆	142	alcohol
ethanol	161.3	alcohol
DMSO-d ₆	168.6	DMSO
50% methanol-d ₄ /ethanol	185.15	alcohol
5% H ₂ O/DMSO-d ₆	187.67	DMSO mixture
50% methanol-d ₄ /DMSO-d ₆	188.8	DMSO mixture
75% methanol-d ₄ /DMSO-d ₆	198.8	DMSO mixture
80% methanol-d ₄ /DMSO-d ₆	200.9	DMSO mixture
10% H ₂ O/DMSO-d ₆	206.74	DMSO mixture
methanol-d ₄	209	alcohol
10% H ₂ O/methanol-d ₄	243.1	water mixture
15% H ₂ O/methanol-d ₄	260.15	water mixture

^asolvent mixtures were reported in v/v % of the first solvent listed. ^bThe *ced* values were calculated from the Hildebrand solubility parameters.^{35–37} The *ced* values of mixed solvents were calculated based on the assumption that *ced* scales linearly with the v/v % solvent composition.

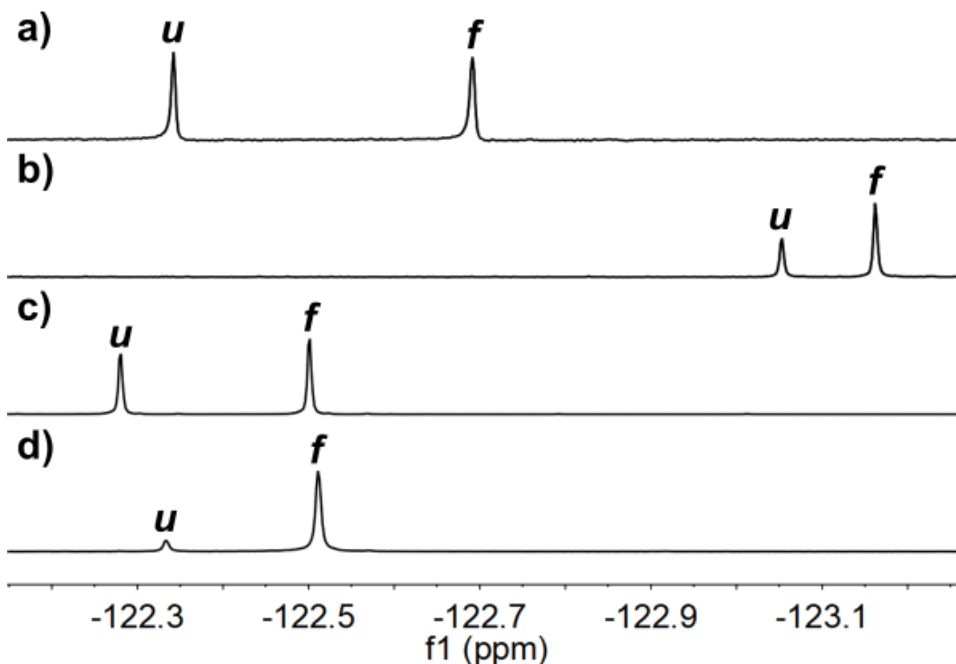


Figure 2.3 Examples of the proton decoupled ¹⁹F NMR spectra (376 MHz) highlighting the region with the *folded* (*f*) and *unfolded* (*u*) conformer singlets for balance a) **1a** in n-hexane at 23 °C after equilibration, b) **1a** in DMSO-d₆ at 23 °C after equilibration, c) crystals of **1a** dissolved in cold CDCl₃ (-50°C) prior to equilibration, d) **1a** in deuterated chloroform at 23 °C after equilibration.

2.4 Results and Discussion

The ability of the rigid *N*-phenyl succinimide framework to position the alkyl ether and alkyl thioether groups in a favorable geometry to form the desired intramolecular interaction was initially confirmed by X-ray crystal structures and later by the solvent folding studies. Balances **1a** and **1b** crystallized exclusively in the *folded* conformers providing evidence of the stabilizing intramolecular alkyl-alkyl interactions (**Figure 2.4**).³⁸ The alkyl groups of the ether and thioethers were in VDW contact. In **1a**, the entire length

of the decyl ether is involved in an alkyl-alkyl interaction with the opposing dodecyl thioether. In **1b**, the first 6 carbons of the decyl ether form alkyl-alkyl interactions with the shorter hexyl thioether.

The crystals of *folded-1a* and *folded-1b* also provided the means for assigning the conformer peaks in the ^{19}F NMR spectra. The crystals were dissolved in cold CDCl_3 (-50°C). Under these conditions the rate of interconversion is minimal, therefore the major peak was assigned as the *folded* conformer (**Figure 2.3c**). The sample was allowed to slowly warm to 25°C and monitored by ^{19}F NMR, which confirmed that the *folded* and *unfolded* peaks maintained the same relative positions in the room temperature spectra (**Figure 2.3d**). The conformer peaks in CDCl_3 were used to assign the peaks in other solvent systems by following the *folded* and *unfolded* peaks in mixtures of CDCl_3 and the second solvent system. In all solvent systems, the *folded* conformer was the more upfield peak.

The folding ratios of **1a-c** were measured in 46 solvent systems (**Table 2.1**) using proton decoupled ^{19}F NMR. These included solvents commonly used in organic synthesis and separations, including many that are not readily available in deuterated forms such as *n*-hexane, triethylamine, diethyl ether, cyclohexane, *N,N*-diethylamine, 1,2-dimethoxyethane, ethyl acetate, furan, cyclohexanone, propionic acid, dioxane, *t*-butanol, pyridine, acetophenone, *i*-propanol, and ethanol. The folding energies were calculated from the ^{19}F NMR measured folding ratios. The solvent systems were selected to span a wide range of *ced* values from 50.3 cal/cm^3 for *n*-pentane to 274.1 cal/cm^3 for a 60% water/THF mixture. Solvents with diverse functional groups were chosen including alcohol, amine, aromatic, ether, carboxylic acid, carboxylic ester, ketone, alkyl halide, sulfoxide, nitrile, and water mixtures. These allowed testing for specific solvent-solute interactions.

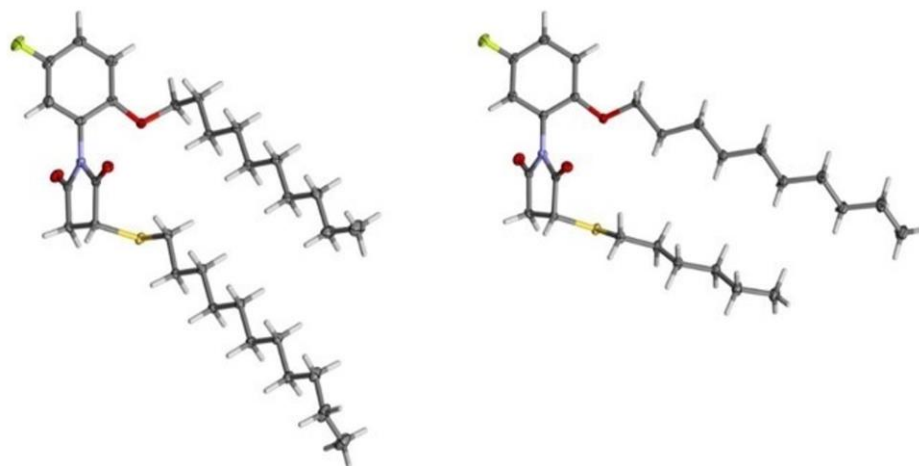


Figure 2.4 X-ray crystallography structures of **1a** (left) and **1b** (right). Both structures crystallized in the *folded* conformers with the alkyl groups of the ether and thioethers forming intramolecular alkyl-alkyl interactions.

The ability to measure the organic solvophobic effects was first verified by correlating the measured folding energies (ΔG) in the 46 solvent systems against the solvent *ced* values (**Figure 2.5**). The ΔG values for **1a-c** became more negative with increasing solvent *ced* values, which corresponded with the expected increase in solvophobic effects in more cohesive solvents.^{12,13,21} However, the analysis also revealed specific solvent effects due to hydrogen bonding solvent-solute interactions. Discrete trendlines were observed for the aprotic and protic solvents. The trendline in the protic solvents (alcohols, water, and carboxylic acids) had weaker correlation with a less steep slope. The separate solvent trends for the protic solvents were attributed to hydrogen bonding interactions with the oxygen ether and sulfur thioether linkers of the balances in the *unfolded* conformers.

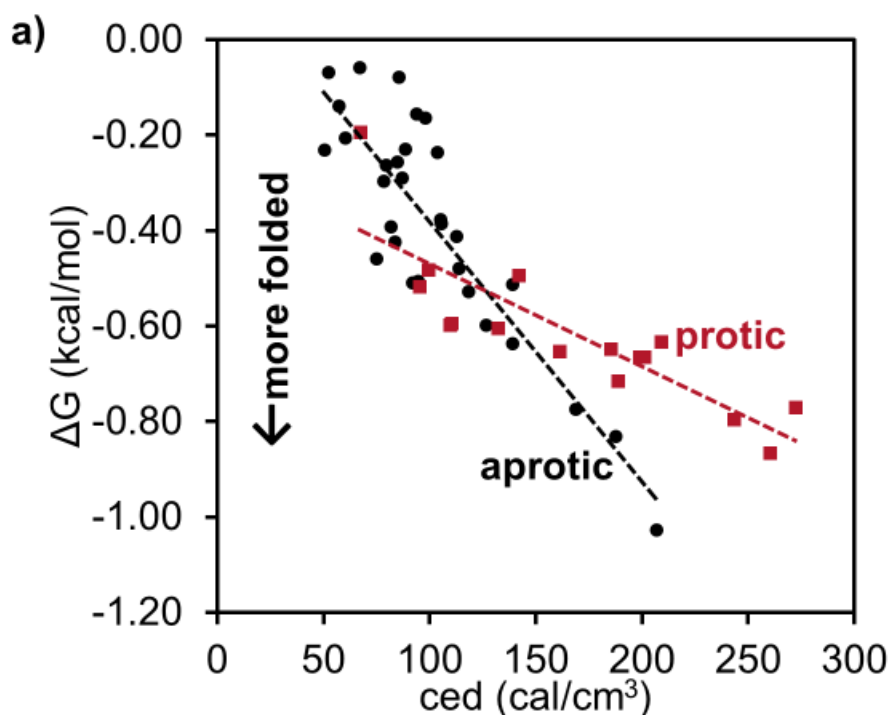
The hydrogen bonding solvent effects were removed using the short alkyl balance **1c** as a control. Balance **1c** shares the same N-phenylsuccinimide framework and linkers as **1a** and **1b**, and thus can remove folding equilibria biases arising from the framework and solvent interactions with the linkers. The $\Delta\Delta G$ versus *ced* plot for **1a** was linear across the entire range of protic and aprotic solvent *ced* values (**Figure 2.6a**), which was consistent with previous reports of the organic solvophobic effects.^{13,21} The trendline had a negative slope. The solvophobic interactions were weakest in the low *ced* alkane solvents (n-pentane, n-hexane, and cyclohexane) and were the strongest in high *ced* water mixtures (10% H₂O/methanol-d₄, 15% H₂O/methanol-d₄, 40% H₂O/THF).

Solvent specific interactions were not observed. The $\Delta\Delta G$ values in solvents containing the same functional groups (ether, carboxylic acid, ketone/aldehyde/ester, aromatic, alcohol, or amine) did not show systematic deviations from the trendline (**Figure 2.6a**).

Comparison of the $\Delta\Delta G_{\text{fold}}$ vs *ced* correlation plots for **1a** and **1b** (**Figure 2.6b**) were consistent with the ability to measure the solvophobic effects. The trendline for **1a** had a steeper slope than **1b**, which is consistent with the longer alkyl thioether of **1a** forming stronger solvophobic effects than the shorter alkyl thioether of **1b**. In addition, the magnitudes of the solvophobic effects were consistent with previous reports of the organic solvophobic effects (0.09 to -0.41 kcal/mol).^{22,39} The solvophobic interaction energies for **1a** and **1b** spanned a similar range from 0.11 to -0.30 kcal/mol.

Further confirmation of the ability of balances **1** to measure the organic solvophobic effects was provided by comparison of the $\Delta\Delta G_{\text{fold}}$ vs *ced* correlation plots with similar analysis reported by Cockroft for balances **5** (**Figures 2.7 and 2.8**).^{13,19} Balance **5a** forms

similar alkyl-alkyl interactions in the *folded* conformer. The folding ratios were reported for a comparable range of organic solvents. Finally, the folding ratios were measured for a control balance **5b** in which has one truncated alkyl group like **1c**. Therefore $\Delta\Delta G$ versus *ced* analyses could be performed for **5a** and directly compared with **1a** and **1b**. The strong linear correlation and range of $\Delta\Delta G$ values were similar for **1a**, **1b**, and **5a**. Even the levels of scatter were congruent with R^2 values of 0.85, 0.71, and 0.83 for **1a**, **1b**, and **5a**, which is an important consideration when measuring a weak non-covalent interaction. The modest R^2 values were commensurate with the relatively small range of $\Delta\Delta G$ values (0.41 kcal/mol) in comparison to the experimental errors (± 0.02 and ± 0.03 kcal/mol).



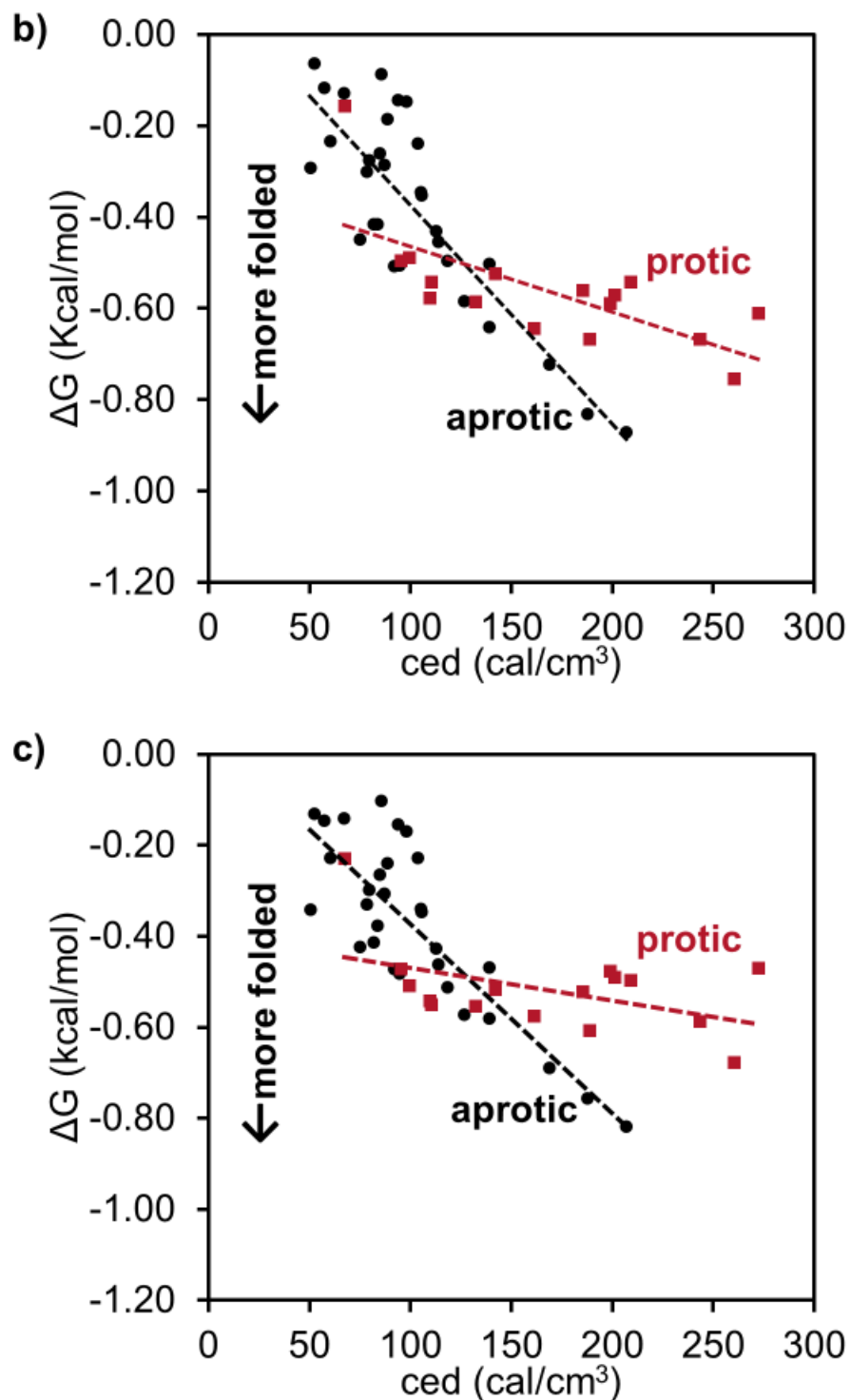


Figure 2.5 Correlation plots for the folding energies versus solvent ced (ΔG) for balances a) **1a**, b) **1b**, and c) **1c**. Separate trendlines were drawn for the aprotic (black) and protic (red) solvents. 9: Solvent ced vs. ΔG between folded and unfolded conformers of balances a) **1a**, b) **1b**, and c) **1c**.

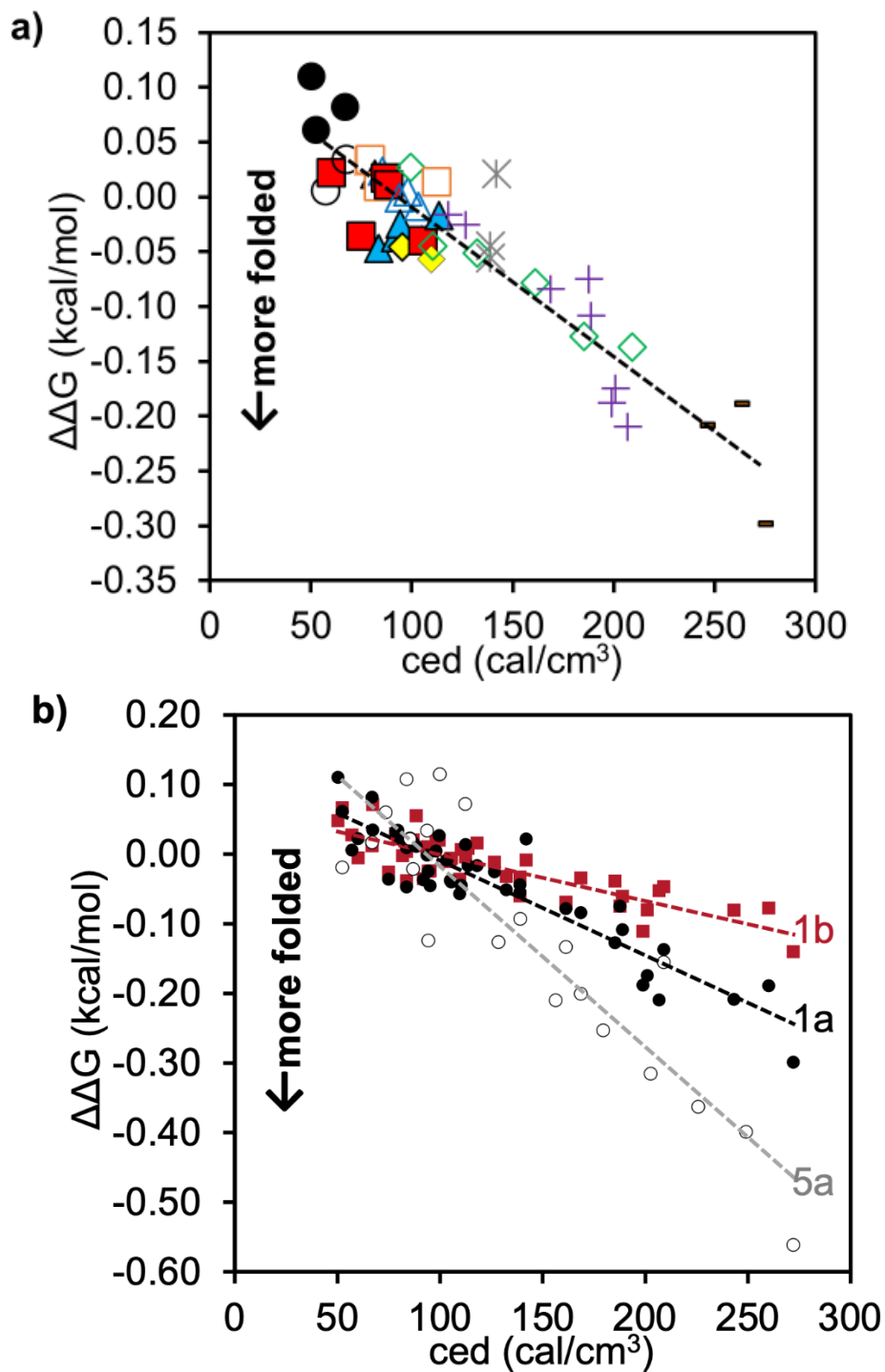


Figure 2.6 a) The $\Delta\Delta G$ versus solvent ced correlation plot for **1a** with the different solvent types highlighted based on their functional groups: alkanes (black solid circles), amines (black empty circle), ethers (red solid square), aromatics (orange empty square), carboxylic acids (yellow solid squares), alcohols (green hollow diamonds) ketones, aldehydes, and carboxylic esters (light blue solid triangles), alkyl halides (dark blue hollow triangles), DMSO and mixtures with DMSO (purple +), mixtures with water (brown -), and other

groups (gray *). b) The $\Delta\Delta G$ versus solvent *ced* correlation plots for balances **1a**, **1b**, and **5a**.

The solvophobic effects of interest can be isolated using the slope of the $\Delta\Delta G$ versus *ced* trendlines ($\text{slope}_{\Delta\Delta G/\text{ced}}$), as the solvophobic effects will vary with the solvent environment. The slope removed other terms which are not solvent dependent. For example, the positive values of $\Delta\Delta G$ in low *ced* alkane solvents were attributed to conformational entropy and dispersion contributions. Ideally, the solvophobic interaction should be zero when the solvent *ced* is zero. However, the y-intercepts for the trendlines for **1a**, **1b**, and **5a** do not go through the origin and are slightly positive (0.13, 0.07, and 0.24 kcal/mol). The entropic penalty from restricting the alkyl chain conformational space favors the *unfolded* conformer. The stabilizing alkyl-alkyl dispersion interactions favor the *folded* conformer. Thus, these components mostly cancel leaving only a small positive contribution to $\Delta\Delta G$.

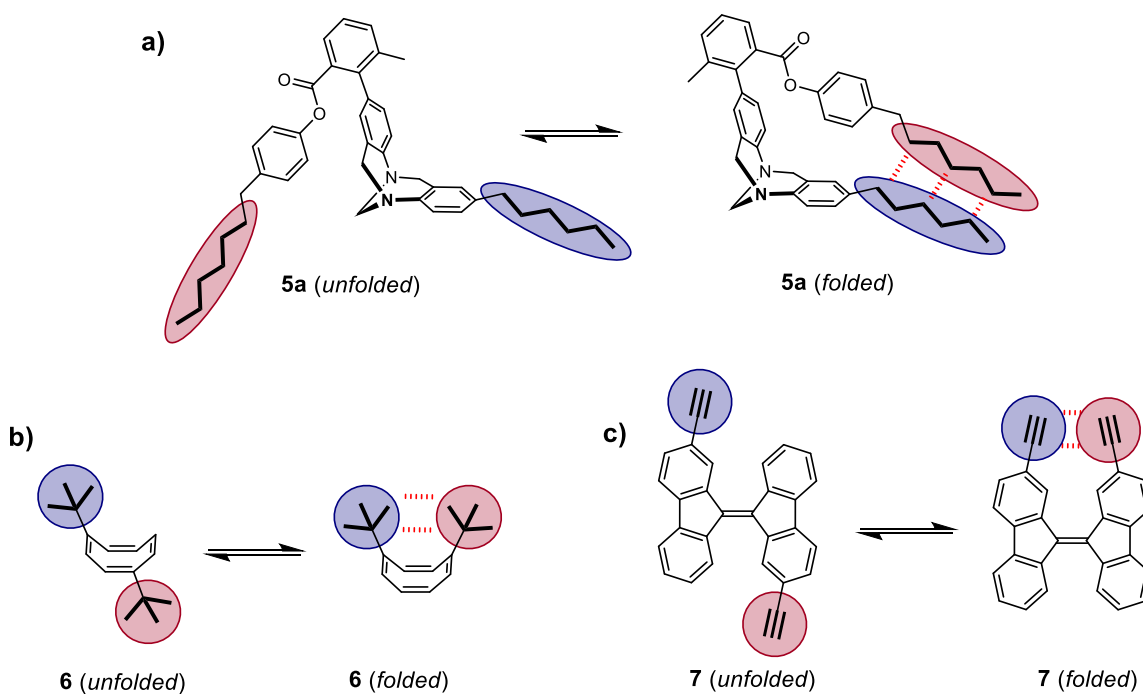


Figure 2.7 Molecular balances designed to measure the organic solvophobic effects from a) Cockroft (a)¹⁸ and Schreiner (b and c)^{21,36} that were compared with balances **1**.

To test the accuracy of the solvophobic measurements, the $\text{slope}_{\Delta\Delta G/ced}$ values were compared with the changes in solvent accessible surface areas (ΔSASA) upon folding of our balances **1a-c** and Cockroft's balance **5**. The solvophobic effect is expected to show a strong correlation with ΔSASA . The ΔSASA were defined as the difference in SASA for the *folded* and *unfolded* structures. The SASA for the *folded* conformers were calculated in Spartan18 using the geometry of the crystal structures of **1a** and **1b**.³⁷ A crystal structure was not available for **1c**. Therefore, the *folded* **1c** structure was generated from the similar crystal structure of **1b** by truncating the terminal four carbons of the alkyl thioether. The *unfolded* structures were generated by rotating the $\text{C}_{\text{phenyl}}\text{-N}_{\text{imide}}$ bond of the *folded* structures 180° . The ΔSASA for **1a-c** (42, 26, and 13 \AA^2) followed the expected trends, decreasing with the length of the alkyl thioethers. The ΔSASA for Cockroft's balances **5a** and **5b** (59 and 12 \AA^2) were also calculated, using the crystal structure of *folded* **5a** (for details see Section 2.6.8). To compare the SASA values across the two balance platforms, the SASA values were normalized ($\Delta\Delta\text{SASA}$) using the control balances **1c** and **5b**. For example, the $\Delta\Delta\text{SASA}$ for **1a** was 29 \AA^2 , which is the difference between the ΔSASA of **1a** and **1c** ($42 - 13 \text{ \AA}^2$). The $\Delta\Delta\text{SASA}$ for **5a** was 35 \AA^2 , which is the difference between the ΔSASA of **5a** and **5b** ($59 - 14 \text{ \AA}^2$). The $\Delta\Delta\text{SASA}$ values for balances **1a** and **1b** were lower than the values for **5a**, even though they had longer or similar length alkyl groups than **5a**. The differences were attributed to the better geometric overlap of the alkyl groups in **5a** in comparison to balances **1** and to the alkyl groups forming weak solvophobic interactions in the *unfolded* conformers of **1**.

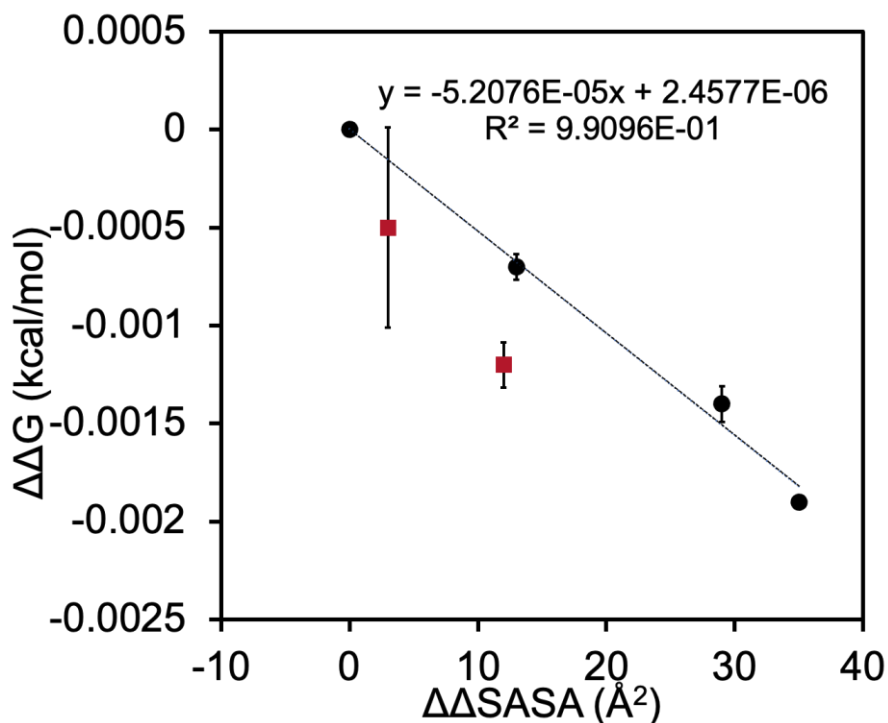


Figure 2.8 The correlation plot of $\text{slope}_{\Delta\Delta G/\text{ced}}$ versus $\Delta\Delta\text{SASA}$ for balances **1a**, **1b**, **1c**, and **5a** (black circles). Data points for balances **6** and **7** (red squares) were plotted for comparison but use unnormalized surface area values (ΔSASA).

Comparison of the solvophobic effects per unit area provided confirmation of the consistency in the solvophobic analysis across the different sized alkyl groups and across the two balance systems. The analysis also included a data point for the control balances **1c** and **5b** at the origin. The $\text{slope}_{\Delta\Delta G/\text{ced}}$ values were strongly correlated with $\Delta\Delta\text{SASA}$ (**Figure 2.8**, $R^2 = 0.98$), as expected for a measurement of the solvophobic effect. Furthermore, the slope of **Figure 2.8** provides the dependence of the solvophobic effect with respect to the *ced* of the solvent and the change in solvent accessible surface area of the interaction. Therefore, this slope ($-0.0526 \text{ cm}^3 \text{ \AA}^{-2} \text{ kcal mol}^{-1}$) was used to generate a model of the solvophobic effect (**Equation 2.1**), which can predict the solvophobic interaction energy for two alkyl surfaces in a specific organic solvent.

The accuracy of **Equation 2.1** was tested by comparison with previous measures of the solvophobic effect. First, the solvophobic interaction energies calculated using equation 1 were compared with the experimental values from Schreiner's balances **6** and **7** (**Figure 2.7b and c**). These balances also contain non-polar alkynyl and *t*-butyl groups, their folding ratios were measured over a range of organic solvents, and they have crystal structures of the *folded* conformers allowing comparison with solvophobic analyses of balances **1** and **5**. One difference was the absence of control balances for **6** and **7**, which was why these balances were not included in the above analysis. Thus, some of the framework biases could not be removed, and only the ΔG and $\Delta SASA$ values for **6** and **7** could be calculated and compared with the $\Delta\Delta G$ and $\Delta\Delta SASA$ for **1** and **5**. Despite the lack of control structures, the solvophobic effects per unit area for **6** and **7** (**Figure 2.8**, red squares) were close to those predicted by **Equation 2.1** as represented by the trendline for balances **1** and **5**. While there are only two data points for Schreiner's balances, it was also reassuring that their slope is similar to the trendline for the balances with controls.

The second test of **Equation 2.1** was to compare the predicted solvophobic effect per unit area for water with the previously measured values for the hydrophobic effect.^{26,40} Using the *ced* value for water (550 cal/cm³), the predicted hydrophobic effect for water from **Equation 2.1** was 0.029 kcal/mol Å⁻². This value fell in the middle of the experimentally measured range of hydrophobic effect values for non-polar alkyl surfaces (0.020 to 0.033 kcal mol⁻¹ Å⁻²).^{37,38}

Next, the organic solvophobic effect was explored using **Equation 2.1**. A contour plot was generated (**Figure 2.9**) by calculating the solvophobic interaction energies (kcal/mol) for $\Delta SASA$ values (0 to 100 Å²) across a range of solvent *ced* values (0 to 600

cal/cm³). The solvophobic energies increase linearly with respect to solvent *ced* and Δ SASA. To enhance the utility of the contour plot, the Δ SASA axis was calibrated to the corresponding values for modeled alkane dimers with optimal surface area contact (density functional theory, B3LYP, 6-311+G*). Most experimental systems will have less than optimal surface contact. Therefore, the Δ SASA will be lower for similar length alkane surfaces as was observed for balance **1**.

The contour plot analysis confirmed that organic solvophobic effects are very weak (< 1.0 kcal/mol). The largest solvophobic effect was 2.5 kcal/mol for the decane-decane dimer (Δ SASA = 86 Å²). But this was in water which has a *ced* of 550 cal/cm³. Most organic solvents had significantly lower *ced* values. The highest value for a pure organic solvent used in this study was methanol with a *ced* of 209 cal cm⁻³. Therefore, in methanol, the solvophobic effect for the decane-decane dimer was 0.94 kcal/mol, which was only 38% of the solvophobic effect in water. In common non-protic organic solvents like benzene, THF, or chloroform, the solvophobic effect for the decane dimer was even smaller (~0.4 kcal/mol), which is around 20% of the hydrophobic effect. For smaller alkane surfaces, the organic solvophobic effect is much lower than 1.0 kcal/mol. For example, the solvophobic effect for the methane dimer is 0.54 kcal/mol in water, 0.2 kcal/mol in methanol, and only 0.1 kcal/mol in benzene, THF, and chloroform.

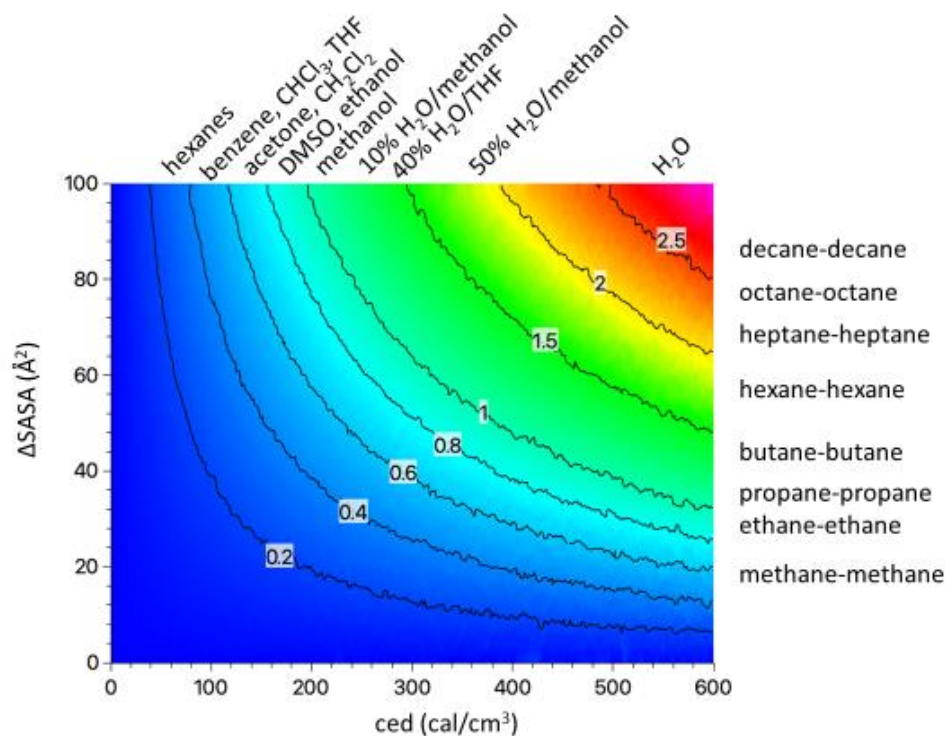


Figure 2.9. A contour plot of the solvophobic interaction energies in kcal/mol calculated for the differences in surface area on the formation of complexes of non-polar surfaces in solvent systems with *ced* values from 0 to 600 cal/cm³.

This analysis also provides strategies for enhancing the solvophobic effect. Even small percentages of water can greatly increase the solvophobic effects in miscible organic solvents such as THF, alcohols, DMSO, or DMF due to the very high *ced* value for water. The alcohol solvents have the highest solvophobic effects among the organic solvents as they have the highest *ced* values. Interestingly, not all the protic solvents had high *ced* values and solvophobic effects. For example, diethyl amine and acetic acid had lower *ced* values (67.2 and 109.5 cal/cm³) than t-butanol and pyridine. Among the non-protic organic solvents, DMSO, acetonitrile, and DMF had the highest solvophobic effects and *ced* values, but these were only 25% to 30% the solvophobic effect in water.

2.5 Conclusions

In conclusion, we designed a molecular torsional balance to quantitatively measure the organic solvophobic effects and to develop an empirical predictive model for the organic solvophobic effect. The modularity of balances **1** and the ability to measure the folding ratios by ^{19}F NMR enabled measurement of the solvophobic effect in 46 different organic solvent systems and also with different length alkyl surfaces. To isolate the solvophobic effects from the dispersion and conformational entropy terms of the folding energies, a control balance was essential to remove solvent interactions with the framework and linkers. The ability to measure the weak organic solvophobic effects was established by the linear relationship of the folding equilibrium energies with the solvent *ced* and with the normalized change in solvent accessible surface area. The combination of these relationships enabled the development of a simple predictive model. Furthermore, this relationship was extrapolated as to predict the association energies in a series of simple dimers across a spectrum of solvent *ced* as demonstration of its practical use. This study has yielded important information on how particular solvents and mixtures affect hydrocarbon dimerization in solution.

2.6 Experimental Section

2.6.1 General Experimental Information

NMR spectra were recorded on Bruker 300 MHz, 400 MHz, and 500 MHz spectrometers. Chemical shifts are reported in ppm (δ) referenced to NMR solvent peaks. All spectra given for characterization purposes were taken at room temperature. All chemicals were purchased from commercial suppliers and used as received unless

otherwise specified. Flash chromatography was carried out using silica gel from Fisher Scientific (230x400 Mesh). HRMS were measured using a magnetic sector spectrometer (VG 70S) using EI sources.

2.6.2 Synthetic Procedures



Figure 2.10. Synthesis of nitrobenzene **2**.

1-Decanol (5.65 g, 35.7 mmol) was added to a solution of DMF (10 mL) and potassium hydroxide (1.35 g, 24.0 mmol). A solution of 1,4-difluoro-2-nitrobenzene (1.87 g, 11.7 mmol) in *N,N*-dimethylformamide (3 mL) was added dropwise to the mixture. The reaction vessel was flushed with nitrogen and sealed. The reaction was then stirred at 23°C for 8 h. The solvent was removed by washing the reaction in water and ethyl acetate three times in a separatory funnel, followed by the organic phase being dried with magnesium sulfate. The solvent was removed under reduced pressure. The product was then purified using a silica column using a solvent mixture of 10:1 hexanes to ethyl acetate. The final product was an oily yellow substance (2.31 g, 66.2% yield). ¹H NMR (400 MHz, CDCl₃) δ = 7.57 (*dd* J = 3.15, J = 7.83 1H) 7.26 (*ddd* J = 3.15, J = 7.34, J = 9.27 1H) 7.05 (*dd* J = 4.31, J = 9.27, 1H) 1.84 (*m* 6.52, 7.29, 2H) 1.29 (*m* 14H) 0.89 (*t* 6.42, 3H). ¹³C NMR (100 MHz, CDCl₃) δ = 155.1 (*d* J = 243.3 Hz), 149.1 (*d* J = 2.6 Hz), 139.5 (*d* J = 8.6 Hz) 120.9 (*d* J = 23.0 Hz), 115.8 (*d* J = 7.7 Hz), 112.7 (*d* J = 27.4 Hz), 70.4, ,

29.5, 29.5, 29.3, 29.2, 29.0, 25.8, 22.7, 14.1. ^{19}F NMR (376 MHz, CDCl_3) $\delta = -121.4$.

HRMS (EI) $(\text{C}_{16}\text{H}_{24}\text{FNO}_3)^+ \text{M}^+$ calculated 297.1740; observed 297.1746.

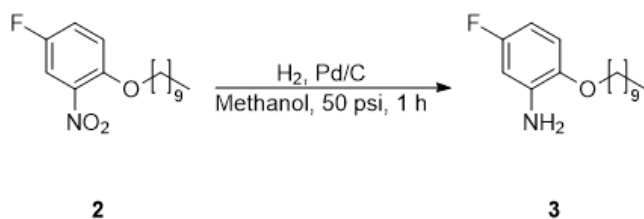


Figure 2.11 Synthesis of aniline **3**.

Nitrobenzene **2** (0.68 g, 2.27 mmol) was dissolved in 7 mL of methanol and palladium on carbon catalyst (0.07 g, 0.68 mmol) was added to the solution. The solution was reacted with hydrogen gas (50 psi) for 1 h in a Parr shaker, after which the palladium on carbon catalyst was removed by filtering through celite, and the methanol was removed under reduced pressure. The product required no further purification. The product (0.41 g, 66.7 % yield) was isolated as a brown oil. ^1H NMR (400 MHz, CDCl_3) $\delta = 6.66$ (*dd* $J = 4.94$, $J = 8.76$ 1 H) 6.45 (*dd* $J = 2.98$, $J = 9.78$, 1 H) 6.37 (*ddd* $J = 3.03$, $J = 8.57$, $J = 8.57$ 1 H) 3.94 (*t* 6.27 2 H) 1.79 (*m* 2 H) 1.26 (*m* 14 H) 0.88 (*t* 5.78, 6.95, 3 H). ^{13}C NMR (100 MHz, CDCl_3) $\delta = 158.6$ ($dJ = 236.5$ Hz), 142.9 ($dJ = 2.2$ Hz), 137.3 ($dJ = 10.9$ Hz), 111.9 ($dJ = 9.9$ Hz), 103.5 ($dJ = 22.9$ Hz), 102.2 ($dJ = 26.6$ Hz), 69.1, 31.9, 29.5, 29.5, 29.3, 29.2, 29.0, 25.8, 22.7, 14.1. ^{19}F NMR (376 MHz, CDCl_3) $\delta = -123.0$. HRMS (EI) $(\text{C}_{16}\text{H}_{26}\text{FNO})^+ \text{M}^+$ calculated for 267.1998; observed 267.1995.

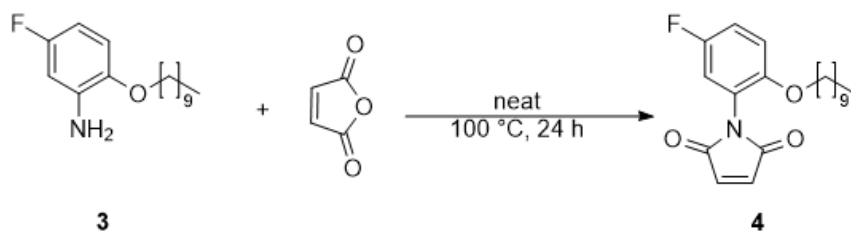


Figure 2.12 Synthesis of maleimide **4**.

Aniline **3** (0.84 g, 3.14 mmol) was added to maleic anhydride (3.00 g, 30.7 mmol) without solvent in a sealed, 2 mL dram vial. The mixture was heated to 100 °C for 24 h. The product was purified in a silica column using 9:1 hexanes to ethyl acetate mixture. Product was a yellow oily substance (1.65 g, 46.8% yield). ¹H NMR (400 MHz, CDCl₃) δ = 7.06 (*ddd*, J = 3.09, J = 7.95, J = 9.08, 1 H) 6.95 (*dd*, J = 3.01, J = 8.22, 1 H) 6.92 (*dd*, J = 4.82, J = 9.27, 1 H) 6.85 (*s* 2 H) 3.91 (*t*, 6.48 2 H) 1.65 (*m*, 6.83 2 H) 1.18 (*m*, 14 H) 0.88 (*t*, 6.50 3 H). ¹³C NMR (100 MHz, CDCl₃) δ = 169.3, 156.1 ($d J$ = 241.1 Hz), 151.3 ($d J$ = 2.8 Hz), 134.5, 120.4 ($d J$ = 10.3 Hz), 117.3 ($d J$ = 24.6 Hz), 116.8 ($d J$ = 22.4 Hz), 113.5 ($d J$ = 8.65 Hz), 68.19, 31.92, 29.56, 29.54, 29.34, 29.26, 29.03, 25.80, 22.71, 14.15. ¹⁹F NMR (376 MHz, CDCl₃) δ = -122.6. HRMS (EI) (C₂₀H₂₆FNO₃)⁺ M⁺ calculated for 347.1905; observed 347.1897.

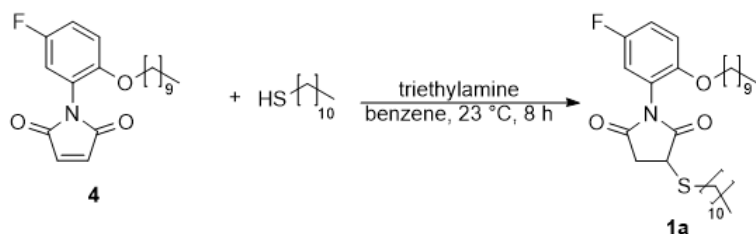


Figure 2.13 Synthesis for balance **1a**.

Maleimide **4** (0.09 g, 0.27 mmol) was dissolved in benzene (3 mL) and triethylamine (0.06 g, 0.55 mmol) and 1-undecanethiol (0.15 g, 0.81 mmol) were directly added. The mixture was stirred for 8 h at 23 °C. Solvent was removed via rotary evaporation and crude product was purified in a silica column (ethyl acetate/hexanes = 1:9, v/v). Product (0.06 g, 47% yield) was a white crystalline powder. ¹H NMR (400 MHz, CDCl₃) δ = 7.12-7.06 (*m*, 1 H major and minor) 6.96-6.87 (*m*, 2 H major and minor) 3.92 (*t*, J = 6.66 Hz, 2 H major and minor) 3.88 (*dd*, J = 3.10, J = 9.10 Hz, 1 H major) 3.87 (*dd*,

$J = 3.10, J = 9.10$ Hz, 1 H minor) 3.32 (*dd*, $J = 9.10, J = 18.7$ Hz, 1 H major) 3.27 (*dd*, $J = 9.10, J = 18.7$ Hz 1 H minor) 2.98-2.89 (*m*, 1 H major and minor) 2.78-2.68 (*m*, 1 H major and minor) 2.65 (*dd*, $J = 3.65, 18.7$ Hz, 1 H major) 2.60 (*dd*, $J = 3.63, 18.7$ Hz, 1 H minor) 1.75-1.59 (*m*, 4 H major and minor) 1.44-1.34 (*m*, 4 H major and minor) 1.34-1.20 (*m*, 26 H major and minor) 0.87 (*m*, 6 H major and minor). ^{13}C NMR (100 MHz, CDCl_3) $\delta = 175.1$ (minor), 174.9 (major), 173.4 (major), 173.2 (minor), 156.2 ($d J = 240.7$ Hz minor), 156.1 ($d J = 240.7$ Hz major), 150.8 ($d J = 2.6$ Hz minor), 150.6 ($d J = 2.6$ Hz major), 121.1 ($d J = 10.0$ Hz minor), 120.9 ($d J = 10.0$ Hz major), 117.1 ($d J = 22.5$ Hz minor), 117.0 ($d J = 22.5$ Hz major), 116.3 ($d J = 25.0$ Hz), 113.7 ($d J = 8.4$ Hz minor), 113.6 ($d J = 8.4$ Hz major), 69.3 (major), 69.1 (minor), 39.5 (major), 39.4 (minor), 36.4 (major), 36.4 (minor), 31.9, 31.6, 29.6, 29.5, 29.5, 29.5, 29.4, 29.4, 29.3, 29.3, 29.2, 29.2, 29.1, 29.0, 29.0, 28.9, 25.8, 25.8, 25.9, 25.7, 22.6, 14.1. ^{19}F NMR (376 MHz, CDCl_3) $\delta = -122.3$ (*s*, 1 F minor) -122.5 (*s*, 1 F major). HRMS (EI) $(\text{C}_{31}\text{H}_{50}\text{FNO}_3\text{S})^+ \text{M}^+$ calculated for 535.3492; observed 535.3495.

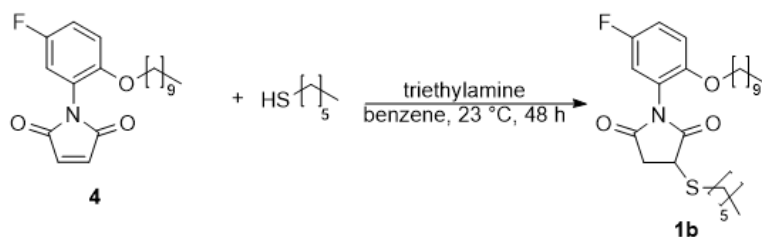


Figure 2.14 Synthesis for balance **1b**.

Maleimide **4** (0.04 g, 0.11 mmol) was dissolved in benzene (3 mL) and triethylamine (0.05 g, 0.51 mmol) and 1-hexanethiol (0.04 g, 0.35 mmol) were directly added. The mixture was stirred for 48 h at 23°C . Solvent was removed under reduced pressure and crude product was purified in a silica column (ethyl acetate/hexanes = 1:8,

v/v). Product (0.04 g, 90% yield) was a yellow oil. ^1H NMR (300 MHz, CDCl_3), δ = 7.13-7.04 (*m*, 1 H major and minor) 6.96-6.86 (*m*, 2 H major and minor) 4.00-3.83 (*m*, 3 H major and minor) 3.31 (*dd*, J = 9.3, 18.8 Hz. 1 H major) 3.28 (*dd*, J = 9.3, 18.8 Hz. 1 H minor) 3.00-2.87 (*m*, 1 H major and minor) 2.86-2.62 (*m*, 1 H major and minor) 1.77-1.60 (*m*, 4 H major and minor), 1.46-1.37 (*m*, 2 H major and minor) 1.36-1.20 (*m*, 18 H major and minor) 0.93-0.83 (*m*, 6 H major and minor). ^{13}C NMR (100 MHz, CDCl_3) δ = 175.1 (minor), 174.9 (major), 173.5 (major), 173.2 (minor), 156.2 ($d J$ = 239.9 Hz major), 156.1 ($d J$ = 239.9 Hz minor), 150.8 ($d J$ = 13.2 Hz major), 150.7 ($d J$ = 13.2 Hz minor), 121.1 ($d J$ = 9.8 Hz minor), 120.9 ($d J$ = 9.8 Hz major), 117.1 ($d J$ = 21.9 Hz minor), 117.0 ($d J$ = 21.9 Hz minor), 116.4 ($d J$ = 25.1 Hz), 113.7 ($d J$ = 8.0 Hz minor), 113.6 ($d J$ = 8.0 Hz major), 69.3 (major), 69.2 (minor), 39.5 (major), 39.4 (minor), 36.5 (major), 36.4 (minor), 31.9, 31.6, 31.4, 31.3, 29.7, 29.6, 29.5, 29.4, 29.3, 29.3, 29.3, 29.2, 29.0, 29.0, 28.9, 28.5 (major), 28.5 (minor), 22.7 (major), 22.5 (minor), 14.1 (major), 14.0 (minor). ^{19}F NMR (376 MHz, CDCl_3) δ = -122.3 (minor) -122.5 (major). HRMS (EI) $(\text{C}_{26}\text{H}_{40}\text{FNO}_3\text{S})^+ \text{M}^+$ calculated for 465.2719; observed 465.2713.

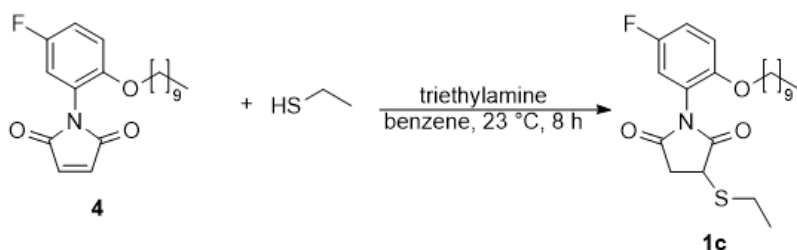


Figure 2.15. Synthesis for balance **1c**.

Maleimide **4** (0.13 g, 0.27 mmol) was dissolved in benzene (10 mL). Triethylamine (0.11 g, 0.55 mmol) and 1-undecanethiol (0.08 g, 0.81 mmol) were directly added. The mixture was stirred for 8 h at 23 °C. Solvent was removed under reduced

pressure and crude product was purified in a silica column (ethyl acetate/hexanes = 1:9, v/v). Product (0.12 g, 76% yield) was a white crystalline powder. ^1H NMR (500 MHz, CDCl_3) δ = 7.12-7.06 (*m*, 1 H major and minor) 6.95-6.88 (*m*, 2 H major and minor) 3.97-3.87 (*m*, 3 H major and minor) 3.31 (*dd*, J = 9.3, 18.7 Hz. 1 H major) 3.30 (*dd*, J = 9.3, 18.7 Hz. 1 H minor) 3.02-2.76 (*m*, 2H major and minor) 2.70 (*dd*, 3.8, 18.7 Hz. major and minor) 1.76-1.64 (*m*, 1 H major and minor) 1.34 (*q*, 7.4 Hz 2 H) 1.30-1.24 (*m*, 14 H) 0.88 (*t*, 6.8 Hz 3H). ^{13}C NMR (100 MHz, CDCl_3) δ = 175.0 (minor), 174.8 (major), 173.4 (major), 173.1 (minor), 156.1 (dJ = 240.7 Hz minor), 156.0 (dJ = 240.7 Hz major), 150.8 (dJ = 2.7 Hz major), 150.6 (dJ = 2.7 Hz minor), 121.1 (dJ = 10.1 Hz minor), 120.9 (dJ = 10.1 Hz major), 117.0 (dJ = 22.4 Hz minor), 116.9 (dJ = 22.4 Hz major), 116.3 (dJ = 24.9 Hz major), 116.3 (dJ = 24.9 Hz minor), 113.7 (dJ = 8.6 Hz minor), 113.6 (dJ = 8.6 Hz major), 69.2 (major), 69.1 (minor), 39.3 (major), 39.1 (minor), 36.4 (major), 36.3 (minor), 31.8, 29.5, 29.5, 29.5, 29.3, 29.2, 29.2, 29.1, 29.0, 25.9, 25.8, 25.8, 25.5, 22.6, 14.1, 14.0, 13.9. ^{19}F NMR (376 MHz, CDCl_3) δ = -122.3 (minor), -122.5 (major). HRMS (EI) ($\text{C}_{22}\text{H}_{32}\text{FNO}_3\text{S}$) $^+$ M^+ calculated for 409.2091; observed 409.2087.

2.6.3 Crystallographic Data

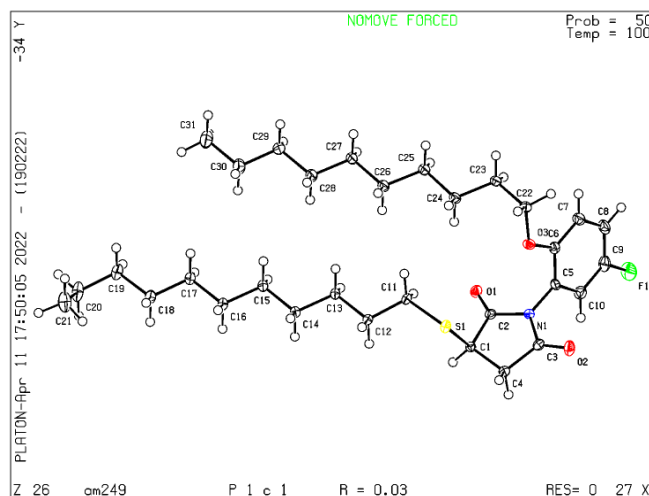


Figure 2.16. X-ray structure of compound **1a**. Compound **1a** was crystallized in methanol for 2 days in 2 mL dram.

Table 2.2 General information about calculated crystal structure for compound **1a**. These data can be obtained free of charge from The Cambridge Crystallographic Data Centre via www.ccdc.cam.ac.uk/data_request/cif.

Empirical Formula	C ₃₁ H ₅₀ NO ₃ FS
Formula weight	535.78
Temperature/K	100(2)
Crystal system	Monoclinic
Space group	Pc
a/Å	18.2753(11)
b/Å	8.9802(6)
c/Å	9.2403(6)
α/°	90
β/°	102.256(3)
γ/°	90
Volume/Å ³	1481.92(17)
Z	2
ρ _{calc} /cm ³	1.201
μ/mm ⁻¹	0.147
F(000)	584.0
Crystal size/mm ³	0.46 × 0.14 × 0.02
Radiation	MoKα (λ = 0.71073)

2 θ range for data collection/ $^{\circ}$	4.562 to 55.16
Index ranges	$-23 \leq h \leq 23$, $-11 \leq k \leq 11$, $-11 \leq l \leq 11$
Reflections collected	20708
Independent reflections	6681 [$R_{\text{int}} = 0.0353$, $R_{\text{sigma}} = 0.0379$]
Data/restraints/parameters	6681/2/337
Goodness-of-fit on F^2	1.066
Final R indexes [$I \geq 2\sigma(I)$]	$R_1 = 0.0330$, $wR_2 = 0.0744$
Final R indexes [all data]	$R_1 = 0.0398$, $wR_2 = 0.0786$
Largest diff. peak/hole / $e \text{ \AA}^{-3}$	0.23/-0.22
Flack parameter	0.02(3)

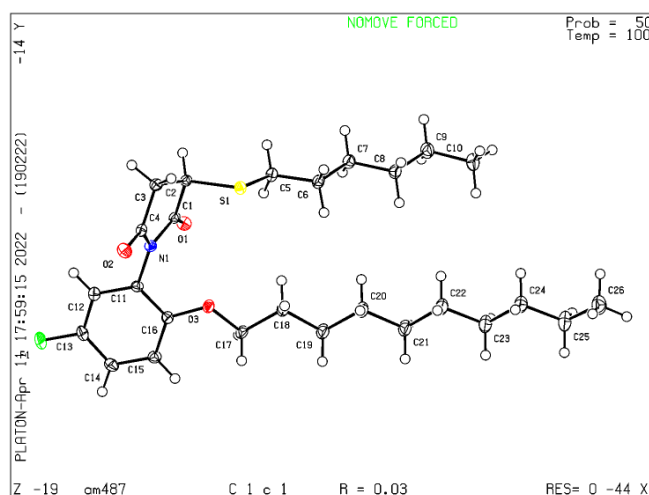


Figure 2.17. X-ray structure of compound **1b**. Compound **1b** was crystallized in n-hexanes for 5 days in 2 mL dram.

Table 2.3 General information about calculated crystal structure for compound **1b**. These data can be obtained free of charge from The Cambridge Crystallographic Data Centre via www.ccdc.cam.ac.uk/data_request/cif.

Empirical Formula	$C_{26}H_{40}NO_3FS$
Formula weight	465.65
Temperature/K	100(2)
Crystal system	Monoclinic
Space group	Cc
a/ \AA	33.3694(11)
b/ \AA	8.7595(3)
c/ \AA	8.8487(3)

$\alpha/^\circ$	90
$\beta/^\circ$	97.1080(10)
$\gamma/^\circ$	90
Volume/ \AA^3	2566.59(15)
Z	4
$\rho_{\text{calc}}/\text{g}/\text{cm}^3$	1.205
μ/mm^{-1}	0.160
F(000)	1008.0
Crystal size/ mm^3	$0.3 \times 0.25 \times 0.05$
Radiation	MoK α ($\lambda = 0.71073$)
2 Θ range for data collection/ $^\circ$	4.81 to 61.052
Index ranges	$-47 \leq h \leq 47, -12 \leq k \leq 12, -12 \leq l \leq 12$
Reflections collected	51666
Independent reflections	7813 [$R_{\text{int}} = 0.0323, R_{\text{sigma}} = 0.0228$]
Data/restraints/parameters	7813/2/291
Goodness-of-fit on F^2	1.040
Final R indexes [$I \geq 2\sigma(I)$]	$R_1 = 0.0254, wR_2 = 0.0634$
Final R indexes [all data]	$R_1 = 0.0271, wR_2 = 0.0645$
Largest diff. peak/hole / $e \text{\AA}^{-3}$	0.23/-0.16
Flack parameter	0.017(12)

2.6.4 ^1H , ^{13}C , and ^{19}F NMR Spectra

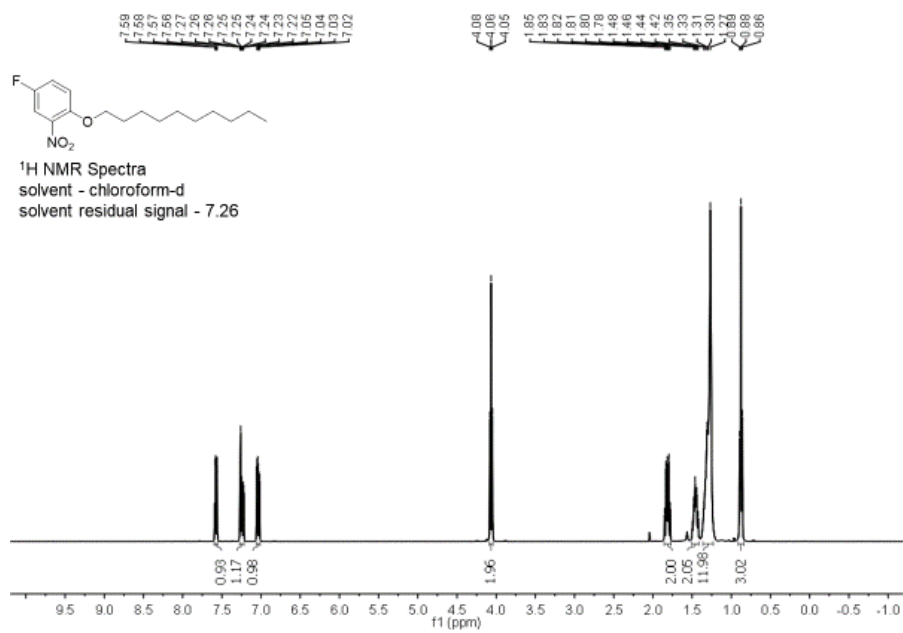


Figure 2.18 ^1H NMR spectrum of nitrobenzene **2** (400 MHz, chloroform-d).

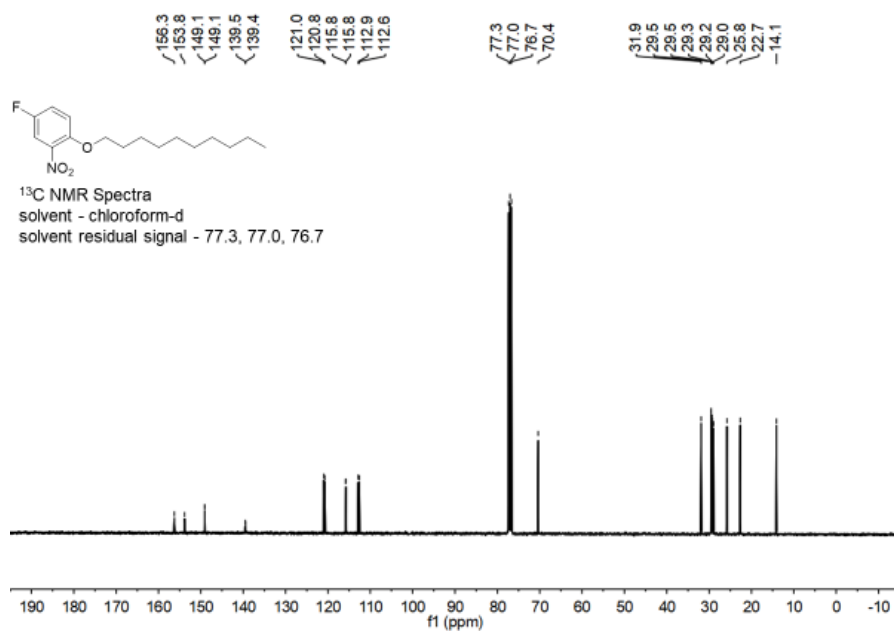


Figure 2.19 ¹³C NMR spectrum of nitrobenzene **2** (100 MHz, chloroform-d).

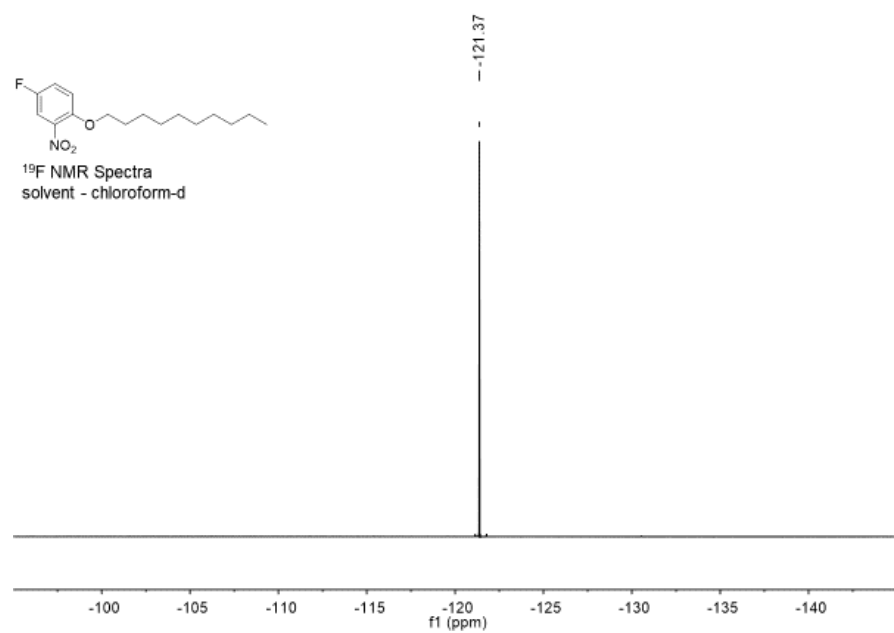


Figure 2.20 ¹⁹F NMR spectrum of nitrobenzene **2** (376 MHz, chloroform-d).

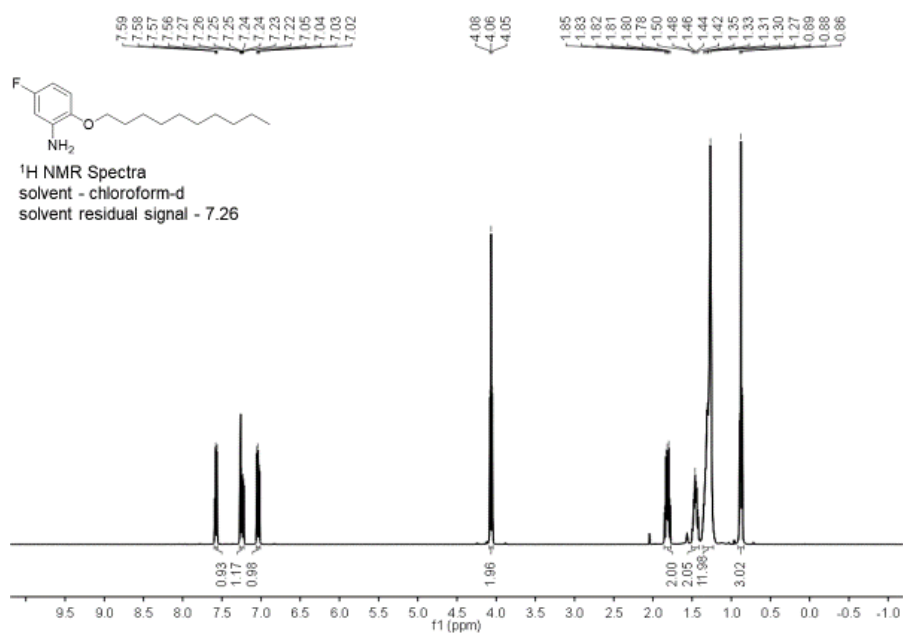


Figure 2.21 ¹H NMR spectrum of aniline **3** (400 MHz, chloroform-d).

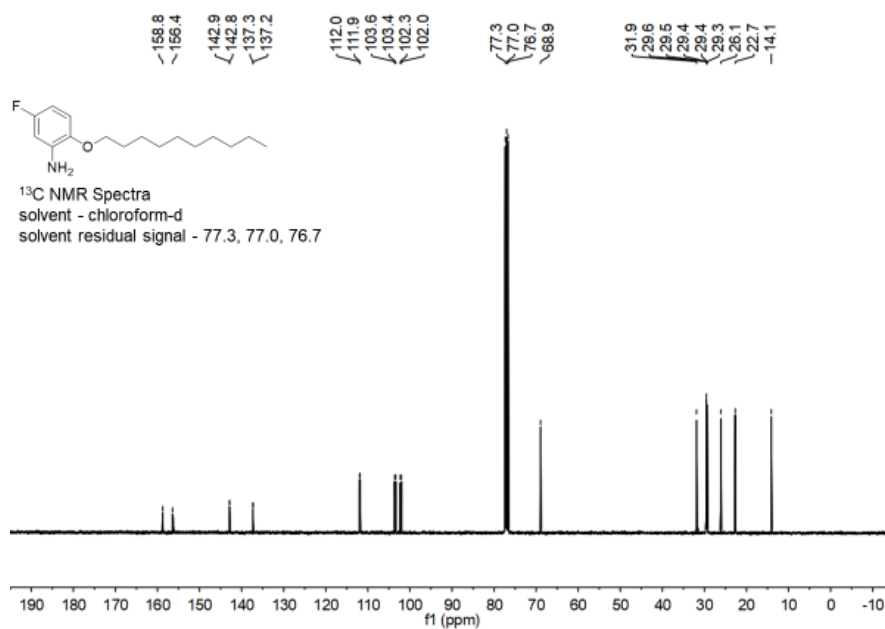


Figure 2.22 ¹³C NMR spectrum of aniline **3** (100 MHz, chloroform-d).

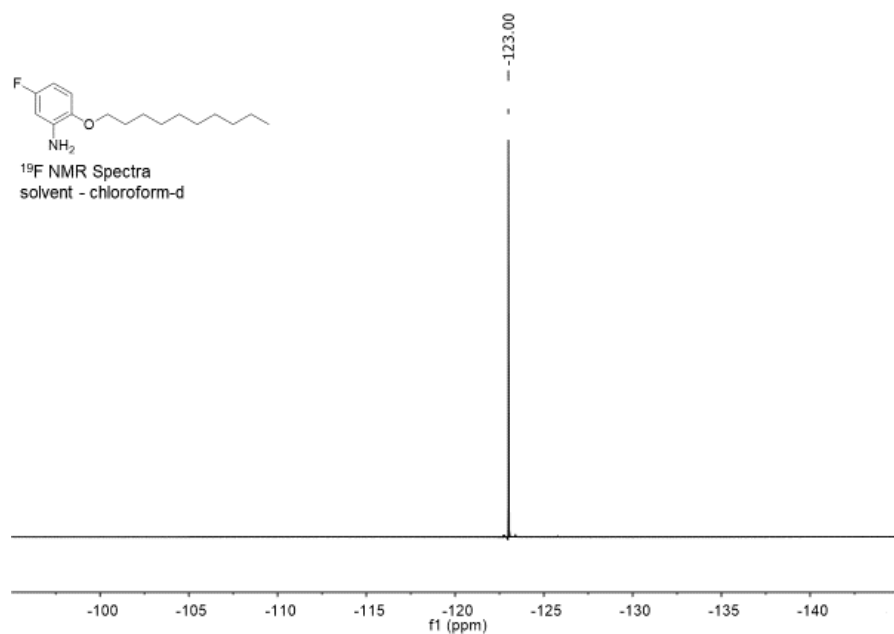


Figure 2.23 ¹⁹F NMR spectrum of aniline **3** (376 MHz, chloroform-d).

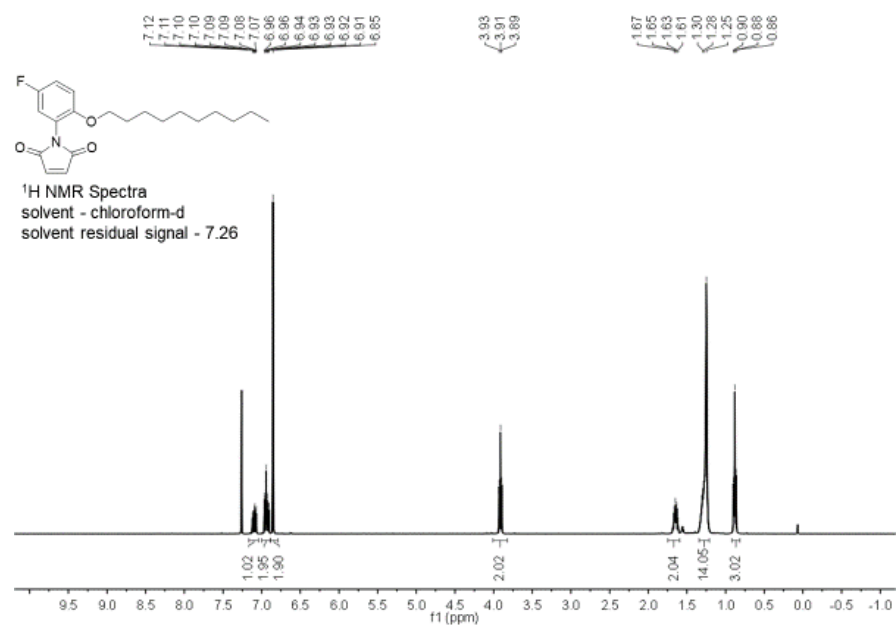


Figure 2.24 ¹H NMR spectrum of maleimide **4** (400 MHz, chloroform-d).

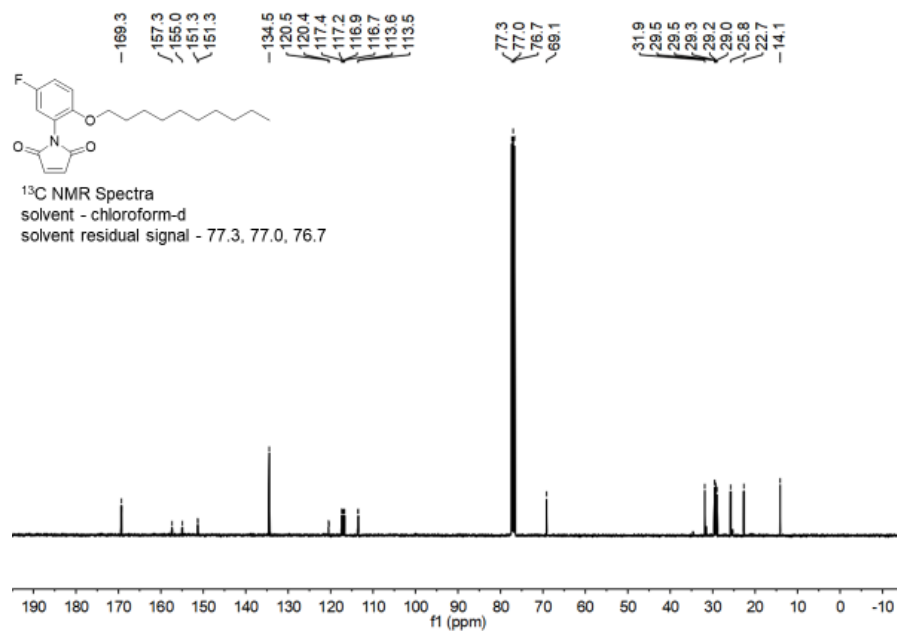


Figure 2.25 ¹³C NMR spectrum of maleimide **4** (100 MHz, chloroform-d).

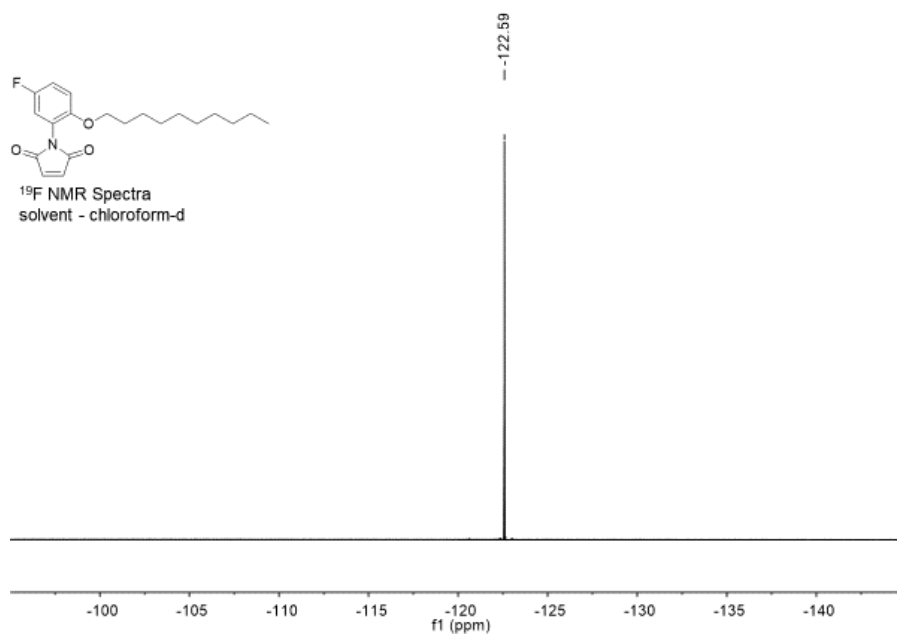


Figure 2.26 ¹⁹F NMR spectrum of maleimide **4** (376 MHz, chloroform-d).

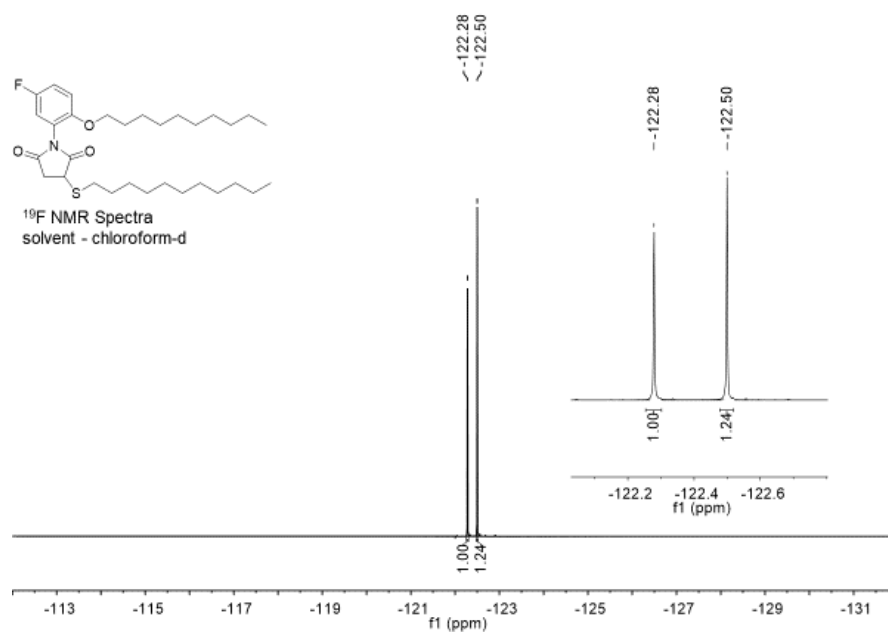


Figure 2.29 ¹⁹F NMR spectrum of balance **1a** (376 MHz, chloroform-d).

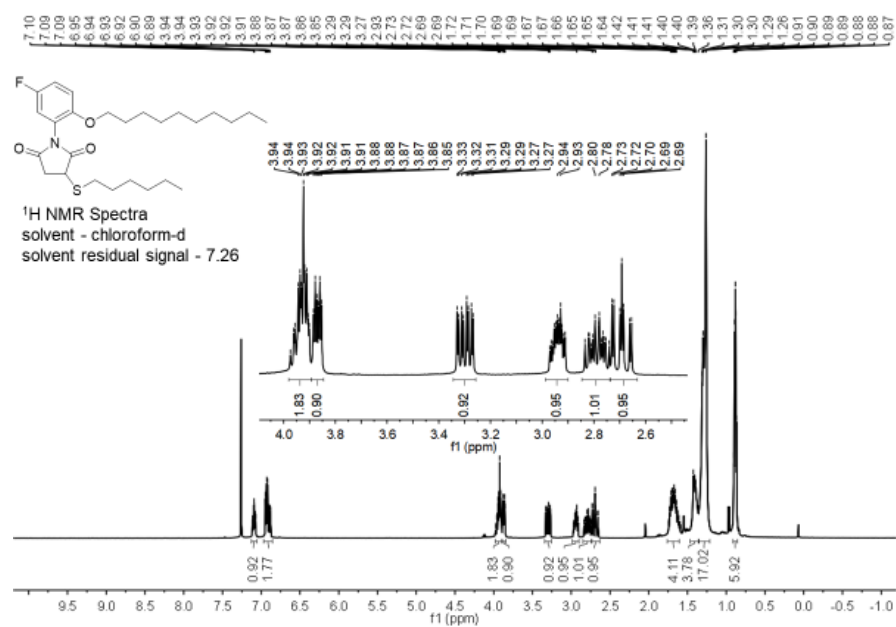


Figure 2.30 ¹H NMR spectrum of balance **1b** (400 MHz, chloroform-d).

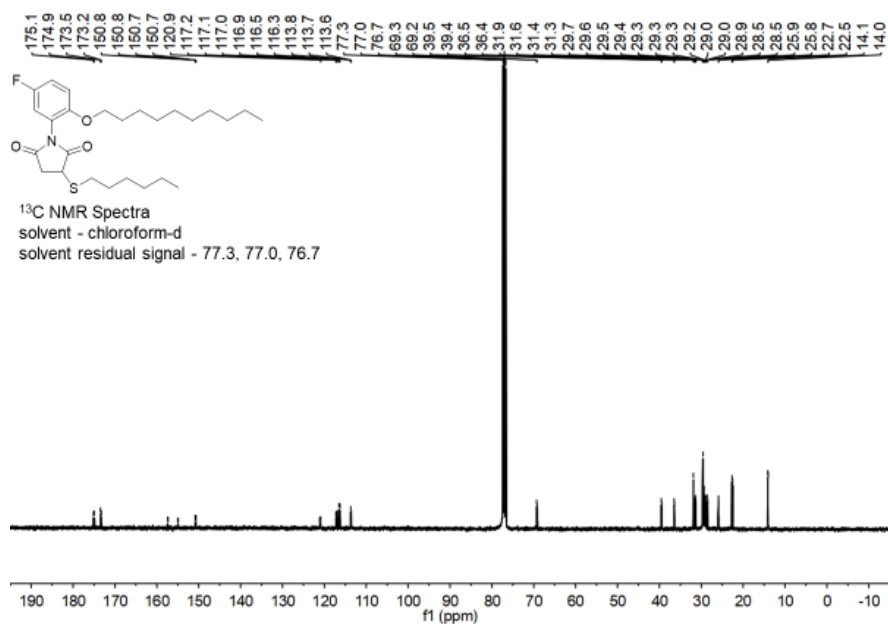


Figure 2.31 ¹³C NMR spectrum of balance **1b** (100 MHz, chloroform-d).

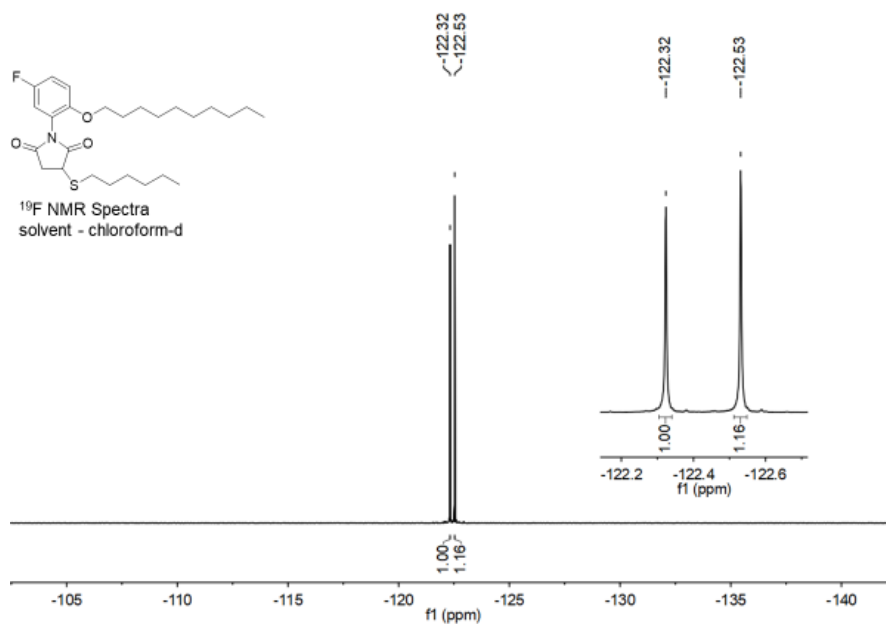


Figure 2.32 ¹⁹F NMR spectrum of balance **1b** (376 MHz, chloroform-d).

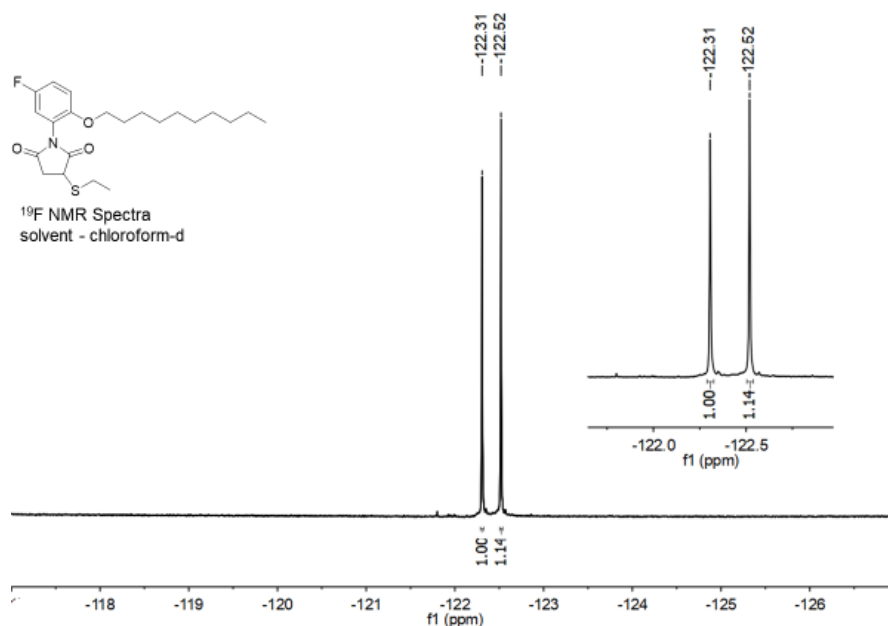


Figure 2.35 ¹⁹F NMR spectrum of balance **1c** (376 MHz, chloroform-d).

2.6.5 Determination of Conformer Identities

The identity of the two signals present in the decoupled ¹⁹F NMR with respect to the two conformations, namely the *folded* and *unfolded*, of the molecular balances was confirmed via several direct and indirect methods. Firstly, it was expected that the presence of the *folded* conformer would increase as solvent *ced* increased due to solvophobicity. The ratio of the downfield to upfield signals of the decoupled ¹⁹F NMR increased with the *ced* of the solvent environments for all balances. This suggests that the downfield signals belonged to the *folded* conformation while the upfield signals belonged to the *unfolded* conformation.

Furthermore, low temperature decoupled ¹⁹F NMR was employed to determine the identity of the signals. According to previous x-ray crystallography experiments, balances **1a** and **1b** are both crystallized in the *folded* conformation. Therefore, we designed an experiment where decoupled ¹⁹F NMR was conducted with crystals of **1a** and **1b** in cold

temperatures in order to slow down the equilibrium exchange between the conformers. This way, the *folded* conformation will have a greater presence than after equilibrium at 23 °C. Chloroform-d in an NMR tube was frozen (-63.5 °C) using a dry ice and acetone mixture. A small sample of the balance crystals was quickly placed into a liquid nitrogen chilled NMR machine set to -50 °C. A decoupled ^{19}F NMR experiment was then immediately conducted. The process was completed for both balance **1a** and **1b**.

In both spectra, the upfield signal to downfield signal significantly increased from their runs at equilibrium and 23 °C. Considering that equilibrium was prevented by the short time and low temperatures, it can be assumed that the dominant signal would belong to the *folded* conformer. Therefore, this experiment demonstrates that the upfield signals in the decoupled ^{19}F NMR belong to the *folded* conformer, while the downfield conformers belong to the *unfolded* conformer in both **1a** and **1b**.

While a crystal structure for **1c** could not be obtained, conformer signals therein were reasonably assumed to be consistent with **1a** and **1b** due to the similar structures and chemical shifts in all three molecules. Furthermore, it can be reasonably assumed that conformer signal identities were consistent throughout all solvent systems due to no significant changes in chemical shifts in any of the solvent mixtures.

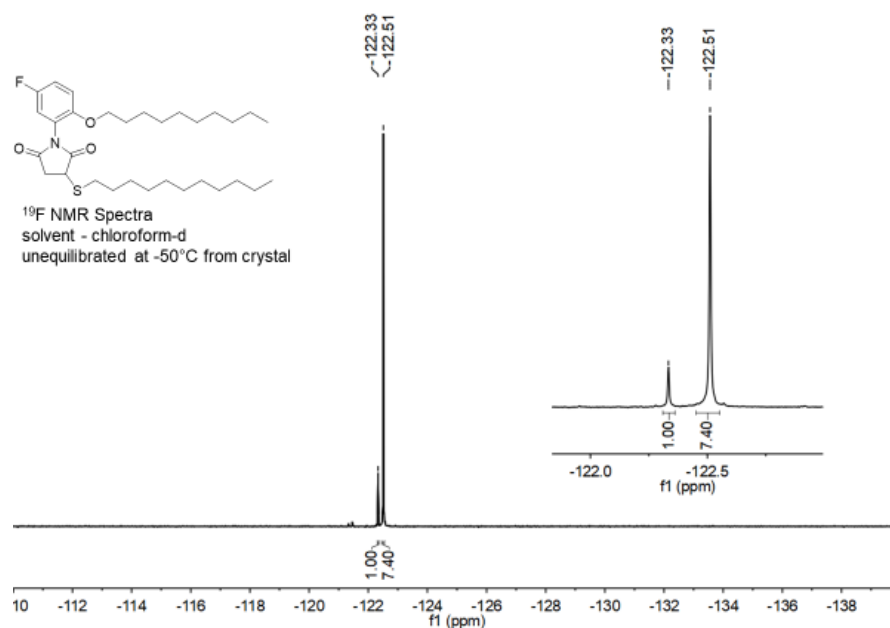


Figure 2.36 Decoupled ¹⁹F NMR spectrum of crystalline compound 1a, taken immediately after sample was introduced to solution at -50 °C.

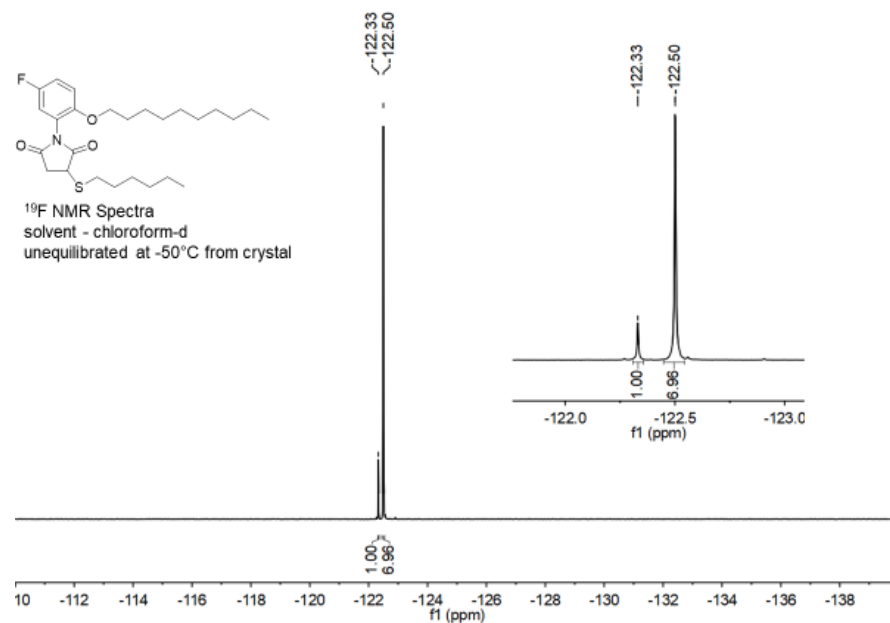


Figure 2.37 Decoupled ¹⁹F NMR spectrum of crystalline compound 1b, taken immediately after sample was introduced to solution at -50 °C.

2.6.6 Error Analysis

The NMR samples for this work were prepared by dissolving ~ 5 mg of purified molecular compound in 0.2 mL to 0.5 mL of solvent, giving an average concentration of 58 to 21 mM (assuming the average molecular weight to be 470 g/mol). NMR signals were measured using the Mestrenova line fitting function to reduce the error in integration. The error of the quantitative NMR analysis is considered to be 1% for concentrations >10 mM.

Therefore, the error for a 1:1 *folded:unfolded* ratio is 1.4% as both conformers have a concentration greater than 10 mM. This error is equal to the square root of the sum of the squares of 1% and 1%, which is only 1.4% (**Equation 2.2**). The minor conformers were at no less than ~ 4.8 mM but no greater than 10 mM. It is safe to estimate the maximum error for integration of the minor conformer is 2.5%, and the maximum error of the major conformer is 1%, based on estimations from Rizzo et al.⁴¹ The total integration error for each measurement was no more than 2.7% (**Equation 2.2**).

$$\text{Equation 2.2 Error}\left(\frac{folded}{unfolded}\right) = \sqrt{(\text{Error}_{folded})^2 + (\text{Error}_{unfolded})^2}$$

The folding energies (ΔG) calculated also have some associated uncertainty. this uncertainty was calculated to be no more than ± 0.016 kcal/mol at 23°C (**Equation 2.3**). Therefore, the uncertainty of the calculated interaction energies ($\Delta\Delta G$) was no more than ± 0.022 kcal/mol (**Equation 2.4**).

$$\text{Equation 2.3 Error}_{\Delta G} = -RT\text{Error}([folded]/[unfolded])$$

$$\text{Equation 2.4 Error}_{\Delta\Delta G} = \sqrt{(\text{Error}_{\Delta G})^2 + (\text{Error}_{\Delta G})^2}$$

To experimentally validate error estimations, redundant folding energy measurements of **1a**, **1b**, and **1c** were conducted in chloroform-d. The compounds used

were synthesized separately from each other to ensure results would not be artificially biased towards similarity. Results demonstrate that all $\Delta\Delta G$ measurements were within ± 0.02 kcal/mol of each other, in accordance with our error calculations.

Table 2.4 Redundant folding energy measurements of **1a**, **1b**, and **1c** in chloroform-d₃.

	1c folding energy (kcal/mol)	1b folding energy (kcal/mol)	1a folding energy (kcal/mol)	1b Interaction energy (kcal/mol)	1a Interaction energy (kcal/mol)
Trial 1	-0.1	-0.09	-0.08	0.01	0.02
Trial 2	-0.12	-0.08	-0.08	0.03	0.04
Trial 3	-0.11	-0.08	-0.09	0.02	0.02

2.6.7 Solvent Data

Folding energies were calculated using Gibbs free energy equation . Solvent mixtures reported in v/v %. Interaction energies for **4b** and **4c** were calculated by subtracting the folding energies from balances **4b** and **4c** from the folding energy of the control balance **4a** for all of the different solvent systems. Cohesive energy densities of mixtures were calculated assuming these values scale linearly with respect to the volume of their components. Cohesive energy densities values were calculated using Hildebrandt and Hansen solubility parameters.^{36,42,43,44}

Table 2.5 Solvents used for decoupled ¹⁹F NMR experiments and the measure energy difference between the *folded* and *unfolded* conformers (folding energy).

Solvent	ced (cal/mL)	1c folding energy (kcal/mol)	1b folding energy (kcal/mol)	1a folding energy (kcal/mol)	1b interaction energy (kcal/mol)	1c interaction energy (kcal/mol)	unfolded shift (ppm)	folded shift (ppm)
n-pentane	50.27	-0.34	-0.29	-0.23	0.05	0.11	-122.5	-122.7
hexane	52.4	-0.13	-0.06	-0.07	0.07	0.06	-122.4	-122.7
triethylamine	57	-0.14	-0.12	-0.14	0.03	0.01	-122.7	-123.1
diethyl ether	60	-0.23	-0.23	-0.21	-0.01	0.02	-123.5	-123.7
cyclohexane	66.9	-0.14	-0.13	-0.06	0.01	0.08	-122.4	-122.6
N,N-diethylamine	67.24	-0.23	-0.16	-0.19	0.07	0.03	-123.2	-123.6
1,2-dimethoxyethane	74.88	-0.42	-0.45	-0.46	-0.03	-0.04	-123.8	-124.1
<i>p</i> -xylene	78.3	-0.33	-0.3	-0.3	0.03	0.03	-122.3	-122.8
toluene	79.4	-0.3	-0.27	-0.26	0.02	0.03	-122.4	-122.8

ethyl acetate	81.7	-0.41	-0.41	-0.39	0	0.02	-123.8	-124.2
methyl acetate	83.61	-0.38	-0.41	-0.42	-0.04	-0.05	-124	-124.3
benzene-d6	83.7	-0.26	-0.26	-0.25	0	0.01	-122.4	-122.9
CDCl3	85.4	-0.1	-0.09	-0.08	0.01	0.02	-122.3	-122.5
THF	86.9	-0.31	-0.28	-0.29	0.02	0.02	-124.2	-124.4
furan	88.36	-0.24	-0.18	-0.23	0.06	0.01	-122.9	-123.1
cyclohexanone	91.86	-0.47	-0.51	-0.51	-0.03	-0.04	-123.6	-123.9
methylene chloride	93.7	-0.15	-0.14	-0.15	0.01	0	-123.2	-123.4
acetone-d6	94.3	-0.48	-0.51	-0.51	-0.02	-0.02	-123.6	-123.9
propanoic acid	95.15	-0.47	-0.5	-0.52	-0.02	-0.05	-123.2	-123.6
1,1,2,2-tetrachloroethane	98.01	-0.17	-0.15	-0.16	0.02	0	-122.2	-124.2
1-decanol	99.5	-0.51	-0.49	-0.48	0.02	0.03	-122.3	-122.6
1,2-dichloroethane	103.4	-0.23	-0.24	-0.24	-0.01	-0.01	-123.2	-123.3
1,4-dioxane	105.06	-0.34	-0.35	-0.38	-0.01	-0.04	-123.2	-123.5
25% DMSO-d6/chloroform-d3	105.52	-0.35	-0.35	-0.39	-0.01	-0.04	-124.5	-124.7
acetic acid	109.5	-0.54	-0.58	-0.6	-0.04	-0.06	-123.1	-123.4
tert-butanol	110.3	-0.55	-0.54	-0.59	0.01	-0.04	-122.5	-122.9
pyridine	112.4	-0.43	-0.43	-0.41	0	0.01	-122.9	-123

acetophenone	113.63	-0.46	-0.45	-0.48	0.01	-0.02	-122.6	-122.8
40% DMSO-d6/chloroform-d3	118.02	-0.51	-0.49	-0.53	0.02	-0.02	-117.9	-118.1
50% DMSO-d6/chloroform-d3	126.55	-0.57	-0.58	-0.6	-0.01	-0.03	-118	-118.2
isopropanol	132.3	-0.55	-0.58	-0.6	-0.03	-0.05	-122.9	-123.3
acetonitrile-d4	138.9	-0.47	-0.5	-0.51	-0.03	-0.04	-124.4	-124.5
N,N-dimethylformamide	138.9	-0.58	-0.64	-0.64	-0.06	-0.06	-123.9	-124.1
75% ethanol/benzene-d6	142	-0.52	-0.52	-0.49	-0.01	0.02	-123.8	-124.1
ethanol	161.3	-0.58	-0.64	-0.65	-0.07	-0.08	-123.6	-123.8
DMSO-d6	168.6	-0.69	-0.72	-0.77	-0.03	-0.08	-123	-123.3
50% methanol-d4/ethanol	185.15	-0.52	-0.56	-0.65	-0.04	-0.13	-124.5	-124.8
5% H2O/DMSO-d6	187.67	-0.75	-0.83	-0.83	-0.07	-0.07	-123	-123.2
50% methanol-d4/DMSO-d6	188.8	-0.61	-0.67	-0.71	-0.06	-0.11	-124	-124.2
75% methanol-d4/DMSO-d6	198.8	-0.48	-0.59	-0.66	-0.11	-0.19	-124.5	-124.7
80% methanol-d4/DMSO-d6	200.9	-0.49	-0.57	-0.66	-0.08	-0.17	-124.5	-124.8
10% H2O/DMSO-d6	206.74	-0.82	-0.87	-1.03	-0.05	-0.21	-123	-123.2
methanol-d4	209	-0.5	-0.54	-0.63	-0.05	-0.14	-124.1	-124.3
10% H2O/methanol-d4	243.1	-0.58	-0.65	-0.79	-0.07	-0.22	-124.6	-124.8

15% H ₂ O/methanol-d ₄	260.15	-0.69	-0.81	-0.87	-0.12	-0.17	-123.7	-123.9
40% H ₂ O/THF	272.14	-0.47	-0.54	-0.61	-0.07	-0.14	-124.2	-124.3

2.6.8 SASA Calculations

The difference of the solvent accessible alkyl surface area between the *folded* and *unfolded* conformers between balances was modeled and calculated using Spartan 18. Structures for the folded conformations of **1a**, **1b**, and **5**¹⁹ were derived from their respective CIF coordinates, while the structure for **4c** was derived from the truncated model of **1c** and **6** was derived from the truncated model of **5**. Unfolded conformations were derived by rotating the *N*-aryl bond 180°. Accessible surface areas were measured after ground state energetics of the conformers were calculated using density functional theory methodology, at the B3LYP-D3, 6-311+G* level of theory. There were zero imaginary frequencies in all of the GS state structures. Surface areas were measured using a 1 Å probe. Δ SASA (Å²) was measured by subtracting the *folded* conformer SASA from the *unfolded* conformer SASA. $\Delta\Delta$ SASA was calculated by subtracting the Δ SASA of **1c** from that of balances **1a**, **1b**, and **1c**, and the Δ SASA of **6** from that of **5** and **6**.

Table 2.6 Calculated solvent accessible surface area (SASA) of *folded* and *unfolded* conformers balances **1a**, **1b**, and **1c** from this study, as well as **5** and **6** from Cockcroft et al.¹⁹ and Schreiner et al.^{20,39} *measurements taken with a 2.63 Å probe to match the molecular radius of benzene.

	<i>folded</i> conformer SASA(Å ²)	<i>Unfolded</i> conformer SASA(Å ²)	ΔSASA (Å ²)	ΔΔSASA (Å ²)	slope(L/mol)	y- intercept
1a	323.56	365.42	41.86	29.02	-0.0012 (±9.1E-05)	0.1097
1b	292.9	318.57	25.67	12.83	-0.00060 (±6.6E-05)	0.0614
1c	266.19	279.03	12.84	0	0	0
5a	358.1	417.21	59.11	31.31	-0.0019 (±1.3E-05)	0.1470
5b	330.42	358.22	27.80	0	0	0
6	264.89	289.29	24.40	0	-0.00040 (±0.00052)	-0.2755
7	891.11*	879.28*	11.83	0	-0.0012 (±0.000112)	0.2444

Table 2.7 Xyz coordinates of the *folded* conformer structure of **1a**.

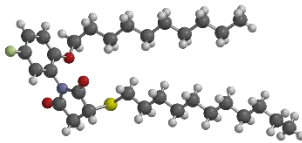
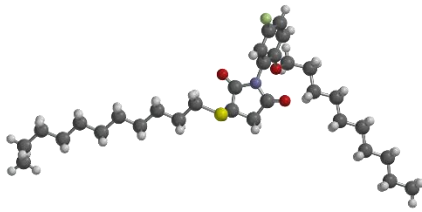
											
S	2.521321	-2.382970	2.692632	H	-0.641979	-0.907270	0.085232	H	3.171493	0.548034	6.865374
F	8.875937	2.538541	2.924268	H	0.518021	-0.939770	-1.014768	C	2.545771	2.125741	5.689214
O	4.518521	0.000630	1.393132	C	-0.952079	-2.351670	-1.360768	H	2.982050	2.784848	5.092538
O	6.230621	-2.223170	4.985933	H	-1.523479	-2.934070	-0.800368	H	2.108403	2.625472	6.422986
O	4.353973	0.524380	5.248964	H	-0.376879	-2.936770	-1.915068	C	1.480306	1.369043	4.898768
N	5.541021	-0.847570	3.273232	C	-1.842579	-1.521970	-2.279168	H	1.897402	0.974606	4.092200
C	4.220421	-2.344570	2.035232	H	-1.270979	-0.941970	-2.841868	H	1.134286	0.626703	5.454063
H	4.274121	-2.705670	1.104432	H	-2.415579	-0.934970	-1.725268	C	0.311925	2.254183	4.469534
C	4.746421	-0.926570	2.131832	C	-2.731879	-2.368770	-3.185768	H	-0.086192	2.674507	5.272919
C	5.698521	-2.076970	3.916132	H	-2.157279	-2.961170	-3.731968	H	0.652411	2.978121	3.886644
C	5.105621	-3.127570	3.013132	H	-3.305780	-2.944470	-2.620468	C	-0.770971	1.483625	3.724101
H	4.567421	-3.775170	3.533732	C	-3.621080	-1.553370	-4.116668	H	-0.367693	1.067106	2.921332
H	5.816621	-3.617570	2.529232	H	-4.191780	-0.953470	-3.573668	H	-1.098541	0.753173	4.307108
C	6.101921	0.391730	3.715732	H	-3.049880	-0.986870	-4.693368	C	-1.958309	2.328798	3.289200
C	5.460337	1.121372	4.718505	C	-4.509580	-2.419070	-4.996168	H	-1.640043	3.043988	2.683163
C	5.986127	2.347462	5.101883	H	-5.077480	-2.985170	-4.416168	H	-2.354105	2.762699	4.086764
H	5.556234	2.859625	5.777056	H	-3.935480	-3.020870	-5.533668	C	-3.034952	1.518653	2.579869
C	7.146665	2.826917	4.494834	C	-5.406580	-1.629670	-5.938868	H	-3.335468	0.794500	3.183529
H	7.512235	3.665293	4.751202	H	-4.844480	-1.009670	-6.467468	H	-2.635137	1.094581	1.779385
C	7.755844	2.072949	3.519318	H	-6.030480	-1.082370	-5.398968	C	-4.253001	2.326620	2.144477
C	7.252460	0.859395	3.108413	C	-6.218380	-2.494470	-6.898768	H	-4.658816	2.751266	2.941777
H	7.683739	0.357628	2.427112	H	-6.713780	-1.902770	-7.519268	H	-3.958754	3.049317	1.534822
C	1.585621	-1.450970	1.447432	H	-5.595680	-3.042270	-7.438768	C	-5.303904	1.488071	1.444278
H	0.955221	-0.843370	1.909232	C	-7.206880	-3.414970	-6.207068	H	-5.581076	0.753064	2.046491
H	2.215021	-0.892470	0.925932	H	-7.737380	-3.890070	-6.880268	H	-4.902381	1.080533	0.636212
C	0.803921	-2.334670	0.490232	H	-7.801980	-2.885870	-5.635868	C	-6.537834	2.281663	1.034193
H	0.229821	-2.952370	1.009132	H	-6.719380	-4.064270	-5.657868	H	-6.926417	2.711924	1.824439
H	1.435921	-2.880570	-0.041968	C	3.605199	1.213643	6.275201	H	-7.196995	1.676692	0.634485
C	-0.067479	-1.507570	-0.453368	H	4.227462	1.750708	6.827529	H	-6.283811	2.966201	0.380974

Table 2.8 Xyz coordinates of the *unfolded* conformer structure of **1a**.



S	2.521321	-2.382970	2.692632	H	-0.641979	-0.907270	0.085232	H	9.742352	-0.553539	1.621499
F	5.089223	3.315838	5.547237	H	0.518021	-0.939770	-1.014768	C	10.391274	-0.671372	3.578297
O	4.518521	0.000630	1.393132	C	-0.952079	-2.351670	-1.360768	H	10.158834	-0.227704	4.432647
O	6.230621	-2.223170	4.985933	H	-1.523479	-2.934070	-0.800368	H	11.338287	-0.464835	3.378411
O	8.111546	-0.285025	2.752859	H	-0.376879	-2.936770	-1.915068	C	10.236051	-2.181631	3.744537
N	5.541021	-0.847570	3.273232	C	-1.842579	-1.521970	-2.279168	H	9.321592	-2.377401	4.069407
C	4.220421	-2.344570	2.035232	H	-1.270979	-0.941970	-2.841868	H	10.342556	-2.615202	2.861461
H	4.274121	-2.705670	1.104432	H	-2.415579	-0.934970	-1.725268	C	11.247011	-2.783792	4.718288
C	4.746421	-0.926570	2.131832	C	-2.731879	-2.368770	-3.185768	H	12.161922	-2.561374	4.411588
C	5.698521	-2.076970	3.916132	H	-2.157279	-2.961170	-3.731968	H	11.119209	-2.374596	5.610477
C	5.105621	-3.127570	3.013132	H	-3.305780	-2.944470	-2.620468	C	11.119228	-4.297171	4.842583
H	4.567421	-3.775170	3.533732	C	-3.621080	-1.553370	-4.116668	H	10.203438	-4.513441	5.150992
H	5.816621	-3.617570	2.529232	H	-4.191780	-0.953470	-3.573668	H	11.235204	-4.699808	3.945258
C	6.101921	0.391730	3.715732	H	-3.049880	-0.986870	-4.693368	C	12.117229	-4.936645	5.795628
C	7.450091	0.664540	3.475790	C	-4.509580	-2.419070	-4.996168	H	11.986538	-4.557885	6.700908
C	7.994782	1.847367	3.956377	H	-5.077480	-2.985170	-4.416168	H	13.035067	-4.707689	5.502055
H	8.912728	2.043432	3.808355	H	-3.935480	-3.020870	-5.533668	C	11.982727	-6.451750	5.866431
C	7.192850	2.748146	4.656903	C	-5.406580	-1.629670	-5.938868	H	12.095810	-6.822479	4.956000
H	7.558349	3.559334	4.989507	H	-4.844480	-1.009670	-6.467468	H	11.066195	-6.673685	6.168390
C	5.866499	2.448514	4.862360	H	-6.030480	-1.082370	-5.398968	C	12.979587	-7.134103	6.797390
C	5.299739	1.278674	4.409361	C	-6.218380	-2.494470	-6.898768	H	13.898593	-6.917687	6.498575
H	4.383396	1.086670	4.568718	H	-6.713780	-1.902770	-7.519268	H	12.866534	-6.771231	7.711772
C	1.585621	-1.450970	1.447432	H	-5.595680	-3.042270	-7.438768	C	12.817716	-8.640662	6.841163
H	0.955221	-0.843370	1.909232	C	-7.206880	-3.414970	-6.207068	H	12.909051	-8.999701	5.923302
H	2.215021	-0.892470	0.925932	H	-7.737380	-3.890070	-6.880268	H	11.905204	-8.855681	7.159546
C	0.803921	-2.334670	0.490232	H	-7.801980	-2.885870	-5.635868	C	13.830264	-9.332816	7.744606
H	0.229821	-2.952370	1.009132	H	-6.719380	-4.064270	-5.657868	H	14.737572	-9.103047	7.453732
H	1.435921	-2.880570	-0.041968	C	9.518614	-0.105974	2.475354	H	13.706017	-10.303331	7.690627
C	-0.067479	-1.507570	-0.453368	H	9.710092	0.860146	2.372087	H	13.698751	-9.037205	8.669340

Table 2.9 Xyz coordinates of the *folded* conformer structure of **1b**.

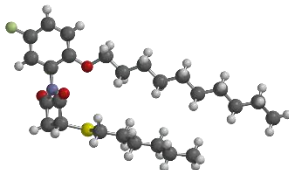
											
S	12.503696	7.392276	0.913038	C	7.883714	12.051238	0.444545	H	6.494842	7.930066	-3.220847
O	11.529998	5.708567	3.668485	H	8.502591	12.773217	0.719870	C	4.553558	8.599818	-3.004719
O	14.574502	3.523935	1.055215	H	7.326047	11.814145	1.227502	H	4.106039	7.802501	-3.383787
O	10.465229	3.919920	1.406603	C	6.983062	12.563858	-0.674308	H	3.995588	8.933062	-2.257664
N	12.909600	4.330800	2.436600	H	7.535796	12.890265	-1.414786	C	4.638491	9.676678	-4.077102
C	12.470835	5.562201	2.924348	H	6.425543	13.295282	-0.335735	H	5.083383	10.473675	-3.693666
C	13.361825	6.635693	2.329934	H	6.409293	11.835466	-0.991353	H	5.204887	9.344053	-4.817915
H	13.628463	7.317727	3.011121	C	9.061813	3.934034	1.105595	C	3.288999	10.093953	-4.642712
C	14.569487	5.859552	1.797218	H	8.526756	3.889272	1.937281	H	2.796094	9.285600	-4.931695
H	14.853893	6.211425	0.916639	H	8.821235	3.164534	0.530887	H	2.760879	10.530883	-3.927888
H	15.331197	5.917552	2.426918	C	8.812559	5.234255	0.383323	C	3.413209	11.047415	-5.820624
C	14.080029	4.433841	1.674505	H	9.387346	5.262330	-0.422157	H	3.885370	11.858161	-5.536787
C	11.268883	8.446470	1.718485	H	9.088695	5.980034	0.973050	H	2.519479	11.286312	-6.143702
H	10.692136	7.904336	2.313150	C	7.368706	5.463579	-0.043669	H	3.915651	10.612750	-6.541223
H	11.716022	9.141611	2.263306	H	6.803668	5.602818	0.757117	C	12.208849	3.066658	2.709976
C	10.430518	9.095850	0.619168	H	7.033057	4.664818	-0.522580	C	10.888160	0.684158	3.225200
H	9.830533	8.413203	0.226855	C	7.274191	6.683119	-0.954386	C	12.810655	2.096602	3.496308
H	11.033185	9.416171	-0.097889	H	7.857214	6.528724	-1.739535	C	10.946699	2.845463	2.181256
C	9.588124	10.268048	1.119676	H	7.637810	7.463269	-0.465386	C	10.286353	1.654213	2.438868
H	9.024921	9.966147	1.875866	C	5.880289	7.043567	-1.458858	C	12.150310	0.905352	3.753920
H	10.187494	10.982451	1.452335	H	5.473106	6.249574	-1.887665	H	13.808590	2.271492	3.914347
C	8.693400	10.833406	0.020271	H	5.311377	7.299810	-0.690176	H	9.288419	1.479323	2.020829
H	9.258491	11.081003	-0.753953	C	5.916841	8.191677	-2.460872	H	10.366050	-0.257719	3.428884
H	8.069611	10.124798	-0.278043	H	6.332202	8.978034	-2.025952	F	12.750734	-0.062478	4.538448

Table 2.10 Xyz coordinates of the *unfolded* conformer structure of **1b**.

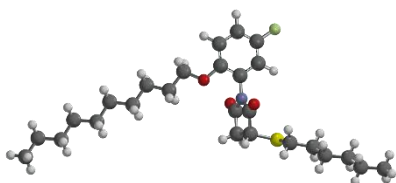
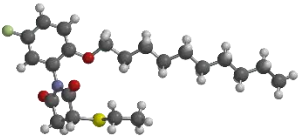

											
S	12.503696	7.392276	0.913038	C	7.883714	12.051238	0.444545	H	20.361600	2.602700	7.689400
O	11.529998	5.708567	3.668485	H	8.502591	12.773217	0.719870	C	21.931900	1.263700	7.618000
O	14.574502	3.523935	1.055215	H	7.326047	11.814145	1.227502	H	21.590600	0.638000	8.304800
O	14.090500	2.462400	3.959500	C	6.983062	12.563858	-0.674308	H	22.377200	0.727200	6.914900
N	12.909600	4.330800	2.436600	H	7.535796	12.890265	-1.414786	C	22.957100	2.189500	8.257300
C	12.470835	5.562201	2.924348	H	6.425543	13.295282	-0.335735	H	23.298800	2.811500	7.567000
C	13.361825	6.635693	2.329934	H	6.409293	11.835466	-0.991353	H	22.506600	2.731200	8.952900
H	13.628463	7.317727	3.011121	C	14.921800	1.416200	4.483700	C	24.135900	1.464300	8.889500
C	14.569487	5.859552	1.797218	H	15.030100	0.691100	3.818500	H	23.794400	0.767400	9.504000
H	14.853893	6.211425	0.916639	H	14.524900	1.035700	5.307100	H	24.655500	1.012000	8.178000
H	15.331197	5.917552	2.426918	C	16.250400	2.063100	4.784900	C	25.057300	2.397100	9.659500
C	14.080029	4.433841	1.674505	H	16.102100	2.804400	5.424000	H	25.413000	3.079800	9.052700
C	11.268883	8.446470	1.718485	H	16.605800	2.456600	3.948800	H	25.798200	1.882500	10.042200
H	10.692136	7.904336	2.313150	C	17.302300	1.126700	5.364800	H	24.554600	2.831300	10.380200
H	11.716022	9.141611	2.263306	H	17.583100	0.474700	4.674900	C	12.208849	3.066658	2.709976
C	10.430518	9.095850	0.619168	H	16.916400	0.623800	6.125200	C	10.888160	0.684158	3.225200
H	9.830533	8.413203	0.226855	C	18.513700	1.922000	5.839800	C	10.946698	2.845463	2.181256
H	11.033185	9.416171	-0.097889	H	18.207900	2.576500	6.516800	C	12.810655	2.096603	3.496307
C	9.588124	10.268048	1.119676	H	18.867300	2.435700	5.071000	C	12.150311	0.905352	3.753920
H	9.024921	9.966147	1.875866	C	19.659400	1.113800	6.441100	C	10.286354	1.654213	2.438868
H	10.187494	10.982451	1.452335	H	19.307600	0.538600	7.166000	H	10.470873	3.612449	1.559533
C	8.693400	10.833406	0.020271	H	20.043800	0.524700	5.744400	H	12.626136	0.138366	4.375643
H	9.258491	11.081003	-0.753953	C	20.756900	2.011500	7.000700	H	10.366050	-0.257719	3.428884
H	8.069611	10.124798	-0.278043	H	21.096900	2.587800	6.271100	F	9.027099	1.433524	1.911362

Table 2.11 Xyz coordinates of the *folded* conformer structure of **1c**.



O	11.268200	7.356700	9.947400	H	1.786000	8.783700	1.941300
C	10.348100	8.253700	10.609000	H	2.888700	9.937800	1.826800
C	9.627300	9.154400	9.625700	S	9.772700	4.071800	8.021100
C	8.749100	8.381200	8.644100	C	8.837000	5.003800	6.775900
C	7.876200	9.288200	7.779100	H	8.206600	5.611400	7.237700
C	6.966700	8.509600	6.836400	H	9.466400	5.562300	6.254400
C	6.072400	9.378000	5.965000	C	8.055300	4.120100	5.818700
H	10.846800	8.812600	11.256800	H	7.481200	3.502400	6.337600
H	9.681900	7.723800	11.113800	H	8.687300	3.574200	5.286500
H	10.297000	9.676700	9.116300	H	7.430134	4.713484	5.141736
H	9.063300	9.794200	10.127700	F	16.485600	8.605400	8.885000
H	9.328200	7.835900	8.054700	O	11.769900	6.455400	6.721600
H	8.166500	7.763000	9.151600	O	13.482000	4.231600	10.314400
H	7.319300	9.856900	8.368200	N	12.792400	5.607200	8.601700
H	8.459200	9.884600	7.246000	C	11.471800	4.110200	7.363700
H	7.528800	7.944300	6.249000	H	11.525500	3.749100	6.432900
H	6.395100	7.905700	7.374300	C	11.997800	5.528200	7.460300
H	6.639900	9.964200	5.404300	C	12.949900	4.377800	9.244600
H	5.521100	9.959000	6.547700	C	12.357000	3.327200	8.341600
C	5.153400	8.565300	5.063000	H	11.818800	2.679600	8.862200
H	4.602300	7.968400	5.627900	H	13.068000	2.837200	7.857700
H	5.710600	7.993200	4.477600	C	13.353300	6.846500	9.044200
C	4.225400	9.399600	4.186200	C	12.546800	7.770600	9.711400
H	3.663500	9.972300	4.766700	C	13.089800	8.991000	10.088900
H	4.772100	9.994700	3.613900	H	12.551400	9.633600	10.536300
C	3.324600	8.558100	3.304000	C	14.427100	9.273000	9.810800
H	2.794700	7.948300	3.875900	H	14.805800	10.106100	10.065300
H	3.887700	8.001000	2.710000	C	15.191900	8.331800	9.162400
C	2.372400	9.383400	2.448000	C	14.679700	7.117700	8.764200
H	1.829600	9.959100	3.026400	H	15.222500	6.484300	8.310200

Table 2.12 Xyz coordinates of the *unfolded* conformer structure of **1c**.



H	1.568605	-1.597497	-7.465531	H	13.020286	-1.483658	-2.680990
C	2.005647	-1.384116	-6.495245	H	13.511620	-0.714778	-4.191925
C	3.081225	-0.833551	-3.942625	C	14.338589	0.207874	-2.422390
C	3.071032	-0.498444	-6.370554	H	14.034753	0.409258	-1.387884
C	1.507204	-2.011242	-5.360311	H	14.526234	1.177968	-2.898599
C	2.034931	-1.753050	-4.096307	C	15.622488	-0.621451	-2.426657
C	3.618868	-0.249078	-5.107539	H	15.441390	-1.590837	-1.947908
H	3.486992	-0.015482	-7.250570	H	15.932933	-0.822100	-3.458678
H	1.583589	-2.257928	-3.247329	C	16.749170	0.092342	-1.696868
F	0.489424	-2.873378	-5.482239	H	16.483037	0.279390	-0.651630
O	4.738271	0.542758	-5.052539	H	16.977309	1.052397	-2.170771
C	5.923504	-0.248422	-5.214173	H	17.657356	-0.518295	-1.712098
H	5.819871	-1.231530	-4.735778	N	3.598490	-0.530384	-2.653941
H	6.112968	-0.394118	-6.284190	C	4.061415	0.710049	-2.280081
C	7.081586	0.508433	-4.570946	C	3.821923	-1.477283	-1.680834
H	6.818983	0.759623	-3.536085	O	4.065780	1.737042	-2.946952
H	7.221407	1.467589	-5.084709	O	3.775424	-2.696288	-1.769948
C	8.372878	-0.305658	-4.603040	C	4.237684	-0.791369	-0.415321
H	8.205022	-1.280007	-4.128172	H	5.123901	-1.285837	-0.004411
H	8.660143	-0.498807	-5.643625	H	3.420740	-0.866049	0.308499
C	9.506386	0.422154	-3.879546	C	4.566195	0.619207	-0.860319
H	9.208893	0.625919	-2.843529	H	5.653172	0.757020	-0.884757
H	9.688044	1.390741	-4.360841	S	3.864735	1.893719	0.245739
C	10.792082	-0.406011	-3.887117	C	2.090345	1.778125	-0.162929
H	10.606556	-1.376434	-3.410690	H	1.922550	2.141724	-1.180677
H	11.094111	-0.606282	-4.922289	H	1.761284	0.738051	-0.101996
C	11.922886	0.316083	-3.152933	C	1.280432	2.615096	0.811872
H	11.619348	0.517239	-2.118306	H	0.215561	2.545821	0.565441
H	12.109925	1.286016	-3.629596	H	1.562676	3.672365	0.766201
C	13.207808	-0.513657	-3.157398	H	1.403953	2.264123	1.842073

Table 2.13 Xyz coordinates of the *folded* conformer structure of **5a**.

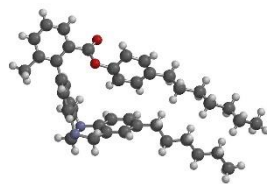
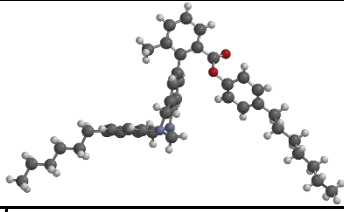
											
C	-7.581929	-3.495789	2.431415	C	1.350372	-1.446089	-5.281186	C	2.802272	1.917512	0.240015
H	-8.156629	-3.118089	1.730915	H	0.497272	-1.806289	-5.631186	C	2.820672	2.607312	1.514315
H	-8.045029	-3.450589	3.293215	H	2.037172	-1.553089	-5.986086	H	3.475072	3.248012	1.767715
H	-7.379729	-4.430789	2.217115	N	1.746672	-2.210389	-4.110186	C	1.708372	2.192112	2.353015
C	-6.299529	-2.707589	2.507015	C	3.130472	-1.831589	-3.762686	H	1.500672	2.739212	3.101915
H	-6.519229	-1.748289	2.611115	H	3.753972	-2.250089	-4.407686	C	0.935572	1.079612	2.154915
H	-5.796729	-2.990989	3.311615	H	3.346572	-2.179789	-2.861486	C	1.167772	0.338211	1.011915
C	-5.416228	-2.874689	1.298415	C	2.373472	0.513711	-4.350286	H	0.652172	-0.445189	0.857615
H	-5.209529	-3.837289	1.194015	C	2.568472	1.898812	-4.356086	C	2.133972	0.707011	0.081015
H	-5.925729	-2.591489	0.498115	H	1.906272	2.467812	-4.730286	H	2.336572	0.138711	-0.651685
C	-4.148228	-2.127689	1.330915	C	3.720272	2.445012	-3.820586	C	-0.070428	0.521012	3.175715
H	-3.631228	-2.432289	2.118015	H	3.847372	3.385812	-3.838486	H	-0.200628	-0.445789	3.002815
H	-4.357728	-1.170089	1.468215	C	4.699072	1.624812	-3.251186	H	0.308272	0.616412	4.085815
C	-3.252628	-2.248289	0.095315	C	4.485672	0.249511	-3.234086	C	-1.378428	1.196412	3.128615
H	-3.076528	-3.206389	-0.082585	H	5.141272	-0.314689	-2.843086	H	-1.736528	1.152712	2.205615
H	-3.731828	-1.877589	-0.688585	C	3.332572	-0.324189	-3.777686	H	-1.262928	2.150612	3.366915
C	-1.945828	-1.533089	0.253415	C	5.950572	2.202612	-2.674886	C	-2.450528	0.510112	4.155015
H	-1.504828	-1.862489	1.076515	C	6.951672	2.713912	-3.518186	H	-2.494928	-0.456689	3.947615
H	-2.129428	-0.568989	0.378315	C	8.134972	3.200712	-2.958786	H	-2.090228	0.596511	5.074415
C	-0.985028	-1.693489	-0.903385	H	8.798172	3.574112	-3.527486	C	-3.666728	0.977512	4.155015
C	-0.946428	-0.777489	-1.948286	C	8.362772	3.149912	-1.593886	H	-3.994628	0.984412	3.221715
H	-1.548428	-0.042989	-1.942086	H	9.185673	3.461612	-1.234685	H	-3.635928	1.918012	4.463715
C	-0.045428	-0.908689	-3.009886	C	7.384072	2.643112	-0.756985	C	-4.740528	0.187811	5.058215
C	0.831772	-1.993289	-3.022786	H	7.537972	2.594412	0.180115	H	-4.753328	-0.756789	4.763315
C	0.811772	-2.904289	-1.970886	C	6.176472	2.204312	-1.285186	H	-4.421428	0.199311	5.996115
H	1.423872	-3.631089	-1.965186	C	6.788572	2.759912	-5.014186	C	-6.048629	0.661112	5.042115
C	-0.091228	-2.758189	-0.937486	H	6.242272	2.001312	-5.306286	H	-6.406329	0.688612	4.120415
H	-0.103128	-3.398489	-0.234685	H	7.669372	2.711612	-5.439986	H	-6.103329	1.567412	5.438415
C	-0.010128	0.121911	-4.117586	H	6.348472	3.597812	-5.269486	C	-6.847929	-0.416789	5.947715
H	-0.823728	0.027811	-4.672686	O	5.387072	1.217212	0.732915	H	-6.372429	-0.556989	6.793315
H	-0.018728	1.027612	-3.716386	C	5.148772	1.801212	-0.281185	H	-6.908429	-1.270289	5.463815
N	1.183472	-0.012889	-4.981386	O	3.921472	2.252012	-0.598485	H	-7.752529	-0.086189	6.132015

Table 2.14 Xyz coordinates of the *unfolded* conformer structure of **5a**.



C	-1.176668	-2.031344	-12.946582	C	-1.229949	0.017675	-1.145304	C	1.525233	0.933289	4.000034
H	-1.616389	-2.877417	-12.713247	H	-2.033553	-0.387000	-1.558197	C	1.543632	1.623089	5.274334
H	-0.777272	-2.105902	-13.837720	H	-1.477779	0.327292	-0.238251	H	2.198033	2.263789	5.527734
H	-1.839391	-1.308968	-12.944296	N	-0.808629	1.159519	-1.939742	C	0.431332	1.207889	6.113034
C	-0.099931	-1.730393	-11.935844	C	0.219448	1.894236	-1.176592	H	0.223632	1.754989	6.861934
H	0.500268	-2.514021	-11.864783	H	-0.217029	2.399040	-0.445442	C	-0.341468	0.095389	5.914934
H	0.439157	-0.965933	-12.260635	H	0.663344	2.547193	-1.773842	C	-0.109268	-0.646011	4.771934
C	-0.632935	-1.401645	-10.565921	C	1.053982	-0.415305	-0.553432	H	-0.624868	-1.429411	4.617634
H	-1.240709	-0.624216	-10.646158	C	2.026297	-1.261489	-0.010166	C	0.856932	-0.277211	3.841034
H	-1.172076	-2.169022	-10.248540	H	1.886083	-2.200964	-0.005515	H	1.059532	-0.845511	3.108334
C	0.383450	-1.094007	-9.546505	C	3.190749	-0.738308	0.520938	C	-1.347468	-0.463211	6.935734
H	0.903221	-0.310710	-9.856151	H	3.839995	-1.320692	0.896288	H	-1.477668	-1.430011	6.762834
H	1.008115	-1.859929	-9.492679	C	3.422033	0.640589	0.508833	H	-0.968768	-0.367811	7.845834
C	-0.131912	-0.797938	-8.135797	C	2.455948	1.471355	-0.051337	C	-2.655468	0.212189	6.888634
H	-0.796606	-0.065419	-8.182836	H	2.607467	2.408203	-0.070622	H	-3.013568	0.168489	5.965634
H	-0.591544	-1.602118	-7.784253	C	1.267920	0.964189	-0.585794	H	-2.539968	1.166389	7.126934
C	0.960679	-0.405397	-7.189018	C	4.673533	1.218389	1.085133	C	-3.727568	-0.474111	7.915034
H	1.456993	0.356785	-7.580463	C	5.674633	1.729689	0.241833	H	-3.771968	-1.440911	7.707634
H	1.591988	-1.162794	-7.107806	C	6.857933	2.216489	0.801233	H	-3.367268	-0.387711	8.834434
C	0.496745	-0.015679	-5.803400	H	7.521133	2.589889	0.232533	C	-4.943768	-0.006711	7.915034
C	0.430597	-0.944461	-4.771242	C	7.085733	2.165689	2.166134	H	-5.271668	0.000189	6.981734
H	0.667699	-1.847424	-4.945523	H	7.908633	2.477389	2.525334	H	-4.912968	0.933789	8.223734
C	0.022981	-0.585545	-3.482429	C	6.107033	1.658889	3.003034	C	-6.017568	-0.796411	8.818234
C	-0.334293	0.739090	-3.230036	H	6.260933	1.610189	3.940134	H	-6.030368	-1.741011	8.523334
C	-0.252880	1.678507	-4.253599	C	4.899433	1.220089	2.474834	H	-5.698468	-0.784911	9.756134
H	-0.473230	2.586167	-4.078853	C	5.511533	1.775689	-1.254167	C	-7.325668	-0.323111	8.802134
C	0.145360	1.299437	-5.519451	H	4.965233	1.017089	-1.546267	H	-7.683368	-0.295611	7.880434
H	0.179845	1.950207	-6.211812	H	6.392333	1.727389	-1.679967	H	-7.380368	0.583189	9.198434
C	-0.010828	-1.615525	-2.374106	H	5.071433	2.613589	-1.509467	C	-8.124968	-1.401011	9.707734
H	-0.758627	-2.242313	-2.538027	O	4.110033	0.232989	4.492934	H	-7.649468	-1.541211	10.553334
H	0.831763	-2.136170	-2.391307	C	3.871733	0.816989	3.478834	H	-8.185468	-2.254511	9.223834
N	-0.174952	-1.005498	-1.036223	O	2.644433	1.267789	3.161534	H	-9.029568	-1.070411	9.892034

Table 2.15 Xyz coordinates of the *folded* conformer structure of **5b**.

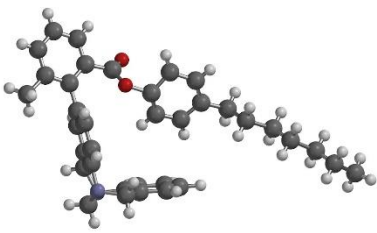
											
C	-0.985028	-1.693489	-0.903385	C	4.485672	0.249511	-3.234086	H	0.652172	-0.445189	0.857615
C	-0.946428	-0.777489	-1.948286	H	5.141272	-0.314689	-2.843086	C	2.133972	0.707011	0.081015
H	-1.548428	-0.042989	-1.942086	C	3.332572	-0.324189	-3.777686	H	2.336572	0.138711	-0.651685
C	-0.045428	-0.908689	-3.009886	C	5.950572	2.202612	-2.674886	C	-0.070428	0.521012	3.175715
C	0.831772	-1.993289	-3.022786	C	6.951672	2.713912	-3.518186	H	-0.200628	-0.445789	3.002815
C	0.811772	-2.904289	-1.970886	C	8.134972	3.200712	-2.958786	H	0.308272	0.616412	4.085815
H	1.423872	-3.631089	-1.965186	H	8.798172	3.574112	-3.527486	C	-1.378428	1.196412	3.128615
C	-0.091228	-2.758189	-0.937486	C	8.362772	3.149912	-1.593886	H	-1.736528	1.152712	2.205615
H	-0.103128	-3.398489	-0.234685	H	9.185673	3.461612	-1.234685	H	-1.262928	2.150612	3.366915
C	-0.010128	0.121911	-4.117586	C	7.384072	2.643112	-0.756985	C	-2.450528	0.510112	4.155015
H	-0.823728	0.027811	-4.672686	H	7.537972	2.594412	0.180115	H	-2.494928	-0.456689	3.947615
H	-0.018728	1.027612	-3.716386	C	6.176472	2.204312	-1.285186	H	-2.090228	0.596511	5.074415
N	1.183472	-0.012889	-4.981386	C	6.788572	2.759912	-5.014186	C	-3.666728	0.977512	4.155015
C	1.350372	-1.446089	-5.281186	H	6.242272	2.001312	-5.306286	H	-3.994628	0.984412	3.221715
H	0.497272	-1.806289	-5.631186	H	7.669372	2.711612	-5.439986	H	-3.635928	1.918012	4.463715
H	2.037172	-1.553089	-5.986086	H	6.348472	3.597812	-5.269486	C	-4.740528	0.187811	5.058215
N	1.746672	-2.210389	-4.110186	O	5.387072	1.217212	0.732915	H	-4.753328	-0.756789	4.763315
C	3.130472	-1.831589	-3.762686	C	5.148772	1.801212	-0.281185	H	-4.421428	0.199311	5.996115
H	3.753972	-2.250089	-4.407686	O	3.921472	2.252012	-0.598485	C	-6.048629	0.661112	5.042115
H	3.346572	-2.179789	-2.861486	C	2.802272	1.917512	0.240015	H	-6.406329	0.688612	4.120415
C	2.373472	0.513711	-4.350286	C	2.820672	2.607312	1.514315	H	-6.103329	1.567412	5.438415
C	2.568472	1.898812	-4.356086	H	3.475072	3.248012	1.767715	C	-6.847929	-0.416789	5.947715
H	1.906272	2.467812	-4.730286	C	1.708372	2.192112	2.353015	H	-6.372429	-0.556989	6.793315
C	3.720272	2.445012	-3.820586	H	1.500672	2.739212	3.101915	H	-6.908429	-1.270289	5.463815
H	3.847372	3.385812	-3.838486	C	0.935572	1.079612	2.154915	H	-7.752529	-0.086189	6.132015
C	4.699072	1.624812	-3.251186	C	1.167772	0.338211	1.011915	H	-1.681343	-1.577243	-0.065025

Table 2.16 Xyz coordinates of the *unfolded* conformer structure of **5b**.

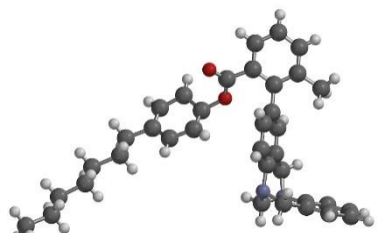
											
C	-0.985028	-1.693489	-0.903385	C	4.485672	0.249511	-3.234086	H	4.381005	1.67936	-9.37004
C	-0.946428	-0.777489	-1.948286	H	5.141272	-0.314689	-2.843086	C	5.223256	1.600195	-7.52322
H	-1.548428	-0.042989	-1.942086	C	3.332572	-0.324189	-3.777686	H	4.463294	1.911194	-7.0472
C	-0.045428	-0.908689	-3.009886	C	5.950572	2.202612	-2.674886	C	6.213552	1.225524	-11.177
C	0.831772	-1.993289	-3.022786	C	6.140627	2.241296	-1.283064	H	5.422944	1.767198	-11.4281
C	0.811772	-2.904289	-1.970886	C	7.294744	2.833648	-0.766115	H	7.016216	1.675517	-11.5431
H	1.423872	-3.631089	-1.965186	H	7.436630	2.831975	0.173324	C	6.093161	-0.10936	-11.7876
C	-0.091228	-2.758189	-0.937486	C	8.235730	3.424016	-1.592817	H	5.323963	-0.58609	-11.3837
H	-0.103128	-3.398489	-0.234685	H	9.001678	3.845865	-1.220375	H	6.91194	-0.63221	-11.5957
C	-0.010128	0.121911	-4.117586	C	8.053489	3.394781	-2.964325	C	5.879416	-0.01677	-13.4061
H	-0.823728	0.027811	-4.672686	H	8.689579	3.808178	-3.537654	H	5.101117	0.570206	-13.5776
H	-0.018728	1.027612	-3.716386	C	6.940832	2.762351	-3.504571	H	6.674839	0.430389	-13.7934
N	1.183472	-0.012889	-4.981386	C	5.137905	1.657102	-0.323898	C	5.691728	-1.13233	-14.0526
C	1.350372	-1.446089	-5.281186	H	4.237339	1.747703	-0.698079	H	4.960837	-1.62804	-13.6068
H	0.497272	-1.806289	-5.631186	H	5.186687	2.134603	0.529953	H	6.512965	-1.67947	-13.9689
H	2.037172	-1.553089	-5.986086	H	5.338284	0.708534	-0.178950	C	5.330693	-1.00513	-15.6165
N	1.746672	-2.210389	-4.110186	O	7.287078	3.544767	-5.726774	H	4.522978	-0.43934	-15.6995
C	3.130472	-1.831589	-3.762686	C	6.913997	2.678536	-4.994177	H	6.072929	-0.52665	-16.0657
H	3.753972	-2.250089	-4.407686	O	6.506032	1.472755	-5.429863	C	5.099359	-2.18918	-16.3093
H	3.346572	-2.179789	-2.861486	C	6.379789	1.232206	-6.841876	H	4.377292	-2.71516	-15.8848
C	2.373472	0.513711	-4.350286	C	7.657592	1.140805	-7.519275	H	5.920564	-2.7416	-16.3526
C	2.568472	1.898812	-4.356086	H	8.500363	1.191331	-7.083234	C	4.663866	-1.68141	-17.7835
H	1.906272	2.467812	-4.730286	C	7.481978	0.961347	-8.951048	H	5.31125	-1.02281	-18.1121
C	3.720272	2.445012	-3.820586	H	8.236616	0.666735	-9.448073	H	3.773798	-1.26676	-17.7374
H	3.847372	3.385812	-3.838486	C	6.321523	1.181280	-9.643214	H	4.632318	-2.44423	-18.3989
C	4.699072	1.624812	-3.251186	C	5.196208	1.510380	-8.911504	H	-1.68134	-1.57724	-0.06502

Table 2.17 Xyz coordinates of the *folded* conformer structure of **6**.

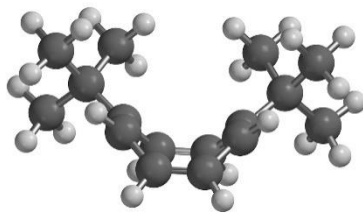
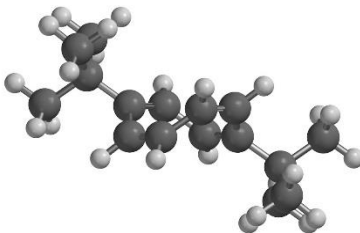
							
C	-0.613379	1.307298	0.659143	C	1.075673	1.355937	-3.420597
H	-0.532776	2.228820	1.231867	H	1.940678	1.219653	-4.080542
C	-0.391251	1.387831	-0.663760	H	1.247077	2.282106	-2.861817
H	-0.146922	2.368714	-1.066112	H	0.195015	1.504924	-4.056194
C	-0.923606	0.113977	1.447943	C	0.888156	-1.122634	-3.387578
C	-0.404178	0.302299	-1.645549	H	1.841990	-1.231585	-3.918062
C	-2.020183	-0.628806	1.182359	H	0.105588	-1.073541	-4.153444
H	-2.279139	-1.473773	1.813924	H	0.740099	-2.035213	-2.798478
C	-1.512549	-0.444760	-1.840895	C	1.500227	-0.209855	2.169404
H	-1.535078	-1.204010	-2.617384	H	2.177347	-0.424557	3.004790
C	-2.788312	-0.315367	-1.168246	H	1.821777	0.745007	1.739564
H	-3.644051	-0.203402	-1.830905	H	1.651112	-0.990590	1.416232
C	-3.009890	-0.395702	0.151382	C	-0.240584	-1.531865	3.334714
H	-4.036741	-0.345775	0.507791	H	0.490647	-1.721522	4.129959
C	0.029600	-0.173590	2.640483	H	-0.170755	-2.365448	2.626178
C	0.890737	0.138620	-2.488078	H	-1.230604	-1.557985	3.804344
C	2.128414	0.017898	-1.571804	C	-0.123164	0.921292	3.719163
H	3.044653	-0.110110	-2.160513	H	0.482501	0.690983	4.603732
H	2.041409	-0.849086	-0.908215	H	-1.165498	1.011662	4.046441
H	2.273588	0.908814	-0.951232	H	0.202373	1.903342	3.359991
C	-0.613379	1.307298	0.659143	C	1.075673	1.355937	-3.420597
H	-0.532776	2.228820	1.231867	H	1.940678	1.219653	-4.080542

Table 2.18 Xyz coordinates of the *unfolded* conformer structure of **6**.

							
C	1.157547	1.008331	1.470149	H	3.117349	2.359015	-1.875270
H	1.328209	1.770667	2.226343	H	2.060111	1.815656	-3.187661
C	1.387160	1.308008	0.181756	C	2.518239	-0.916750	-2.833000
H	1.724720	2.314115	-0.054429	H	3.473727	-1.034964	-3.358447
C	0.743813	-0.281103	1.971220	H	1.761184	-0.711384	-3.598546
C	1.295270	0.383053	-0.950592	H	2.285455	-1.880251	-2.364799
C	-0.384760	-0.924612	1.632539	H	1.401203	-0.726728	2.713761
H	-0.588953	-1.879709	2.110114	C	-2.843490	-0.314370	1.334427
C	0.138831	-0.250630	-1.245823	C	-3.414022	-1.719175	1.625091
H	0.073746	-0.894525	-2.118512	H	-2.834472	-2.250821	2.387263
C	-1.139193	-0.131987	-0.564785	H	-3.423660	-2.337184	0.719702
H	-1.929284	0.184822	-1.239923	H	-4.444332	-1.657545	1.995079
C	-1.421337	-0.431270	0.722418	C	-3.856931	0.404730	0.410032
C	2.595433	0.219493	-1.783398	H	-3.512836	1.410805	0.143298
C	3.790630	-0.116661	-0.861168	H	-4.830853	0.515893	0.902114
H	4.702722	-0.291948	-1.443968	H	-4.033393	-0.157686	-0.514044
H	3.594030	-1.020963	-0.273326	C	-2.801380	0.495026	2.651662
H	4.014800	0.697222	-0.162637	H	-2.368931	1.489536	2.490697
C	2.902861	1.523667	-2.550267	H	-2.211584	-0.007532	3.426373
H	3.780724	1.403730	-3.196178	H	-3.808353	0.634024	3.062732

2.7 References

- (1) Lins, L.; Brasseur, R. The Hydrophobic Effect in Protein Folding. *FASEB J.* **1995**, *9* (7), 535–540.
- (2) Dyson, H. J.; Wright, P. E.; Scheraga, H. A. The Role of Hydrophobic Interactions in Initiation and Propagation of Protein Folding. *Proc. Natl. Acad. Sci.* **2006**, *103* (35), 13057–13061.
- (3) Spolar, R. S.; Ha, J. H.; Record, M. T. Hydrophobic Effect in Protein Folding and Other Noncovalent Processes Involving Proteins. *Proc. Natl. Acad. Sci.* **1989**, *86* (21), 8382–8385.
- (4) Maibaum, L.; Dinner, A. R.; Chandler, D. Micelle Formation and the Hydrophobic Effect. *J. Phys. Chem. B* **2004**, *108* (21), 6778–6781.
- (5) Killian, J. A.; von Heijne, G. How Proteins Adapt to a Membrane–Water Interface. *Trends Biochem. Sci.* **2000**, *25* (9), 429–434.
- (6) Rodrigues, R. C.; Ortiz, C.; Berenguer-Murcia, Á.; Torres, R.; Fernández-Lafuente, R. Modifying Enzyme Activity and Selectivity by Immobilization. *Chem. Soc. Rev.* **2013**, *42* (15), 6290–6307.
- (7) Bert, J.; van Tol, A.; Odenthal, J. B.; Jongejan, J. A.; Duine, J. A. Relation of Enzymatic Reaction Rate and Hydrophobicity of the Solvent *Progress in Biotechnology*; Tramper, J., Vermüe, M. H.; Beftink, H. H.; von Stockar, U.; Eds.; Elsevier, **1992**; Vol. 8, pp 229–235.
- (8) Breslow, R. Hydrophobic Effects on Simple Organic Reactions in Water. *Acc. Chem. Res.* **1991**, *24* (6), 159–164.
- (9) Blokzijl, W.; Engberts, J. B. F. N. Hydrophobic Effects. Opinions and Facts. *Angew. Chem. Int. Ed.* **1993**, *32* (11), 1545–1579.
- (10) Qian, J.; Timko, M. T.; Allen, A. J.; Russell, C. J.; Winnik, B.; Buckley, B.; Steinfeld, J. I.; Tester, J. W. Solvophobic Acceleration of Diels–Alder Reactions in Supercritical Carbon Dioxide. *J. Am. Chem. Soc.* **2004**, *126* (17), 5465–5474.
- (11) Sedov, I. A.; Stolov, M. A.; Solomonov, B. N. Solvophobic Effects and Relationships between the Gibbs Energy and Enthalpy for the Solvation Process: Solvophobic Effects. *J. Phys. Org. Chem.* **2011**, *24* (11), 1088–1094.
- (12) Otto, S. The Role of Solvent Cohesion in Nonpolar Solvation. *Chem. Sci.* **2013**, *4* (7), 2953.
- (13) Yang, L.; Adam, C.; Cockroft, S. L. Quantifying Solvophobic Effects in Nonpolar Cohesive Interactions. *J. Am. Chem. Soc.* **2015**, *137* (32), 10084–10087.
- (14) Pindur, Ulf.; Lutz, Gundula.; Otto, Christian. Acceleration and Selectivity Enhancement of Diels–Alder Reactions by Special and Catalytic Methods. *Chem. Rev.* **1993**, *93* (2), 741–761.
- (15) Cui, D.; Ebrahimi, M.; Rosei, F.; Macleod, J. M. Control of Fullerene Crystallization from 2D to 3D through Combined Solvent and Template Effects. *J. Am. Chem. Soc.* **2017**, *139* (46), 16732–16740.
- (16) Yamagishi, H.; Tsunoda, M.; Iwai, K.; Hengphasatporn, K.; Shigeta, Y.; Sato, H.; Yamamoto, Y. Solvophobicity-Directed Assembly of Microporous Molecular Crystals. *Commun. Chem.* **2021**, *4* (1), 122.

- (17) Greaves, T. L.; Drummond, C. J. Solvent Nanostructure, the Solvophobic Effect and Amphiphile Self-Assembly in Ionic Liquids. *Chem. Soc. Rev.* **2013**, 42 (3), 1096–1120.
- (18) Marmur, A. Dissolution and Self-Assembly: The Solvophobic/Hydrophobic Effect. *J. Am. Chem. Soc.* **2000**, 122 (9), 2120–2121.
- (19) Yang, L.; Adam, C.; Nichol, G. S.; Cockroft, S. L. How Much Do van Der Waals Dispersion Forces Contribute to Molecular Recognition in Solution? *Nat. Chem.* **2013**, 5, 1006–1010.
- (20) Wilming, F. M.; Becker, J.; Schreiner, P. R. Quantifying Solvophobic Effects in Organic Solvents Using a Hydrocarbon Molecular Balance. *J. Org. Chem.* **2022**, 87 (3), 1874–1878.
- (21) Adam, C.; Yang, L.; Cockroft, S. L. Partitioning Solvophobic and Dispersion Forces in Alkyl and Perfluoroalkyl Cohesion. *Angew. Chem. Int. Ed.* **2015**, 54, 1164–1167.
- (22) Yang, L.; Brazier, J. B.; Hubbard, T. A.; Rogers, D. M.; Cockroft, S. L. Can Dispersion Forces Govern Aromatic Stacking in an Organic Solvent. *Angew. Chem. Int. Ed.* **2016**, 55, 912–916.
- (23) Iwase, K.; Komatsu, K.; Hirono, S.; Nakagawa, S.; Moriguchi, I. Estimation of Hydrophobicity Based on the Solvent-Accessible Surface Area of Molecules. *Chem. Pharm. Bull.* **1985**, 33 (5), 2114–2121.
- (24) Nakamura, K.; Houk, K. N. Theoretical Studies of the Wilcox Molecular Torsion Balance. Is the Edge-to-Face Aromatic Interaction Important? *Org. Lett.* **1999**, 1, 2049–2051.
- (25) Tomar, D. S.; Ramesh, N.; Asthagiri, D. Solvophobic and Solvophilic Contributions in the Water-to-Aqueous Guanidinium Chloride Transfer Free Energy of Model Peptides. *J. Chem. Phys.* **2018**, 148 (22), 222822.
- (26) Reynolds, J. A.; Gilbert, D. B.; Tanford, C. Empirical Correlation Between Hydrophobic Free Energy and Aqueous Cavity Surface Area. *Proc. Natl. Acad. Sci.* **1974**, 71 (8), 2925–2927.
- (27) Paliwal, S.; Geib, S.; Wilcox, C. S. Chemistry of Synthetic Receptors and Functional-Group Arrays .24. Molecular Torsion Balance for Weak Molecular Recognition Forces - Effects of Tilted-T Edge-to-Face Aromatic Interactions on Conformational Selection and Solid-State Structure. *J. Am. Chem. Soc.* **1994**, 116, 4497–4498.
- (28) Mati, I. K.; Cockroft, S. L. Molecular Balances for Quantifying Non-Covalent Interactions. *Chem. Soc. Rev.* **2010**, 39, 4195–4205.
- (29) Li, P.; Vik, E.C.; Shimizu, K.D. Arylimide Molecular Balances: A Comprehensive Platform for Studying Aromatic Interactions in Solution. *Acc. Chem. Res.* **2020**, 53 (11), 2705–2714.
- (30) Kishikawa, K.; Yoshizaki, K.; Kohmoto, S.; Yamamoto, M.; Yamaguchi, K.; Yamada, K. Control of the Rotational Barrier and Spatial Disposition of the N-(2'-Methylphenyl) Group in Succinimides by Substituent and Solvent Effects. *J. Chem. Soc. Perkin 1* **1997**, 1233–1239.
- (31) Verma, S. M.; Singh, N. B. A Study of Conformation about the Aryl C-N Bond in N-Aryl Imides by Dynamic N.M.R. Spectroscopy. *Aust J Chem* **1976**, 29, 295–300.
- (32) Grossmann, G.; Potrzebowski, M. J.; Olejniczak, S.; Ziolkowska, N. E.; Bujacz, G. D.; Ciesielski, W.; Prezdo, W.; Nazarov, V.; Golovko, V. Structural Studies of N-(2'-Substituted Phenyl)-9,10-Dihydro-9,10-Ethanoanthracene-11,12-Dicarboximides

- by X-Ray Diffraction and NMR Spectroscopy - Proofs for CH/Pi Interactions in Liquid and Solid Phases. *New J Chem* **2003**, 27, 1095–1101.
- (33) Marshall, K.; Rothchild, R. NMR Studies of Hindered Rotation and Magnetic Anisotropy: The Diels-Alder Adducts of Phencyclone with N-Phenylmaleimide and N-(2-Trifluoromethylphenyl)Maleimide. Ab Initio Calculations for Optimized Structures. *Spectrosc. Lett.* **2004**, 37, 469–492.
 - (34) Cobb, S.; Murphy, C. F-19 NMR Applications in Chemical Biology. *J. Fluor. Chem.* **2009**, 130, 132–143.
 - (35) Abboud, J. L. M.; Notario, R. Critical Compilation of Scales of Solvent Parameters. Part I. Pure, Non-Hydrogen Bond Donor Solvents - Technical Report. *Pure Appl. Chem.* **1999**, 71, 645–718.
 - (36) Marcus, Y. Internal Pressure of Liquids and Solutions. *Chem. Rev.* **2013**, 113 (8), 6536–6551.
 - (37) Dack, M. R. J. The Importance of Solvent Internal Pressure and Cohesion to Solution Phenomena. *Chem. Soc. Rev.* **1975**, 4 (2), 211.
 - (38) Li, P.; Hwang, J.; Maier, J. M.; Zhao, C.; Kaborda, D. V.; Smith, M. D.; Pellechia, P. J.; Shimizu, K. D. Correlation between Solid-State and Solution Conformational Ratios in a Series of N-(o-Tolyl)Succinimide Molecular Rotors. *Cryst. Growth Des.* **2015**, 15, 3561–3564.
 - (39) Schümann, J. M.; Wagner, J. P.; Eckhardt, A. K.; Quanz, H.; Schreiner, P. R. Intramolecular London Dispersion Interactions Do Not Cancel in Solution. *J. Am. Chem. Soc.* **2021**, 143 (1), 41–45.
 - (40) Sharp, K. A.; Nicholls, A.; Fine, R. F.; Honig, B. Reconciling the Magnitude of the Microscopic and Macroscopic Hydrophobic Effects. *Science* **1991**, 252, 106–109.
 - (41) Rizzo, V.; Pincioli, V. Quantitative NMR in Synthetic and Combinatorial Chemistry. *J. Pharm. Biomed. Anal.* **2005**, 38 (5), 851–857.
 - (42) Abboud, J. L. M.; Notario, R. Critical Compilation of Scales of Solvent Parameters. Part I. Pure, Non-Hydrogen Bond Donor Solvents - Technical Report. *Pure Appl. Chem.* **1999**, 71, 645–718
 - (43) Dack, M. R. J. The Importance of Solvent Internal Pressure and Cohesion to Solution Phenomena. *Chem. Soc. Rev.* **1975**, 4 (2), 211.
 - (44) Abbott, S. *Adhesion Science: Principles and Practice*; DEStech Publications, Inc: Lancaster, PA, **2015**.

CHAPTER 3

PROBING SOLVENT EFFECTS IN CH-ARENE INTERACTIONS WITH MOLECULAR TORSIONAL BALANCES AND MULTIPARAMETER LINEAR SOLVATION ENERGY RELATIONSHIPS

3.1. Abstract

The goal of this project was to characterize organic solvent effects of CH-arene interactions for varying size surfaces using molecular devices and correlate the changes with solvent parameters. Molecular torsional balances were employed to determine the relationship between solvent accessible surface area (SASA), solvent parameters, and CH-arene interaction energies in organic solvents. The relative populations of *syn*- and *anti*-conformers were measured using ^1H NMR and used to calculate balance folding energies (ΔG). ΔG was proportional to the ΔSASA of the *syn*- and *anti*- conformers, which is consistent with the solvophobic effect, even with different kinds of CH-arene interactions. Solvent parameters from Kamlet-Taft, Catalán, and Lawrence linear solvation energy relationship (LSER) model parameters were correlated with ΔG . While several parameters correlated well with ΔG for balances which could only form intramolecular CH- π interactions, correlation was poor with balances that could also form CH-arene edge interactions, further suggesting that both interactions experienced similar solvent effects.

3.2 Introduction

Interactions between aliphatic and aromatic systems, i.e. CH-arene interactions present themselves in different forms. CH- π interactions are weak attractive non-covalent interactions between a hydrocarbon and an aromatic π -system acting as a soft-acid and soft-base respectively.¹ CH- π interactions are pervasive in synthetic chemistry and biology, specifically in protein folding,² molecular recognition,³ and reaction catalysis.⁴ CH- π interactions have been examined in aqueous and organic solvent environments.⁵⁻⁸ For example, Emenike et al. demonstrated competitive attractions of the methyl-arene

interactions in a variety of organic solvents and modeled the solvent effects.⁹ Closely related are CH- arene edge interactions, which are driven by stabilizing dispersion forces between the aliphatic group and the edge of an arene.^{9,10}

However, previous studies have either varied the solvent for a fixed-sized surface and do not measure how the interactions vary with solvent accessible surface areas (SASA), or have varied surface area without changing solvent. Thus our studies can provide a more general picture of CH-arene interactions and potentially provide a comprehensive, predictive model for all solvents and varying sized surfaces based on the solvent parameters and the solute's Δ SASA.

Therefore, our goal was to design a system to measure the CH-arene interactions' energy as a function of SASA and solvent parameters. Uniparameter relationships are a common method for estimating thermodynamic and kinetic processes. For example, empirical solvent parameters such as ET(30) and *ced* have been shown to correlate the solvent dependence of solute-solute interaction energies.¹² However, uniparameter relationships are limited in processes that are made of multiple major components. Since CH-arene interactions are combinations of dispersion, charge-transfer^{13,14} and solvophobic which are all multi-component interactions, single parameter models are limited in accuracy and in providing insight into the underlying component forces.

The general composition of most linear solvation energy relationship (LSER) models are four parameters describing both the hydrogen bonding and electrostatic interactions of the solvent with both solute and other solvent molecules. ΔG° is a constant describing gas phase solute-solute interaction. Furthermore, coefficients for the individual

parameters denote the importance or weight of the parameter. The combination of these components allow LSER models to make accurate and comprehensive descriptions of complex solvent effect processes.

Because solvent effects are also heavily correlated with SASA of the solute, an aim of this project was to monitor the change in LSER parameter coefficients with solute SASA in order to generate a more general and comprehensive model of the solvent effects for the CH-arene interaction.

3.3 Description of Solvent LSER Models

The most commonly used solvent LSER parameters are Kamlet-Taft parameters (K-T) α , β , and π^* derived from the shift in wavelength of solvatochromic dyes (**Equation 3.1**).¹⁵⁻¹⁶ Respectively, the parameters describe a solvent's hydrogen bond donating, hydrogen bond accepting, polarizability. The additional δ parameter is used as a correction factor for π^* in aromatics and polychlorinated solvents. Furthermore, each parameter has a coefficient which modifies the overall contribution to ΔG .

$$\text{Equation 3.1 } \Delta G = \Delta G^\circ + a\alpha + b\beta + s(\pi^* + d\delta)$$

The K-T parameters have been extensively used in modeling the behavior and properties of ionic liquids, and have been successfully employed by Emenike in describing trends in CH- π interaction molecular balance systems.¹¹

Other LSER parameters have been developed to model solvent effects. Catalán developed solvent parameters also derived from empirical measurements from solvatochromic dyes for solvent acidity (SA), basicity (SB), dipolarity (SdP), and

polarizability (SP) (**Equation 3.2**).¹⁷ Coefficients b , c , d , and e modify these parameters respectively.

$$\text{Equation 3.2 } \Delta G = \Delta G^\circ + bSA + cSB + dSP + eSdP$$

Laurence and coworkers developed a multiparameter solvent model which gauges the components of dispersion and induction (DI), electrostatics (ES), hydrogen bond acidity ($\alpha 1$), and hydrogen bond basicity ($\beta 1$) (**Equation 3.3**).¹⁸ It was demonstrated that the LSER predict many solvent properties such as solvolysis rates and solvent conformer equilibrium.¹⁸

$$\text{Equation 3.3 } \Delta G = \Delta G^\circ + di(DI) + eES + a\alpha 1 + b\beta 1$$

In our study, we tested all three multiparameter LSER for their ability to model CH-arene interaction energies for a series of molecular balances with varying SASA in solvents of varying polarities to develop a comprehensive predictive model and to determine if any specific solvent parameter was dominant in the observed solvent effects.

3.4 Experimental Design

Molecular torsional balances **1-7** were designed with *ortho*-alkyl groups X which can form intramolecular CH- π position or *meta*-alkyl groups Y groups which form CH-arene interactions with the edge of the aromatic shelf (**Figure 3.1**). The ability for X and Y to for the respective interactions was confirmed with molecular modeling, showing similar interaction distances from the X and Y groups to the arene as previous studies.^{10,19} The X and Y groups are on the opposite side of the *N*-phenyl group, thus only one can form an interaction with the aromatic surface per conformer. Since the X and Y groups form

different types of interactions, another question was whether they could be fitted to a single solvent model, which would suggest that solvent effects were dominant and not specific CH-surface interactions. The *N*-arylsuccinimide framework provided a rotational barrier which allowed for conformer populations to be easily observed on the ^1H NMR timescale.

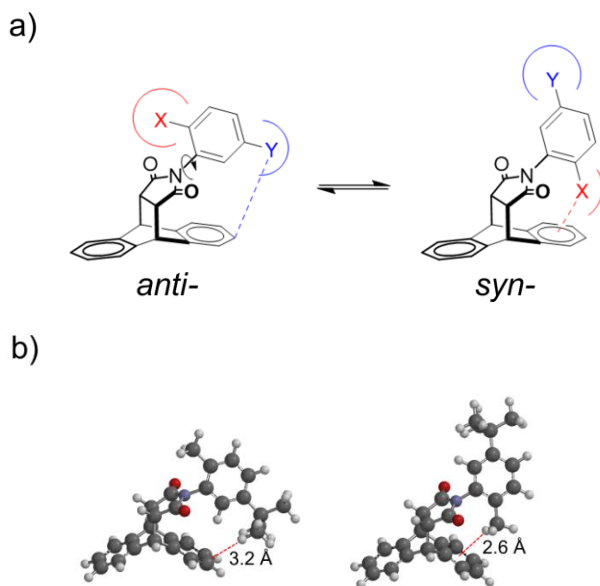


Figure 3.1 a) Equilibrium of torsional molecular balances between the *anti*- and *syn*- conformers, with the total SASA varying between conformers. While X could form CH- π interactions in the *syn*- conformer, while Y could form solvophobic interactions in the *anti*- conformer, b) balance **2** with measured distances from the Y group to the arene edge in the *anti*- conformer and the X group to the arene center in the *syn*- conformer.

Models of the *syn*- and *anti*- conformers of the balances were developed using Spartan18 in order to calculate the ΔSASA between the *syn*- and *anti*- conformers. The lowest energy configurations for the *syn*- and *anti*- conformers were estimated from the density functional theory minimized structures (density functional theory, B3LYP-D3, 6-311G*). The ΔSASA was calculated using the same structures and a 1 Å surface probe.

Table 3.1 Calculated SASA and Δ SASA of alkyl-aryl balances, calculated using a 1 Å surface probe.

	Balance Numbers						
Substituent	1	2	3	4	5	6	7
X	Me	Me	Me	Me	Me	Et	<i>i</i> -Pr
Y	Adm	<i>t</i> -Bu	<i>i</i> -Pr	Me	H	H	H
SASA <i>syn</i> (Å²)	254.2	236.3	230.9	216.6	206.9	208.3	209.3
SASA <i>anti</i> (Å²)	246.7	229.4	227.4	216.6	210.9	215.5	222.0
ΔSASA (<i>syn</i> - <i>anti</i> Å²)	7.4	6.9	3.5	-0.1	-4.0	-6.0	-12.9

The Δ G for the *syn*- and *anti*- equilibria were measured via integration of the 1D ¹H NMR spectra at 23 °C.²⁰ The *syn*-/*anti*- ratio was measured from the separate signals for the 2-methyl groups in balances **1-5**, the 2-ethyl groups in balance **6**, and the 2-*i*-propyl groups in balance **7**. Conformer peak assignments were based on previous work.²¹ The *syn*/*anti* conformer population ratio (*K*), was put into Gibbs free energy equation to provide the Δ G. Negative Δ G values were indicative of systems with more stable *syn*- conformers. Five solvents (chloroform-*d*, benzene-*d*₆, dichloromethane-*d*₂, acetonitrile-*d*₃, and DMSO-*d*₆) and 3 DMSO-*d*₆/water mixtures (91% DMSO-*d*₆, 78% DMSO-*d*₆, and 67% DMSO-*d*₆ by volume) were used to obtain 8 different solvent measurements per balance,

for a total of 56 measurements. Solutions were left for thirty min. before measurements to ensure they had reached equilibrium.

3.5 Results and Discussion

The folding energies (ΔG) of the molecular balances fell between 0.63 and -0.44 kcal/mol. Within a single solvent, balances with larger $\Delta SASA$ values conformers showed a greater preference for the *syn*- conformer, which is consistent with solvophobic effects influencing the conformer ratio. The slopes between $\Delta SASA$ and ΔG were similar to previous studied by Cockroft et al.²² Interestingly, although balances **4-7** were only capable of making CH- π interactions and **1-3** could form CH- π and CH-arene edge interactions (**Figure 3.2**), the solvophobic effects for both systems could be represented with a single model. This would suggest that solvophobicity in both kinds of interactions are similar.

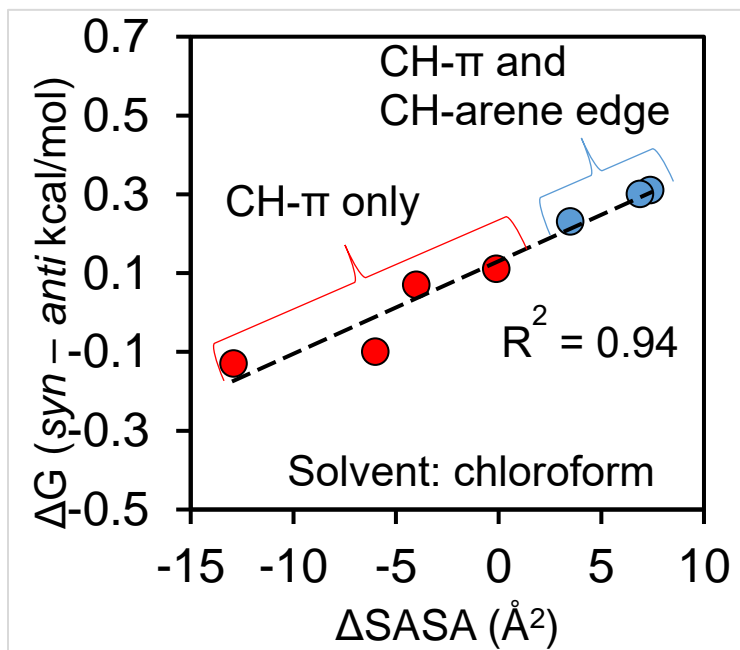


Figure 3.2 ΔG between *syn*- and *anti*- conformers compared against $\Delta SASA$ in chloroform-d, demonstrating similar solvent effects between balances which could only form CH- π interactions and those which could also form CH-arene edge interactions.

While there were several good correlations between ΔG and solvent parameters in balances which could only form CH- π interactions, no individual parameter consistently correlated well with balances which could form CH- π and significant CH-arene edge interactions. Consistent with Emenike's findings, hydrogen accepting and basicity parameters most commonly had the best correlation with ΔG values.⁹ This suggests that preference for the *syn*- conformer is largely driven by the solvation of the aryl protons exposed to the solvent environment. Other parameters which showed modest correlation include dipolarizability and electrostatics, as they are chief components in the CH- π interaction. Solvent *ced* showed a good correlation with ΔG in balances **4-7**, further indicating that solvophobic effects are significant contributors to the overall interaction. However, balances **1-3** which could form significant CH-arene edge interactions did not have good correlations between ΔG solvent parameters. One explanation for this is that CH- arene edge interactions in the *anti*- conformer are driven by similar solvent effects to CH- π interactions. Thus, the solvent effects will promote both conformers, and thus their overall effect on ΔG is masked. Furthermore, because larger Y groups hinder interactions between adjacent aryl hydrogens and solvent molecules, it would make sense that larger Y groups are associated with decreased correlation between ΔG and hydrogen acceptor and basicity parameters.

Table 3.2 Kamlet-Taft parameters' correlation to ΔG . Parameters taken from literature.¹⁶

Kamlet-Taft parameters				
Solvent	α	β	π^*	δ
CDCl₃	0.20	0.10	0.58	0.50
C₆D₆	0.00	0.10	0.59	1.00
CD₂Cl₂	0.13	0.10	0.82	0.50
CD₃CN	0.19	0.40	0.75	0.00
d6-DMSO	0.00	0.76	1.00	0.00
91% d6-DMSO:D₂O	0.11	0.73	1.01	0.00
78% d6-DMSO:D₂O	0.26	0.70	1.02	0.00
67% d6-DMSO:D₂O	0.39	0.66	1.03	0.00
ΔG vs parameter R²				
1	0.01	0.60	0.57	0.30
2	0.01	0.67	0.81	0.68
3	0.02	0.80	0.80	0.40
4	0.00	0.96	0.83	0.54
5	0.03	0.80	0.63	0.31
6	0.03	0.82	0.94	0.58
7	0.01	0.89	0.74	0.84

Table 3.3 Catalán parameters' correlation to ΔG . Parameters taken from literature.¹⁷

Catalán parameters				
Solvent	SP	SdP	SA	SB
CDCl₃	0.78	0.61	0.05	0.07
C₆D₆	0.79	0.27	0.00	0.12
CD₂Cl₂	0.76	0.77	0.04	0.18
CD₃CN	0.65	0.97	0.04	0.29
d6-DMSO	0.83	1.00	0.07	0.65
91% d6-DMSO:D₂O	0.82	1.00	0.16	0.59
78% d6-DMSO:D₂O	0.80	1.00	0.29	0.51
67% d6-DMSO:D₂O	0.78	1.00	0.40	0.44
ΔG vs parameter R²				
1	0.61	0.29	0.35	0.65
2	0.18	0.75	0.33	0.74
3	0.48	0.40	0.44	0.86
4	0.24	0.50	0.55	0.94
5	0.17	0.27	0.40	0.79
6	0.13	0.62	0.70	0.82
7	0.00	0.79	0.35	0.84

Table 3.4 Laurence parameters' correlation to ΔG . Parameters taken from literature.¹⁸

Laurence parameters				
Solvent	DI	ES	α_1	β_1
CDCl₃	0.80	0.40	0.20	0.00
C₆D₆	0.87	0.23	0.00	0.14
CD₂Cl₂	0.78	0.60	0.10	0.00
CD₃CN	0.67	0.84	0.23	0.37
d6-DMSO	0.84	1.00	0.00	0.71
91% d6-DMSO:D₂O	0.82	0.99	0.14	0.68
78% d6-DMSO:D₂O	0.80	0.98	0.34	0.64
67% d6-DMSO:D₂O	0.78	0.96	0.51	0.60
ΔG vs parameter R²				
1	0.23	0.41	0.00	0.53
2	0.00	0.78	0.02	0.54
3	0.15	0.59	0.00	0.75
4	0.05	0.74	0.02	0.95
5	0.07	0.52	0.00	0.89
6	0.00	0.80	0.10	0.78
7	0.06	0.93	0.07	0.87

3.6 Conclusions and Future Work

We developed a molecular torsional balance system for observing how solvent effects influence CH-arene interactions in organic solvents. It was demonstrated that the solvophobic effects are similar between CH- π interactions and CH-arene edge interactions, and that similar solvent parameters dominate the solvent effects between the two interactions. In future studies, it would be advantageous to design balances with only Y groups to further study CH-arene edge interactions.

3.7 Special Acknowledgements

Special thanks to Dr. Sheri Strickland and her students for all synthesis, collecting ^1H NMR data from molecular balances, and preliminary supplemental information entries. Special thanks to Erik Vik for calculating SASA for balances **1-5**.

3.8 Supplemental Information

3.8.1 General Experimental Information

NMR spectra were recorded on Bruker 300 or 400 MHz spectrometers. Chemical shifts are recorded in ppm (δ) and were internally referenced. All chemicals were purchased from commercial suppliers and used as received unless otherwise specified. Flash chromatography was carried out using silica gel from Fisher Scientific (230x400 Mesh). HRMS were measured using a magnetic sector spectrometer (VG 70S) using EI sources.

3.8.2 Synthesis

Table 3.5 References for synthesis procedures of molecular torsional balances

Balance	X	Y	Reference
1	Me	Adm	This project
2	Me	<i>t</i> -Bu	This project
3	Me	<i>i</i> -Pr	This project
4	Me	Me	Weber 1991 ²³ Srivastav 1993 ²⁴
5	Me	H	Weber 1991 ²³ Grossman 2003 ²⁵
6	Et	H	Raimondi 2014 ²⁶
7	<i>i</i> -Pr	H	Raimondi 2014 ²⁶

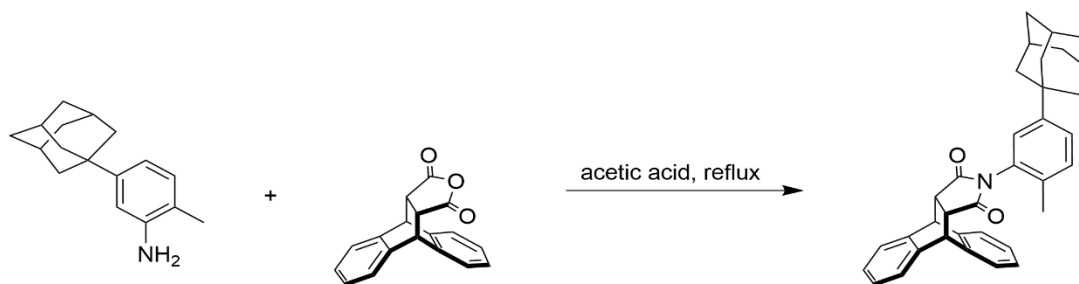


Figure 3.3 Synthesis of balance 1.

The solid 9,10-dihydro-9,10-ethanoanthracene-11,12-dicarboxylic anhydride (0.1151 g, 0.4166 mmol) and the solid 2-methyl-5-adamantylbenzeneamine (0.1040 g, 0.4309 mmol), and 1.0 mL glacial acetic acid were placed in an oven-dried 35-mL high pressure tube equipped with magnetic stir bar. After heating at 125°C for 42 h, the tan suspension was cooled to room temperature, and the acetic acid was removed under vacuum. The residue was mixed with 5 mL methanol, sonicated for 2 min. , and chilled at 0 °C for 1 h, yielding a white solid and a pale-yellow supernatant. Filtration under vacuum yielded the title compound (0.1624 g, 78%) as a white solid. ^1H NMR (400 MHz, CDCl_3) δ = 7.45-7.01 (m, 10 H, major and minor), 6.85 (d, J = 1.85, 1 H minor), 5.42 (d, J = 1.85, 1H, major), 4.91 (s, 1 H, minor), 4.90 (s, 1H, major), 3.40 (s, 1 H, major and minor), 2.12 - 2.02 (m, 3 H, major and minor), 2.01 (s, 3 H, major), 1.87- 1.67 (m, 12 H, major and minor), 1.01 (s, 3 H, minor). ^{13}C NMR (100 MHz, CDCl_3) δ = 176.1, 176.0, 147.5, 147.3, 142.0, 141.3, 139.3, 139.0, 133.3, 132.4, 130.8, 130.4, 127.8, 127.6, 127.3, 127.2, 127.1, 126.8, 126.7, 125.6, 125.5, 125.3, 125.1, 124.3, 124.2, 77.4, 77.0, 76.6, 47.2, 47.1, 45.9, 45.3, 33.4, 33.2, 23.8, 23.7, 17.1 (major), 15.9 (minor). HRMS (EI) ($\text{C}_{35}\text{H}_{33}\text{NO}_2$) $^+$ M calculated 499.2511, observed 499.2509.

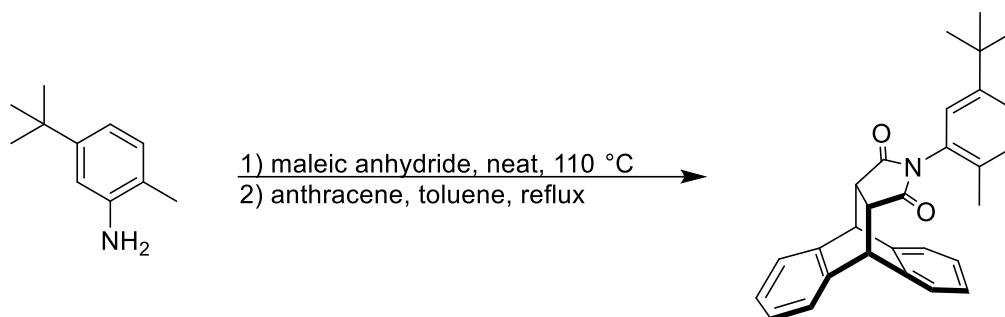


Figure 3.4 Synthesis of balance **2**.

The liquid 2-methyl-5-(1,1-dimethylethyl)benzenamine (0.1046 g, 6.406 mmol) and maleic anhydride (0.1894 g, 1.931 mmol) were added into a 25 ml round bottom flask. The reaction mixture was flushed with N₂ and heated at 110 °C under N₂ for 92 h without solvent. The product mixture was a golden brown solid (0.1160 g, 74%) and was used without further purification. Anthracene (0.1062 g, 0.5958 mmol) was mixed with 7 mL reagent-grade toluene in an oven-dried 35-mL high pressure tube equipped with a magnetic stir bar. A solution of the maleimide in 2 mL toluene was added dropwise with stirring at room temperature, followed by a 1 mL toluene rinse. This golden-brown reaction mixture was heated at 120 °C for 65 h, and the solvent was removed under vacuum. The golden-brown residue was mixed with 10 mL methanol, sonicated for 2 min, and chilled at 0 °C for 1 h. Filtration under vacuum yielded the title compound (0.1253 g, 46%) as a tan solid. ¹H NMR (400 MHz, CDCl₃) δ = 7.44-7.12 (m, 9 H, major and minor), 7.07 (dd, 1 H, major and minor), 6.88 (d, 1.85, 1 H, minor), 5.49 (d, 1.85, 1 H, major), 4.90 (s, 2 H, major and minor), 3.40 (s, 2 H, major and minor), 2.01 (s, 3 H, major), 1.25 (s, 9 H, minor), 1.17 (s, 9 H, major), 1.01 (s, 3 H, minor). ¹³C NMR (100 MHz, CDCl₃) δ = 176.1, 176.0, 150.0, 142.0, 141.4, 141.4, 139.3, 138.9, 130.3, 127.4, 127.2, 126.8, 126.8, 126.6, 125.5, 125.3, 124.5, 124.4, 124.4, 124.2, 47.2, 47.1, 45.9, 45.4, 34.4, 31.2, 17.0. HRMS (EI) (C₂₉H₂₇NO₂)⁺ M calculated 421.2042, observed 421.2048.

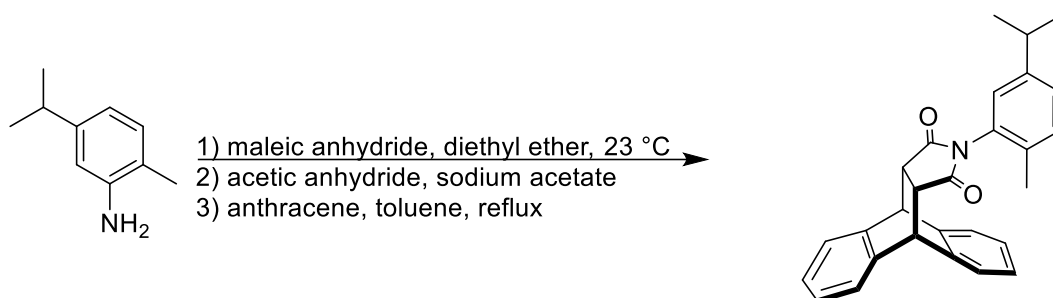


Figure 3.5 Synthesis of balance **3**.

Maleic anhydride (0.2290 g, 2.335 mmol) was dissolved in 25 mL anhydrous diethyl ether, and a mixture of 2-methyl-5-(1-methylethyl)benzenamine (0.5010 g, 3.357 mmol) in 20 mL anhydrous diethyl ether was added dropwise with magnetic stirring at 23 °C. This amber reaction mixture was allowed to stir at room temperature for 48 h, followed by removal of the solvent under vacuum. The residue (a dark brown oil) was used without further purification (0.1817 g, 74%). Anthracene (0.1075 g, 0.6031 mmol) was mixed with 7 mL reagent-grade toluene in an oven-dried 35-mL high pressure tube equipped with a magnetic stir bar. A solution of the maleimide in 2 mL toluene was added dropwise with stirring at room temperature, followed by a 1-mL toluene rinse. This pale yellow reaction mixture was heated at 140 °C for 24 h, and the solvent was removed under vacuum. The off-white solid residue was mixed with 10 mL methanol, sonicated for 2 min., and chilled at 0 °C for 1 h. Filtration under vacuum yielded the title compound (0.1654 g, 67%) as a white solid. ^1H NMR (400 MHz, CDCl_3) δ = 8.40 - 6.97 (m, 11 H, major and minor), 6.76 (s, 1 H, minor), 5.31 (s, 1 H, major), 4.91 (s, 2 H, minor), 4.90 (2, 2 H, major), 3.40 (s, 2 H, major and minor) 2.82 (m, J = 6.87, 1 H, minor), 2.70 (m, J = 6.87, 1 H, major), 2.01 (s, 3 H, major), 1.18 (d, J = 6.87, 6 H, minor), 1.12 (d, J = 6.87, 6 H, major), 1.01 (s, 3 H, minor). ^{13}C NMR (100 MHz, CDCl_3) δ = 176.1, 176.0, 142.0, 141.3, 139.3, 139.0, 132.4, 130.5, 127.9, 127.6, 127.4, 127.1, 126.9, 126.8, 125.7, 125.5, 125.3, 125.1, 124.4, 124.2,

77.5, 77.0, 76.6, 47.2, 47.1, 45.9, 45.4, 33.4, 33.3, 23.8, 23.7, 17.1, 16.0. HRMS (EI) $(C_{28}H_{25}NO_2)^+$ M calculated 407.1885, observed 407.1904.

3.8.3 Crystallography Data

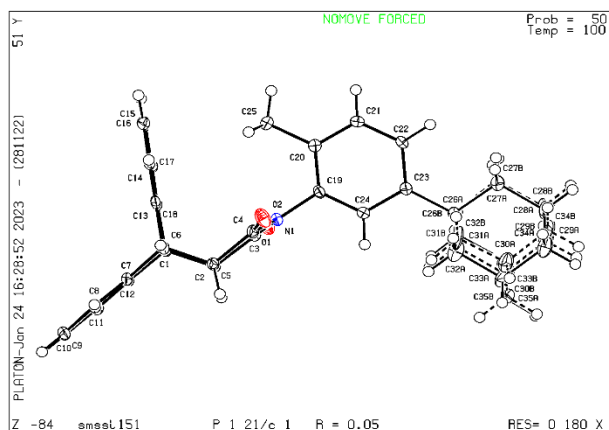


Figure 3.6 X-ray structure of balance **1**. Balance **1** was crystallized in a mixture of methanol and chloroform for 30 days in 2 mL dram.

Table 3.6 General information about calculated crystal structure for balance **1**. These data can be obtained free of charge from The Cambridge Crystallographic Data Centre via www.ccdc.cam.ac.uk/data_request/cif.

Empirical Formula	C ₃₅ H ₃₃ NO ₂
Formula weight	499.62
Temperature/K	100(2)
Crystal system	Monoclinic
Space group	P2 ₁ /c
a/Å	13.4265(6)
b/Å	15.0535(7)
c/Å	12.9181(7)
α/°	90
β/°	104.3933(3)
γ/°	90

Volume/Å ³	2522.8(2)
Z	4
$\rho_{\text{calc}}/\text{cm}^3$	1.315
μ/mm^{-1}	0.080
F(000)	1064.0
Crystal size/mm ³	0.44 × 0.32 × 0.18
Radiation	MoK α (λ = 0.71073)
2 Θ range for data collection/°	4.144 to 55.034
Index ranges	-17 ≤ h ≤ 17, -19 ≤ k ≤ 19, -16 ≤ l ≤ 16
Reflections collected	59291
Independent reflections	5812 [R _{int} = 0.0507, R _{sigma} = 0.0233]
Data/restraints/parameters	5812/30/427
Goodness-of-fit on F ²	1.198
Final R indexes [I ≥ 2 σ (I)]	R ₁ = 0.0546, wR ₂ = 0.1195
Final R indexes [all data]	R ₁ = 0.0619, wR ₂ = 0.1226
Largest diff. peak/hole / e Å ⁻³	0.37/-0.22
Flack parameter	NA

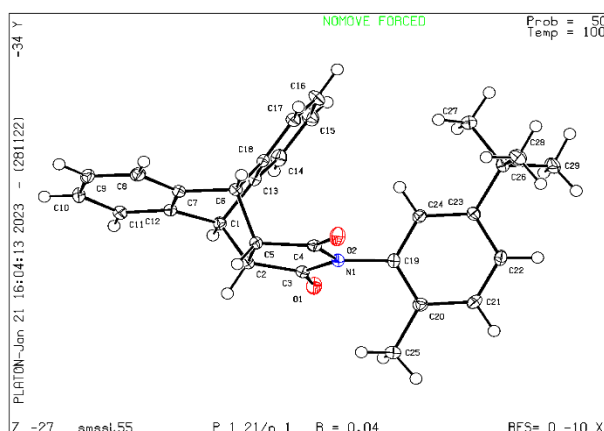


Figure 3.7 X-ray structure of balance **2**. Balance **2** was crystallized in a mixture of methanol and chloroform for 30 days in 2 mL dram.

Table 3.7 General information about calculated crystal structure for balance **2**. These data can be obtained free of charge from The Cambridge Crystallographic Data Centre via www.ccdc.cam.ac.uk/data_request/cif.

Empirical Formula	C ₂₉ H ₂₇ NO ₂
Formula weight	421.51
Temperature/K	100(2)
Crystal system	Monoclinic
Space group	P21/n
a/Å	13.9171(8)
b/Å	10.5494(6)
c/Å	15.4248(6)
α/°	90
β/°	102.256(3)
γ/°	90
Volume/Å ³	2147.0(2)
Z	4
ρ _{calc} /cm ³	1.304
μ/mm ⁻¹	0.081
F(000)	896.0
Crystal size/mm ³	0.54 × 0.28 × 0.2
Radiation	MoKα (λ = 0.71073)
2θ range for data collection/°	4.762 to 56.588
Index ranges	-18 ≤ h ≤ 18, -14 ≤ k ≤ 13, -20 ≤ l ≤ 20
Reflections collected	57178
Independent reflections	5275 [R _{int} = 0.0673, R _{sigma} = 0.0409]
Data/restraints/parameters	5275/0/293
Goodness-of-fit on F ²	1.031
Final R indexes [I ≥ 2σ (I)]	R ₁ = 0.0448, wR ₂ = 0.1120
Final R indexes [all data]	R ₁ = 0.0564, wR ₂ = 0.1193

Largest diff. peak/hole / e Å ⁻³	0.43/-0.25
Flack parameter	NA

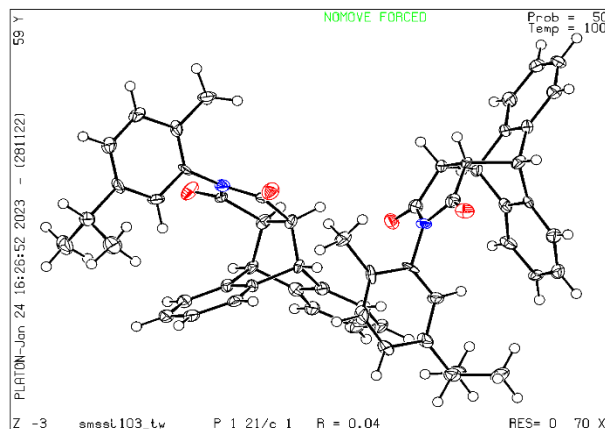


Figure 3.8 X-ray structure of balance **3**. Balance **3** was crystallized in a mixture of methanol and chloroform for 30 days in 2 mL dram.

Table 3.8 General information about calculated crystal structure for balance **3**. These data can be obtained free of charge from The Cambridge Crystallographic Data Centre via www.ccdc.cam.ac.uk/data_request/cif.

Empirical Formula	C ₂₈ H ₂₅ NO ₂
Formula weight	407.49
Temperature/K	100(2)
Crystal system	Monoclinic
Space group	P21/c
a/Å	10.7304(6)
b/Å	20.0539(11)
c/Å	20.0623(10)
α/°	90
β/°	90.088(3)
γ/°	90
Volume/Å ³	4317.1(4)

Z	8
$\rho_{\text{calc}}/\text{cm}^3$	1.254
μ/mm^{-1}	0.078
F(000)	1728.0
Crystal size/ mm^3	$0.42 \times 0.14 \times 0.13$
Radiation	MoK α ($\lambda = 0.71073$)
2 Θ range for data collection/ $^\circ$	3.796 to 55.268
Index ranges	$-13 \leq h \leq 13, -26 \leq k \leq 26, -26 \leq l \leq 26$
Reflections collected	9883
Independent reflections	9883 [$R_{\text{int}} = ?$, $R_{\text{sigma}} = 0.0324$]
Data/restraints/parameters	9883/0/568
Goodness-of-fit on F^2	1.047
Final R indexes [$I \geq 2\sigma(I)$]	$R_1 = 0.0410$, $wR_2 = 0.0945$
Final R indexes [all data]	$R_1 = 0.0495$, $wR_2 = 0.1002$
Largest diff. peak/hole / $\text{e } \text{\AA}^{-3}$	0.29/-0.21
Flack parameter	NA

3.8.4 ^1H and ^{13}C NMR Spectra

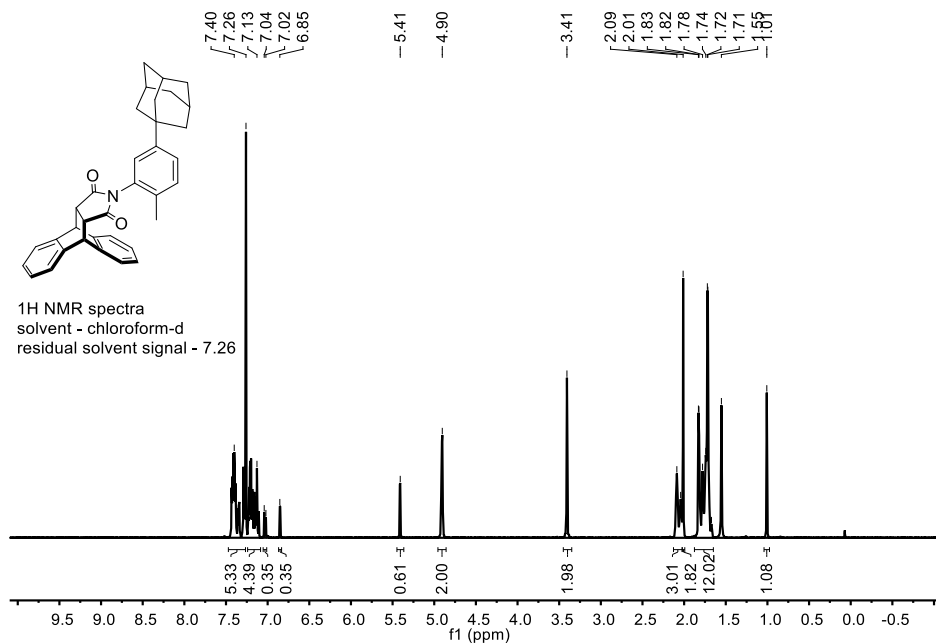


Figure 3.9 ^1H NMR spectrum of balance **1** (400 MHz, chloroform-d).

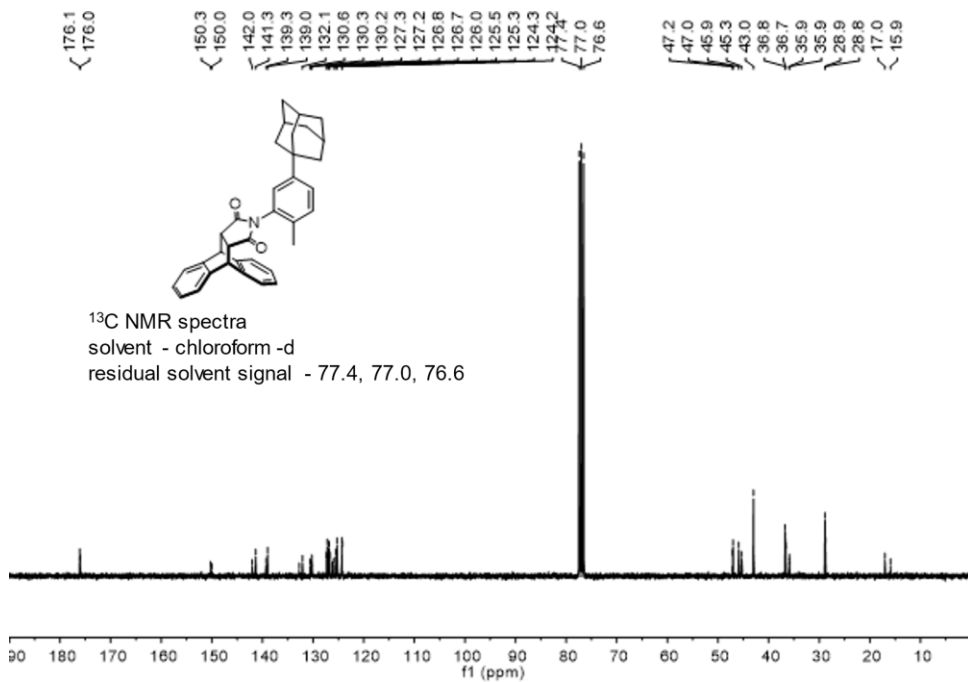


Figure 3.10 ^{13}C NMR spectrum of balance **1** (100 MHz, chloroform-d).

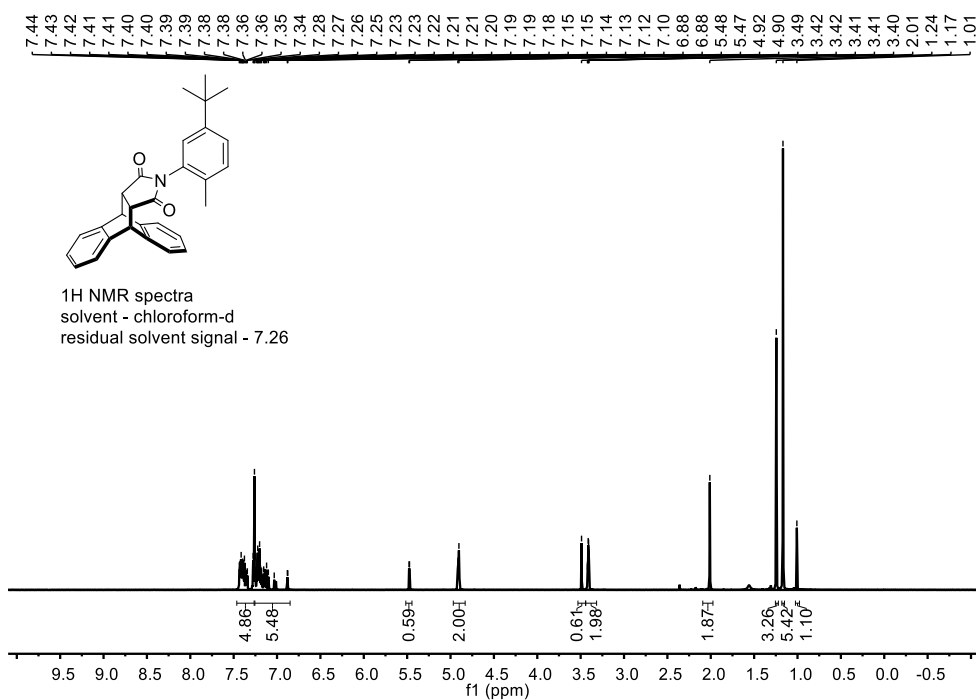


Figure 3.11 ¹H NMR spectrum of balance **2** (400 MHz, chloroform-d).

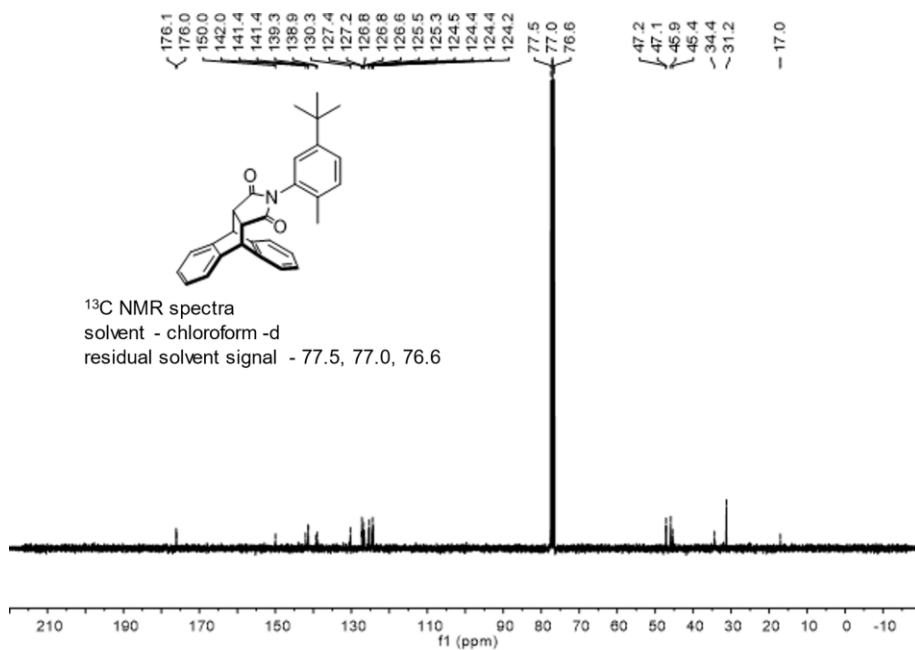


Figure 3.12 ¹³C NMR spectrum of balance **2** (100 MHz, chloroform-d).

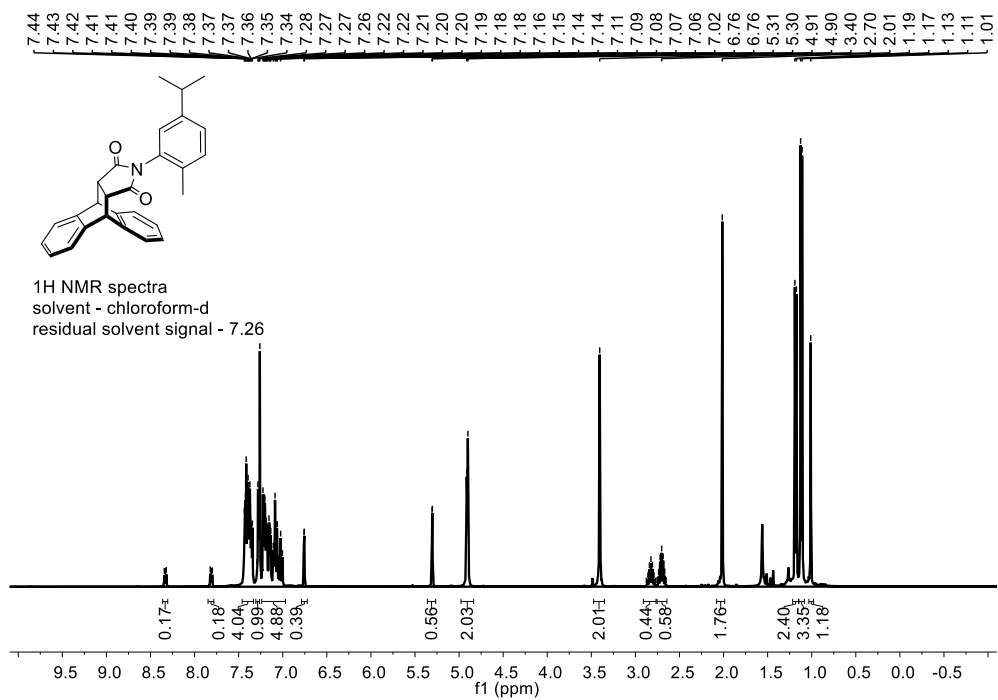


Figure 3.13 ¹H NMR spectrum of balance **3** (400 MHz, chloroform-d).

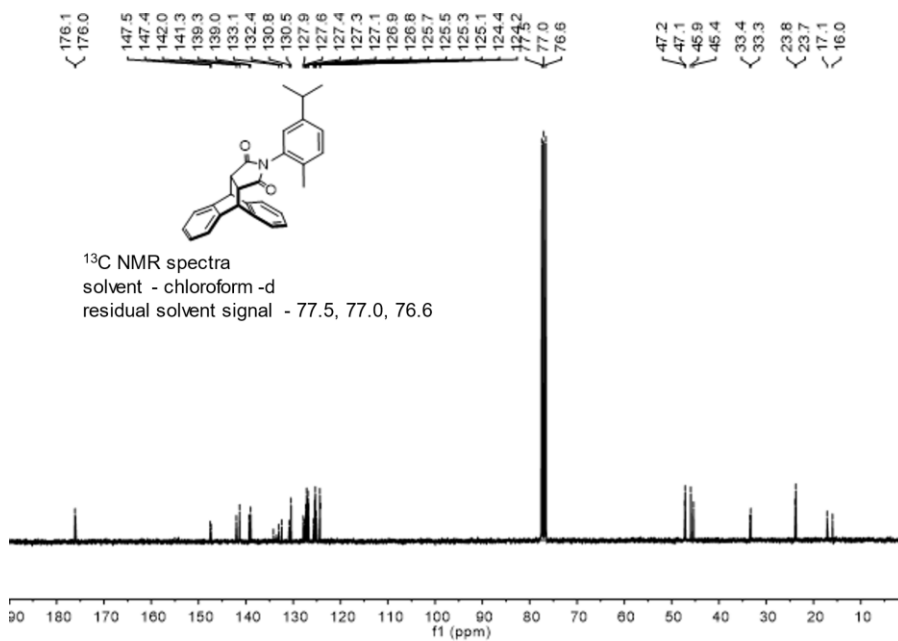


Figure 3.14 ¹³C NMR spectrum of balance **3** (100 MHz, chloroform-d).

3.8.5 SASA Calculations

The difference of the solvent accessible alkyl surface area between the *folded* and *unfolded* conformers between balances was modeled and calculated using Spartan 18. Conformer geometries were optimized using density functional theory methodology, at the B3LYP-D3, 6-311 level of theory. Vibrational analysis confirmed that geometries converged to a ground state. Surface areas were measured using a 1 Å probe. Δ SASA (Å²) was measured by subtracting the *folded* conformer SASA from the *unfolded* conformer SASA.

Table 3.9 Xyz coordinates of the *anti*- conformer structure of **1**.

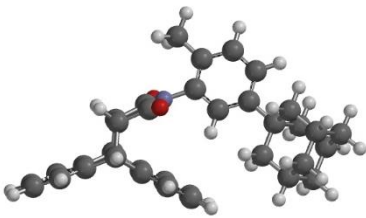
											
C	3.855888	-1.657953	-0.532603	H	2.614311	-0.622885	1.294592	H	-4.937782	0.897482	-0.364235
H	4.311384	-1.484350	-1.507602	C	1.870781	0.383751	1.897465	H	-4.007982	0.573098	1.089318
C	2.720092	-2.738861	-0.648771	C	2.295328	1.813007	-0.008388	C	-3.122489	2.621944	-1.573862
H	3.141440	-3.651937	-1.073148	C	4.238053	-2.424792	1.748901	H	-3.848972	2.239835	-2.298188
C	2.773201	-2.043540	1.801419	C	6.889300	-3.140504	1.296103	H	-2.195401	2.802477	-2.130233
H	2.323115	-2.194271	2.782648	C	4.821967	-2.215371	0.490473	C	-1.830630	2.158316	0.520104
C	2.070909	-2.957520	0.732510	C	4.977958	-2.994211	2.775653	H	-1.628290	1.441102	1.323140
H	2.115799	-3.996384	1.064404	C	6.310099	-3.349047	2.545786	H	-0.880910	2.332193	0.003285
C	1.597005	-2.245675	-1.545268	C	6.142663	-2.573710	0.259908	C	-3.648065	3.932256	-0.961768
C	0.615475	-2.552888	0.557038	C	-1.123792	-3.547893	-2.827620	H	-3.832496	4.654733	-1.765014
N	0.431737	-2.155645	-0.777120	H	-1.941142	-4.007397	-3.386760	C	-2.346278	3.471509	1.132627
O	-0.233605	-2.536941	1.411053	H	-0.805785	-4.256485	-2.057502	H	-1.592308	3.862247	1.826716
O	1.685304	-1.954081	-2.712201	H	-0.279934	-3.405261	-3.507417	C	-4.703443	2.632216	0.919453
C	-0.789996	-1.578746	-1.256705	H	-0.534893	0.084949	0.035878	H	-5.637318	2.432352	1.457491
C	-3.139954	-0.399752	-2.062033	C	-2.858319	1.562210	-0.468880	C	-2.603501	4.498212	0.014935
C	-1.549860	-2.234809	-2.226823	H	4.522311	-3.165866	3.746426	H	-1.670425	4.718465	-0.517582
C	-1.183425	-0.361551	-0.704247	H	6.893999	-3.794653	3.344544	H	-2.957023	5.444335	0.441587
C	-2.373744	0.254189	-1.087912	H	7.922785	-3.423019	1.124318	C	-3.655428	3.197425	1.894083
C	-2.734897	-1.605727	-2.618258	H	6.585552	-2.418546	-0.719439	H	-4.025928	4.121079	2.354044
H	-3.357830	-2.080334	-3.370911	H	1.389901	0.203782	2.853668	H	-3.474102	2.486165	2.708416
H	-4.078920	0.032756	-2.390878	H	1.138108	2.398538	1.707748	C	-4.960295	3.654804	-0.204841
C	3.194869	-0.416644	0.034872	H	2.159321	2.760869	-0.518751	H	-5.719916	3.271428	-0.896430
C	1.721502	1.609736	1.245204	H	3.444644	0.938177	-1.614482	H	-5.355970	4.586640	0.215845
C	3.028391	0.795290	-0.622307	C	-4.182142	1.319680	0.306527				

Table 3.10 Xyz coordinates of the *syn*- conformer structure of **1**.

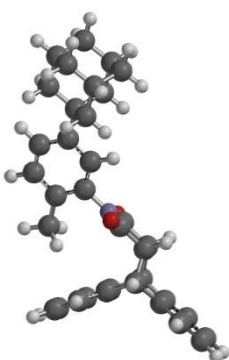
											
C	-3.991842	-0.504438	-0.913535	H	-0.895290	-3.105292	0.140241	H	2.339777	2.221665	-1.522810
H	-3.937695	-0.259399	-1.974434	H	-0.436176	-3.150497	1.831800	H	3.416894	1.156581	-2.403746
C	-2.983143	0.373197	-0.101868	C	-3.675424	-1.960900	-0.631201	C	5.246959	0.698122	-0.402268
H	-3.223596	1.425199	-0.267771	C	-3.278238	-4.589307	0.187154	H	5.325423	-0.036022	-1.212571
C	-4.123913	-1.119865	1.613294	C	-3.357878	-2.930645	-1.572595	H	5.570095	0.196689	0.516815
H	-4.183382	-1.388329	2.668132	C	-3.770148	-2.298343	0.727882	C	3.722504	2.202950	0.896913
C	-3.028877	-0.022524	1.386562	C	-3.572737	-3.609269	1.138099	H	4.004672	1.712518	1.835263
H	-3.242300	0.828756	2.036816	C	-3.163700	-4.251461	-1.159328	H	2.696125	2.559148	1.029525
C	-1.548086	0.136045	-0.539068	C	-5.420913	-0.549263	1.064809	C	4.306645	3.072050	-1.861675
C	-1.621678	-0.519663	1.707250	C	-7.663342	0.439204	-0.257863	H	3.993174	3.556250	-2.793462
N	-0.837948	-0.383882	0.552566	C	-5.353097	-0.228764	-0.300835	C	6.181697	1.885923	-0.688297
O	-1.239139	-0.962389	2.760696	C	-6.606970	-0.373307	1.763247	H	7.208899	1.515535	-0.783330
O	-1.089907	0.342591	-1.634112	C	-7.731951	0.121621	1.095916	C	4.652121	3.394461	0.611576
C	0.550129	-0.736803	0.460703	C	-6.467680	0.266825	-0.961733	H	4.586438	4.110106	1.439285
C	3.230114	-1.313337	0.180291	C	3.780687	1.165976	-0.257844	C	5.755501	2.572709	-1.997917
C	1.459671	0.276978	0.192464	H	-6.414221	0.505318	-2.020013	H	6.427672	3.408645	-2.226010
C	0.947839	-2.074128	0.580161	H	-8.542344	0.815606	-0.771463	H	5.832594	1.867701	-2.834250
C	2.311720	-2.327143	0.443711	H	-8.665005	0.251240	1.635113	C	4.216734	4.077564	-0.698795
C	2.824502	0.015952	0.039214	H	-6.664799	-0.630636	2.816758	H	4.851399	4.948526	-0.901969
H	2.664292	-3.350659	0.532598	H	-3.645764	-3.869658	2.189316	H	3.190083	4.451810	-0.604547
H	4.273118	-1.584883	0.077101	H	-3.128957	-5.617280	0.501476	C	6.099792	2.891170	0.473951
H	1.078647	1.285194	0.086272	H	-2.924517	-5.016181	-1.891243	H	6.781255	3.731741	0.297837
C	-0.040434	-3.182659	0.814235	H	-3.273165	-2.664995	-2.621784	H	6.419430	2.411866	1.406935
H	0.420533	-4.159559	0.656325	C	3.377119	1.878048	-1.579960				

Table 3.11 Xyz coordinates of the *anti*- conformer structure of **2**.

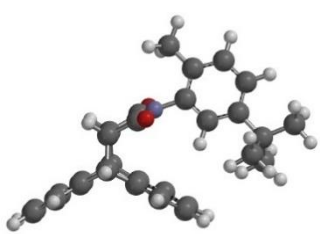
											
C	-2.529973	1.213461	-1.242206	H	5.404690	-0.423160	-0.206776	H	-7.197987	2.023579	-1.185548
H	-2.493097	1.397044	-2.316016	C	-2.037821	-0.172752	-0.870283	H	1.170801	-0.875025	0.366452
C	-1.614029	2.240302	-0.484877	C	-1.172454	-2.620352	0.132300	C	2.771710	3.433089	-0.351665
H	-1.941035	3.253338	-0.724034	C	-1.542003	-1.132836	-1.742094	H	3.720906	3.970930	-0.326637
C	-2.612048	0.742601	1.315288	C	-2.091279	-0.430487	0.508157	H	2.126239	3.847916	0.427847
H	-2.649242	0.532874	2.384216	C	-1.652116	-1.646994	1.012577	H	2.287505	3.632006	-1.311664
C	-1.632863	1.934622	1.026255	C	-1.117847	-2.364236	-1.236350	C	3.435839	-2.400889	0.218582
H	-1.921979	2.796164	1.630590	H	-1.483091	-0.926518	-2.806146	C	2.729633	-3.042603	-0.997138
C	-0.167546	2.057918	-0.913956	H	-1.676743	-1.834639	2.081132	H	3.187484	-2.713943	-1.933916
C	-0.199581	1.536389	1.367125	H	-0.740292	-3.123585	-1.913343	H	1.671609	-2.776837	-1.031982
N	0.562766	1.612893	0.191016	H	-0.836020	-3.577660	0.517044	H	2.800653	-4.134133	-0.947815
O	0.211672	1.177835	2.440167	C	-3.957720	1.126109	0.731226	C	2.752203	-2.892685	1.513464
O	0.276982	2.220876	-2.023297	C	-6.286176	1.779178	-0.649769	H	3.198218	-2.427638	2.396240
C	1.898090	1.098692	0.083635	C	-3.915509	1.371643	-0.650040	H	2.859395	-3.977793	1.609810
C	4.402236	-0.022087	-0.122611	C	-5.161550	1.210187	1.417284	H	1.684194	-2.667062	1.522433
C	2.974325	1.954269	-0.167071	C	-6.329170	1.536013	0.720843	C	4.898938	-2.872000	0.235525
C	2.058933	-0.273863	0.208807	C	-5.073684	1.700094	-1.340818	H	5.454926	-2.440485	1.072587
C	3.317687	-0.872291	0.111499	H	-5.198339	1.011042	2.484232	H	5.421801	-2.616883	-0.690179
C	4.229436	1.354750	-0.263450	H	-7.274872	1.592599	1.250415	H	4.938554	-3.959729	0.339743
H	5.097372	1.978664	-0.455795	H	-5.038731	1.882086	-2.411013				

Table 3.12 Xyz coordinates of the *syn*- conformer structure of **2**.

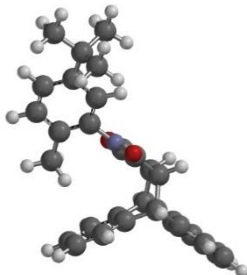
											
C	-2.839058	0.019953	-1.040783	H	5.460613	-0.396775	0.064767	C	-6.662334	0.173289	0.902136
H	-2.781510	0.341737	-2.080732	H	1.996477	2.134190	0.001022	C	-5.372434	0.571738	-1.105226
C	-1.934904	0.925121	-0.141322	C	1.327504	-2.406872	0.835145	H	-5.570901	-0.606372	2.595081
H	-2.259298	1.962058	-0.248936	H	1.878724	-3.331183	0.652996	H	-7.613761	0.185912	1.424278
C	-2.970006	-0.783576	1.432535	H	0.458852	-2.401492	0.174412	H	-5.317389	0.891648	-2.141741
H	-3.026380	-1.130878	2.464299	H	0.947015	-2.425335	1.858534	H	-7.489726	0.931716	-0.932433
C	-1.983753	0.429408	1.315234	C	-2.387627	-1.416078	-0.848616	C	4.675175	2.260302	-0.463751
H	-2.299875	1.208377	2.012203	C	-1.752459	-4.045327	-0.200859	C	4.477796	3.415999	0.539432
C	-0.474503	0.836255	-0.549087	C	-1.946485	-2.277969	-1.843206	H	5.068845	4.286522	0.239765
C	-0.545460	0.050370	1.654402	C	-2.481289	-1.857341	0.479724	H	4.791223	3.120695	1.544427
N	0.253192	0.309403	0.529370	C	-2.166168	-3.169114	0.805644	H	3.434225	3.733942	0.596025
O	-0.152129	-0.396543	2.701898	C	-1.633823	-3.600163	-1.515398	C	4.183944	2.699604	-1.861641
O	-0.012304	1.149471	-1.616982	H	-1.858207	-1.928878	-2.867275	H	4.739705	3.577251	-2.206150
C	1.668591	0.084519	0.452372	H	-2.241035	-3.509147	1.833767	H	3.121264	2.951342	-1.856600
C	4.396053	-0.230794	0.170847	H	-1.301135	-4.283486	-2.290202	H	4.325944	1.897630	-2.591012
C	2.474360	1.173767	0.146145	H	-1.512604	-5.074845	0.044819	C	6.177743	1.948198	-0.552961
C	2.199245	-1.204021	0.600399	C	-4.302154	-0.298574	0.886378	H	6.724101	2.841874	-0.866177
C	3.583647	-1.320846	0.476005	C	-6.592945	0.592700	-0.423621	H	6.388299	1.164191	-1.285456
C	3.854399	1.041888	-0.023918	C	-4.233331	0.124767	-0.451063	H	6.585245	1.633443	0.411869
H	4.036221	-2.300888	0.596124	C	-5.513414	-0.272782	1.563092				

Table 3.13 Xyz coordinates of the *anti*- conformer structure of **3**.

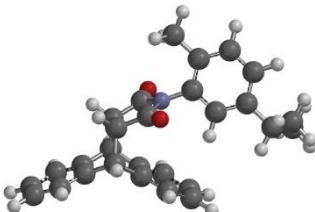
											
C	2.611543	-0.789349	-1.172375	H	-4.893012	-2.319176	-0.487701	C	-3.885446	2.208697	0.179353
H	2.596984	-1.034548	-2.234299	H	-5.514527	0.041868	-0.304492	H	-2.960319	2.768557	0.360095
C	1.768785	-1.841385	-0.362543	C	1.994046	0.564678	-0.878232	H	5.196272	-0.337052	2.585801
H	2.176677	-2.837182	-0.542055	C	0.760216	2.896808	-0.001016	H	7.298625	-0.994837	1.435094
C	2.633799	-0.172054	1.354845	C	1.346373	1.382351	-1.795390	H	7.277482	-1.554784	-0.976403
H	2.645379	0.097929	2.410810	C	2.017774	0.905159	0.482359	H	5.146149	-1.469579	-2.258669
C	1.745337	-1.449492	1.127606	C	1.396853	2.065870	0.924274	H	1.384775	2.306929	1.982111
H	2.089958	-2.250493	1.784191	C	0.732099	2.555288	-1.351989	H	0.272055	3.805157	0.336757
C	0.320057	-1.802147	-0.812464	C	4.003405	-0.518757	0.807269	H	0.219192	3.195961	-2.061767
C	0.283435	-1.144184	1.433103	C	6.357220	-1.266426	-0.479037	H	1.296365	1.095167	-2.841000
N	-0.461191	-1.368630	0.262928	C	3.992954	-0.839895	-0.558671	C	-4.496676	2.729953	-1.131864
O	-0.165696	-0.747867	2.477424	C	5.188372	-0.578046	1.526946	H	-3.823377	2.558961	-1.975513
O	-0.093795	-2.055494	-1.916666	C	6.368733	-0.950762	0.877675	H	-4.701362	3.802792	-1.067265
C	-1.844676	-1.020439	0.122151	C	5.163006	-1.215979	-1.202694	H	-5.441568	2.226297	-1.355050
C	-4.473391	-0.240662	-0.182190	C	-2.438672	-3.463368	-0.268073	C	-4.826496	2.463417	1.368643
C	-2.800372	-2.007583	-0.134746	H	-3.324918	-4.095645	-0.186043	H	-4.385060	2.111987	2.304503
C	-2.188718	0.326871	0.222055	H	-1.730454	-3.776624	0.503707	H	-5.779335	1.942174	1.236429
C	-3.509836	0.740575	0.073712	H	-1.969841	-3.656138	-1.236617	H	-5.044779	3.530602	1.472609
C	-4.122988	-1.580263	-0.285641	H	-1.407411	1.054788	0.408018				

Table 3.14 Xyz coordinates of the *syn*- conformer structure of **3**.

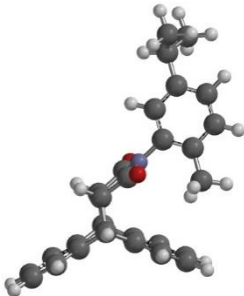
											
C	2.799245	1.170173	-0.242223	H	-4.088354	-0.264086	2.455571	C	-5.085977	0.385276	-2.084690
H	2.818220	2.240695	-0.448060	H	-5.652759	0.078454	0.601233	H	-4.480252	0.615059	-2.969530
C	1.701031	0.465559	-1.108845	H	-2.350389	0.276905	-2.125744	H	5.199714	2.097636	-1.467237
H	1.909387	0.662180	-2.162675	C	-1.368091	-0.436512	2.385929	H	7.147361	0.672602	-2.065656
C	2.771995	-1.379045	0.283569	H	-1.848155	-0.238536	3.346186	H	7.115040	-1.752572	-1.570697
H	2.763179	-2.444276	0.514732	H	-0.484607	0.199259	2.312348	H	5.133293	-2.776659	-0.470374
C	1.674872	-1.041606	-0.783234	H	-1.016308	-1.471272	2.383993	H	2.196763	-2.029772	2.989184
H	1.841585	-1.661070	-1.667400	C	2.489351	0.858537	1.209015	H	1.711895	-0.381847	4.788124
C	0.296534	0.968584	-0.806222	C	1.931873	-0.037134	3.783124	H	1.677173	2.040579	4.277450
C	0.265298	-1.314530	-0.283764	C	2.185971	1.779362	2.202700	H	2.157954	2.839451	1.971626
N	-0.467764	-0.124385	-0.368155	C	2.490324	-0.514361	1.495445	C	-5.846716	-0.921690	-2.371595
O	-0.162859	-2.367016	0.119075	C	2.210586	-0.965135	2.777760	H	-6.495261	-0.810438	-3.246032
O	-0.104687	2.098206	-0.918409	C	1.912517	1.326176	3.495647	H	-6.476625	-1.202806	-1.522276
C	-1.867909	-0.046585	-0.066998	C	4.074711	-0.911179	-0.336559	H	-5.157669	-1.748658	-2.560420
C	-4.587233	0.051122	0.395838	C	6.283271	0.231135	-1.579809	C	-6.064115	1.553092	-1.881199
C	-2.751521	0.161895	-1.123802	C	4.091696	0.464480	-0.616495	H	-6.678945	1.699189	-2.774401
C	-2.318790	-0.202793	1.246009	C	5.155047	-1.711064	-0.679765	H	-5.533609	2.486046	-1.676593
C	-3.701307	-0.146745	1.447719	C	6.265485	-1.133334	-1.301453	H	-6.744692	1.364771	-1.045707
C	-4.128059	0.213067	-0.915563	C	5.191280	1.035618	-1.240695				

Table 3.15 Xyz coordinates of the *anti*- conformer structure of **4**.

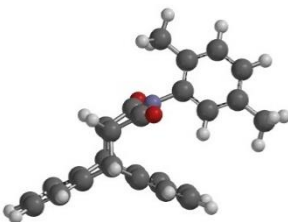
											
C	2.017724	-0.464757	-1.167345	C	-4.093336	1.056283	0.104504	H	-3.917853	-3.777011	-0.180951
H	2.001449	-0.714873	-2.228082	C	-4.710120	-1.258612	-0.275835	H	-2.322095	-3.463385	0.508583
C	1.183540	-1.517786	-0.350161	H	-5.480603	-1.993755	-0.489031	H	-2.562475	-3.335971	-1.231126
H	1.595923	-2.512208	-0.526965	H	-6.096267	0.376625	-0.290810	H	-1.988904	1.365286	0.439265
C	2.043951	0.164410	1.356938	C	1.393994	0.887395	-0.877701	C	-4.472743	2.508414	0.254825
H	2.057059	0.439461	2.411572	C	0.157726	3.221561	-0.009062	H	-5.273157	2.787228	-0.435788
C	1.163191	-1.119914	1.138296	C	0.741744	1.698798	-1.797132	H	-3.621600	3.166923	0.067909
H	1.515631	-1.915676	1.797067	C	1.419963	1.234470	0.481193	H	-4.831770	2.717242	1.268460
C	-0.267011	-1.487278	-0.795557	C	0.798054	2.396230	0.918883	H	4.612254	0.028497	2.579117
C	-0.299408	-0.822812	1.448133	C	0.126378	2.872897	-1.358089	H	6.716666	-0.613343	1.423248
N	-1.047524	-1.055548	0.281293	C	3.414244	-0.174986	0.806484	H	6.691564	-1.185769	-0.985224
O	-0.746478	-0.425591	2.492892	C	5.770290	-0.904923	-0.485502	H	4.554450	-1.128543	-2.259417
O	-0.682428	-1.744375	-1.898279	C	3.401550	-0.502859	-0.557859	H	0.788681	2.642936	1.975449
C	-2.431309	-0.706273	0.142665	C	4.602530	-0.218587	1.521700	H	-0.330454	4.131228	0.325376
C	-5.057889	0.082128	-0.164959	C	5.784038	-0.582355	0.869536	H	-0.389681	3.508878	-2.069934
C	-3.389557	-1.690142	-0.121587	C	4.572750	-0.870297	-1.204629	H	0.689704	1.406384	-2.841189
C	-2.771941	0.640361	0.250411	C	-3.030448	-3.146011	-0.261585				

Table 3.16 Xyz coordinates of the *syn*- conformer structure of **4**.

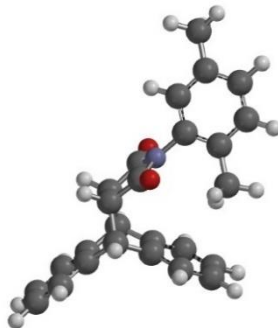
											
C	-1.921286	0.628012	-1.168809	C	4.400560	-1.199130	0.197127	C	-3.278721	0.900662	-0.546370
H	-1.872754	0.880678	-2.228179	C	4.903812	1.141351	-0.197843	C	-4.521644	0.740292	1.523296
C	-0.905440	1.496515	-0.356811	H	4.750038	-2.223050	0.291267	C	-5.649748	1.241589	0.866112
H	-1.140265	2.550826	-0.516497	H	6.371825	-0.430769	-0.147901	C	-4.396460	1.402666	-1.197075
C	-2.039661	-0.005642	1.354246	H	3.175973	2.427828	-0.166380	C	5.880426	2.239648	-0.535072
H	-2.093496	-0.281740	2.407410	C	2.043005	-2.052627	0.539364	H	6.884291	2.012049	-0.168768
C	-0.947276	1.094906	1.130151	H	2.503679	-3.028305	0.373320	H	5.575251	3.196906	-0.105508
H	-1.162189	1.942724	1.784394	H	1.189607	-1.968782	-0.135754	H	5.950934	2.378075	-1.619448
C	0.526964	1.253600	-0.800863	H	1.645331	-2.029723	1.556430	H	-4.348601	1.649751	-2.253647
C	0.461639	0.601082	1.447160	C	-1.603860	-0.830590	-0.898815	H	-6.469536	1.951886	-0.990977
N	1.243038	0.741423	0.291088	C	-1.197902	-3.463833	-0.101397	H	-6.579742	1.367557	1.411439
O	0.847522	0.157276	2.498859	C	-1.290127	-1.793030	-1.848879	H	-4.573959	0.474555	2.575016
O	0.978773	1.449035	-1.900256	C	-1.690196	-1.177426	0.458380	H	-1.555973	-2.759260	1.907758
C	2.632115	0.393587	0.199386	C	-1.488786	-2.491051	0.858106	H	-1.045584	-4.493830	0.204755
C	5.317976	-0.184356	-0.053058	C	-1.091459	-3.116403	-1.446097	H	-0.855463	-3.875570	-2.184801
C	3.543854	1.412936	-0.058403	C	-3.339556	0.569169	0.817034	H	-1.211571	-1.519576	-2.896530
C	3.032770	-0.942237	0.317381	C	-5.588130	1.570348	-0.485341				

Table 3.17 Xyz coordinates of the *anti*- conformer structure of **5**.

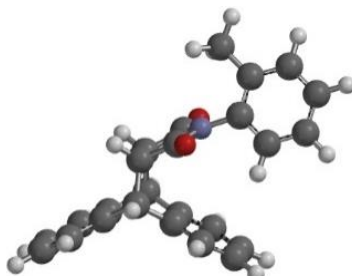
											
C	-1.650599	0.472435	-1.159664	C	2.984982	-1.140154	0.312384	C	-3.069802	0.375542	0.819468
H	-1.612872	0.687089	-2.227652	C	4.259368	-1.680623	0.191594	C	-5.376551	1.172221	-0.522046
C	-0.696040	1.443266	-0.378361	C	5.134469	0.527821	-0.237034	C	-3.025915	0.662210	-0.553815
H	-0.984796	2.474360	-0.588647	H	4.406881	-2.749343	0.305616	C	-4.264471	0.489267	1.517120
C	-1.735296	-0.070793	1.383715	H	5.979739	1.173083	-0.456333	C	-5.421268	0.887511	0.840459
H	-1.774315	-0.310530	2.446315	H	6.335732	-1.252467	-0.183900	C	-4.173282	1.062325	-1.224754
C	-0.722021	1.100119	1.124640	C	-1.197877	-0.937868	-0.831142	H	-4.302538	0.259878	2.577951
H	-0.987634	1.953716	1.750799	C	-0.375293	-3.428632	0.095872	H	-6.359888	0.969439	1.379292
C	0.741259	1.221029	-0.816963	C	-0.720002	-1.879942	-1.731999	H	-4.137048	1.277701	-2.288688
C	0.700597	0.659230	1.454896	C	-1.252253	-1.233890	0.539307	H	-6.279857	1.474804	-1.042178
N	1.464323	0.741284	0.278885	C	-0.836058	-2.473285	1.005872	H	2.124326	-1.771574	0.504813
O	1.105387	0.271497	2.519979	C	-0.315636	-3.132812	-1.264431	C	3.643339	2.574262	-0.298431
O	1.184879	1.386701	-1.926254	H	-0.658779	-1.641435	-2.789203	H	4.584559	3.124301	-0.250276
C	2.799827	0.232440	0.165288	H	-0.862721	-2.692213	2.068486	H	2.976113	2.977498	0.468383
C	5.336342	-0.841139	-0.084558	H	0.048939	-3.877264	-1.965044	H	3.177413	2.770048	-1.267567
C	3.863743	1.097085	-0.113857	H	-0.059404	-4.404199	0.451664				

Table 3.18 Xyz coordinates of the *syn*- conformer structure of **5**.

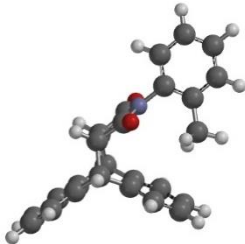
											
C	-1.612359	0.607705	-1.197538	C	3.493503	-0.432251	0.166101	C	-0.432144	-3.047055	-1.397819
H	-1.600614	0.835681	-2.263470	C	4.878702	-0.565923	0.034964	H	-0.736172	-1.510779	-2.886593
C	-0.673051	1.588800	-0.420979	C	5.151232	1.815596	-0.235761	H	-0.857867	-2.640354	1.956263
H	-1.012265	2.611152	-0.599150	H	5.313628	-1.559880	0.079727	H	-0.139271	-3.800327	-2.122182
C	-1.636045	0.028472	1.340505	H	5.783789	2.681235	-0.399784	H	-0.210423	-4.365721	0.286508
H	-1.650107	-0.226292	2.400324	H	6.773251	0.400270	-0.269706	C	-2.990801	0.466384	0.810823
C	-0.654098	1.218054	1.074518	H	3.323230	2.957631	-0.159416	C	-5.338482	1.236351	-0.474287
H	-0.933035	2.057596	1.715106	C	2.603105	-1.630616	0.347159	C	-2.980593	0.768131	-0.560869
C	0.770694	1.479408	-0.882874	H	3.141874	-2.558299	0.147286	C	-4.171709	0.553607	1.534260
C	0.798123	0.857028	1.374948	H	1.742698	-1.592211	-0.322677	C	-5.349379	0.938681	0.885826
N	1.548734	1.068847	0.209513	H	2.209901	-1.673809	1.365292	C	-4.148262	1.154269	-1.203336
O	1.237329	0.452157	2.421286	C	-1.154341	-0.807714	-0.898632	H	-4.183726	0.313023	2.593215
O	1.186823	1.689751	-1.993290	C	-0.472245	-3.365079	-0.042097	H	-6.277604	0.999094	1.445102
C	2.965209	0.863339	0.106747	C	-0.767513	-1.761364	-1.830757	H	-4.138524	1.379813	-2.265705
C	5.702109	0.538563	-0.163243	C	-1.183288	-1.125683	0.467725	H	-6.257812	1.527149	-0.972593
C	3.777294	1.975065	-0.098591	C	-0.839497	-2.399496	0.898153				

Table 3.19 Xyz coordinates of the *anti*- conformer structure of **6**.

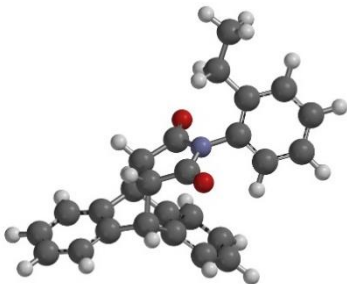
											
H	1.519795	2.486174	2.130317	C	2.757345	2.965243	-2.458117	C	-3.306199	-2.259002	3.261431
C	1.873280	1.497830	1.854872	C	3.655018	2.779713	-3.513762	C	-1.218497	-1.726473	2.204248
C	2.722976	-1.079115	1.142465	C	3.594491	0.386317	-3.166705	C	-3.316048	-1.081863	1.127911
C	2.366263	0.622986	2.826227	H	2.423794	3.963499	-2.190677	C	-3.991123	-1.657210	2.208005
C	1.822724	1.084297	0.530424	H	4.025307	3.638780	-4.063675	C	-1.915587	-2.299470	3.261631
C	2.246773	-0.204822	0.175158	H	3.907596	-0.615471	-3.446930	H	-0.134574	-1.734225	2.178046
C	2.787469	-0.657821	2.472643	H	4.761539	1.359812	-4.692265	H	-5.074261	-1.643382	2.228440
H	2.413145	0.939800	3.862757	C	0.046786	1.040049	-1.192761	H	-1.375904	-2.768547	4.077273
H	3.162171	-1.334913	3.233461	H	-0.409593	1.582371	-2.023493	H	-3.864947	-2.698815	4.081541
H	3.029847	-2.082762	0.864548	C	0.514151	-0.373475	-1.589430	C	-4.038475	-0.432880	-0.036043
C	1.262661	1.870472	-0.640828	H	0.329015	-0.607151	-2.639806	H	-3.791826	0.633237	-0.035915
H	0.937014	2.871347	-0.357735	C	-1.003221	0.822826	-0.112762	H	-3.619557	-0.831818	-0.967789
C	2.050414	-0.521060	-1.296706	C	-0.299015	-1.323820	-0.725497	C	-5.558525	-0.595950	-0.062133
H	2.389416	-1.523324	-1.560363	O	-1.607909	1.679392	0.482327	H	-6.034152	-0.123137	0.801670
C	2.287806	1.862016	-1.758766	O	-0.224389	-2.525635	-0.713915	H	-5.857647	-1.647981	-0.076208
C	4.070417	1.498067	-3.866995	N	-1.140616	-0.555521	0.094249	H	-5.971386	-0.123145	-0.956641
C	2.710803	0.571432	-2.112713	C	-1.914565	-1.126871	1.158985				

Table 3.20 Xyz coordinates of the *syn*- conformer structure of **6**.

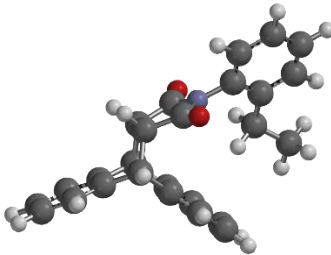
											
H	-2.114652	-1.948439	-1.167633	C	-2.542186	2.225066	-3.192862	C	4.465630	-2.450412	2.131748
C	-2.097291	-1.264017	-0.324971	C	-3.210613	3.449814	-3.269447	C	3.822431	-0.290685	1.311912
C	-2.003644	0.499454	1.851720	C	-2.467625	4.011699	-1.033925	C	2.349807	-2.204205	0.938408
C	-2.542642	-1.675418	0.932879	H	-2.571463	1.529161	-4.026458	C	3.292872	-2.988863	1.611314
C	-1.616062	0.027286	-0.489199	H	-3.763435	3.706916	-4.167442	C	4.732543	-1.092841	1.987171
C	-1.580364	0.914491	0.596644	H	-2.443566	4.701254	-0.195578	H	4.005600	0.770516	1.196939
C	-2.489594	-0.800748	2.015888	H	-3.702697	5.282225	-2.259763	H	3.100298	-4.046701	1.744358
H	-2.921335	-2.683645	1.066668	C	0.394016	1.075164	-1.532298	H	5.638458	-0.659235	2.396883
H	-2.827536	-1.131420	2.992481	H	0.761369	1.555276	-2.440553	H	5.166337	-3.092644	2.655793
H	-1.950824	1.177845	2.696619	C	0.437483	1.996105	-0.300164	C	1.064412	-2.795617	0.400081
C	-1.083862	0.617166	-1.781377	H	0.931304	2.946909	-0.511905	H	0.261090	-2.070178	0.544275
H	-1.130185	-0.085004	-2.614625	C	1.325383	-0.079706	-1.204128	H	1.162284	-2.901331	-0.684390
C	-1.010996	2.270055	0.229117	C	1.274748	1.242290	0.724805	C	0.631221	-4.132358	1.004502
H	-0.988278	2.959777	1.072615	O	1.650431	-0.966458	-1.953647	H	0.559805	-4.082318	2.094597
C	-1.849441	1.899855	-2.035894	O	1.501762	1.589576	1.854740	H	1.315058	-4.946026	0.748152
C	-3.174909	4.336248	-2.195972	N	1.748613	0.058828	0.125503	H	-0.353362	-4.410557	0.619350
C	-1.806680	2.794105	-0.954256	C	2.650286	-0.838256	0.791324				

Table 3.21 Xyz coordinates of the *anti*- conformer structure of **7**.

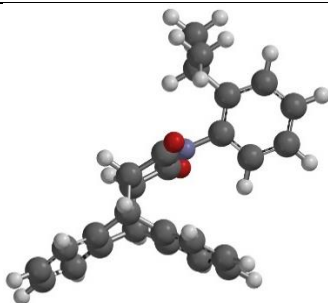
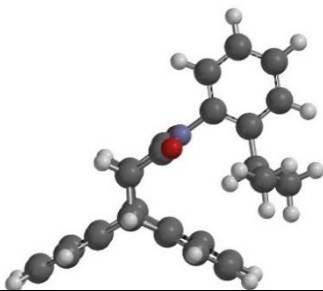
											
H	-2.490654	-2.405351	-1.810797	C	-4.262336	3.177104	-2.844766	C	3.082411	-1.188811	0.940300
C	-2.531232	-1.891241	-0.855246	C	-3.518658	3.379449	-0.549186	C	3.757317	-2.307470	1.445960
C	-2.589258	-0.563567	1.612452	H	-3.456763	1.509105	-3.958538	C	1.934621	-3.770196	0.856080
C	-2.851913	-2.588366	0.311647	H	-4.864362	3.539557	-3.671922	H	0.244918	-2.797485	-0.059240
C	-2.252742	-0.533243	-0.783302	H	-3.543579	3.895176	0.405989	H	4.742912	-2.174649	1.879279
C	-2.285226	0.132729	0.450411	H	-4.907992	4.724164	-1.498945	H	1.490912	-4.759536	0.818455
C	-2.878718	-1.928354	1.538540	C	-0.387522	0.867933	-1.601961	H	3.755576	-4.424251	1.804034
H	-3.073875	-3.649671	0.260576	H	-0.044867	1.517111	-2.409244	C	3.732845	0.182467	0.995290
H	-3.117371	-2.479128	2.442398	C	-0.407684	1.560387	-0.224607	H	3.082326	0.889294	0.474738
H	-2.582803	-0.054216	2.570280	H	-0.010267	2.576399	-0.257798	C	3.865790	0.663768	2.449917
C	-1.827600	0.347404	-1.942021	C	0.580682	-0.293966	-1.455054	H	4.533373	0.010378	3.019898
H	-1.821820	-0.183947	-2.893912	C	0.485294	0.700457	0.660332	H	2.891429	0.672516	2.938905
C	-1.869271	1.586734	0.346418	O	0.886033	-1.085304	-2.310080	H	4.278722	1.676514	2.486503
H	-1.891463	2.100423	1.307193	O	0.677284	0.849151	1.840926	C	5.085085	0.196409	0.264955
C	-2.716297	1.573006	-1.941447	N	1.028773	-0.323290	-0.125073	H	5.815591	-0.453938	0.753882
C	-4.285975	3.843511	-1.622009	C	1.807563	-1.404982	0.405253	H	5.502035	1.207879	0.254549
C	-2.736180	2.244482	-0.709408	C	3.201317	-3.580125	1.406077	H	4.979203	-0.140584	-0.769415
C	-3.472288	2.036332	-3.008830	C	1.236704	-2.678168	0.361565				

Table 3.22 Xyz coordinates of the *syn*- conformer structure of **7**.

											
H	-1.898826	-1.941260	2.007114	C	-3.144621	-3.434625	-3.611168	C	2.303280	1.328580	1.729291
C	-1.989879	-1.028327	1.426897	C	-2.615027	-1.090020	-3.891964	C	3.280377	1.895555	2.556513
C	-2.209774	1.332900	-0.069551	H	-2.369101	-4.377393	-1.829157	C	5.048375	0.739662	1.391600
C	-2.560666	0.114470	1.990963	H	-3.622845	-4.338750	-3.974563	H	4.395495	-0.500146	-0.247660
C	-1.554875	-0.991497	0.109276	H	-2.675838	-0.173884	-4.471853	H	2.974316	2.573563	3.345801
C	-1.658506	0.192237	-0.636344	H	-3.775951	-2.248584	-5.289679	H	6.099483	0.504208	1.265138
C	-2.673551	1.286281	1.246674	C	0.423038	-1.749049	-1.205450	H	5.359404	2.064902	3.060433
H	-2.915861	0.087327	3.015628	H	0.829827	-2.572732	-1.796014	C	0.831122	1.646800	1.929566
H	-3.117579	2.170075	1.692543	C	0.326260	-0.434316	-2.005013	H	0.248032	0.960296	1.313409
H	-2.282701	2.247855	-0.648621	H	0.699881	-0.538389	-3.026168	C	0.384777	1.422943	3.381998
C	-0.995427	-2.156773	-0.687104	C	1.384992	-1.456645	-0.065492	H	0.904750	2.085240	4.079513
H	-0.937136	-3.075892	-0.104121	C	1.225109	0.547590	-1.266984	H	0.565122	0.391017	3.693590
C	-1.163839	0.046315	-2.063584	O	1.716197	-2.214191	0.810014	H	-0.684759	1.620821	3.476089
H	-1.242767	0.972236	-2.633611	O	1.394842	1.709705	-1.537808	C	0.517260	3.074718	1.454009
C	-1.836151	-2.296962	-1.942723	N	1.819094	-0.130078	-0.194539	H	1.067248	3.814665	2.043687
C	-3.230511	-2.258344	-4.351416	C	2.750641	0.476819	0.713357	H	-0.550393	3.284108	1.561082
C	-1.922642	-1.110770	-2.689048	C	4.631216	1.610041	2.396571	H	0.789363	3.198663	0.404990
C	-2.441644	-3.458007	-2.402894	C	4.101369	0.177038	0.546783				

3.8.6 Balance Equilibrium Measurements

Table 3.23 Folding energies of CH-arene molecular balances in various solvents upon equilibrium (kcal/mol).

	1	2	3	4	5	6	7
CDCl₃	0.31	0.30	0.23	0.11	0.07	-0.10	-0.13
C₆D₆	0.38	0.43	0.23	0.07	-0.09	-0.13	-0.13
CD₂Cl₂	0.35	0.25	0.20	0.09	0.02	-0.20	-0.22
CD₃CN	0.41	0.30	0.25	0.03	-0.07	-0.20	-0.53
DMSO-d₆	0.17	0.13	0.00	-0.14	-0.19	-0.29	-0.58
91% DMSO-d₆:D₂O	0.24	0.14	-0.04	-0.15	-0.20	-0.33	-0.63
78% DMSO-d₆:D₂O	0.20	0.17	-0.01	-0.15	-0.21	-0.45	-0.54
67% DMSO-d₆:D₂O	0.23	0.20	0.04	-0.15	-0.21	-0.37	-0.54

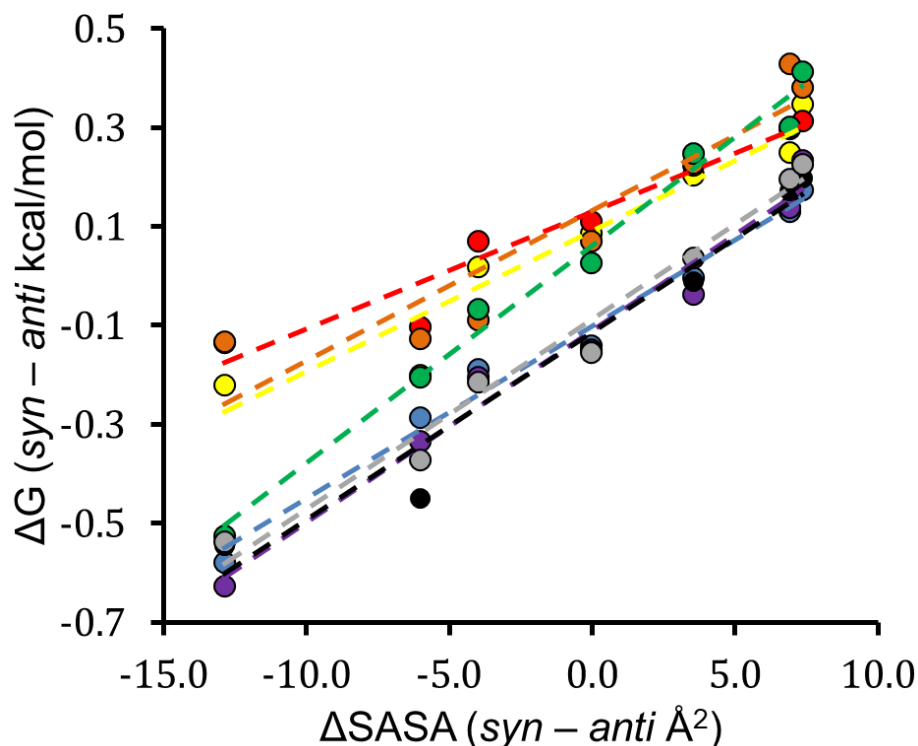


Figure 3.15 Δ SASA between *syn*- and *anti*- conformers compared against ΔG . The study was conducted in 7 different solvent environments: chloroform- d_3 (red), benzene- d_6 (orange), dichloromethane- d_2 (yellow), acetonitrile- d_3 (green), dimethyl sulfoxide- d_6 (blue), 91% dimethyl sulfoxide- d_6 /water mixture (purple), 78% dimethyl sulfoxide- d_6 /water mixture (black), and 67% dimethyl sulfoxide- d_6 /water mixture (gray). The *ced* values of mixed solvents were calculated based on the assumption that *ced* scales linearly with the v/v % solvent composition.

3.8.7 Error Analysis

The NMR samples for this work were prepared by dissolving ~ 5 mg of purified molecular compound in 0.2 mL to 0.5 mL of solvent, giving an average concentration of 61 to 25 mM (assuming the average molecular weight to be 406 g/mol). NMR signals were measured using the Mestrenova line fitting function to reduce the error in integration. The error of the quantitative NMR analysis is considered to be 1% for concentrations >10 mM.

Therefore, the error for a 1:1 *folded:unfolded* ratio is 1.4% as both conformers have a concentration greater than 10 mM. This error is equal to the square root of the sum of the

squares of 1% and 1%, which is only 1.4% (**Equation 3.4**). The minor conformers were at no less than ~ 6.4 mM but no greater than 12 mM. It is safe to estimate the maximum error for integration of the minor conformer is 2.5%, and the maximum error of the major conformer is 1%, based on estimations from Rizzo et. al.²⁷ The total integration error for each measurement was no more than 2.7%.

$$\text{Equation 3.4 Error } \left(\frac{syn}{anti}\right) = \sqrt{(\text{Error}_{(syn)})^2 + (\text{Error}_{(anti)})^2}$$

The folding energies (ΔG) calculated also have some associated uncertainty (**Equation 3.5**). This uncertainty was calculated to be no more than ± 0.016 kcal/mol at 23 °C.

$$\text{Equation 3.5 Error}_{\Delta G} = -RT\text{Error}([syn]/[anti])$$

3.9 References

- (1) Nishio, M.; Hirota, M.; Umezawa, Y. *The CH/ Interaction: Evidence, Nature, and Consequences*; John Wiley & Sons: Nashville, TN, **1998**.
- (2) Diehl, R.C. *CH-[Pi] Interactions Play a Central Role in Protein Recognition of Carbohydrates*; Massachusetts Institute of Technology, **2021**.
- (3) Nishio, M.; Umezawa, Y.; Hirota, M.; Takeuchi, Y. The CH/ π Interaction: Significance in Molecular Recognition. *Tetrahedron* **1995**, *51* (32), 8665–8701.
- (4) Allen, S. E.; Mahatthananchai, J.; Bode, J. W.; Kozlowski, M. C. Oxyanion Steering and CH– π Interactions as Key Elements in an N-Heterocyclic Carbene-Catalyzed [4 + 2] Cycloaddition. *J. Am. Chem. Soc.* **2012**, *134* (29), 12098–12103.
- (5) Nishio, M.; Hirota, M. CH/ π Interaction: Implications in Organic Chemistry. *Tetrahedron* **1989**, *45* (23), 7201–7245.
- (6) Klärner, F.-G.; Schrader, T. Aromatic Interactions by Molecular Tweezers and Clips in Chemical and Biological Systems. *Acc. Chem. Res.* **2013**, *46* (4), 967–978.
- (7) Asensio, J. L.; Ardá, A.; Cañada, F. J.; Jiménez-Barbero, J. Carbohydrate–Aromatic Interactions. *Acc. Chem. Res.* **2013**, *46* (4), 946–954.
- (8) Waters, M. L. Aromatic Interactions in Model Systems. *Curr. Opin. Chem. Biol.* **2002**, *6* (6), 736–741.
- (9) Emenike, B. U.; Spinelle, R. A.; Rosario, A.; Shinn, D. W.; Yoo, B. Solvent Modulation of Aromatic Substituent Effects in Molecular Balances Controlled by CH– π Interactions. *J. Phys. Chem. A* **2018**, *122* (4), 909–915.

- (10) Hwang, J.; Li, P.; Smith, M. D.; Shimizu, K. D. Distance-Dependent Attractive and Repulsive Interactions of Bulky Alkyl Groups. *Angew. Chem. Int. Ed.* **2016**, *128* (28), 8218–8221.
- (11) Reichardt, C. Empirical Parameters of Solvent Polarity as Linear Free-Energy Relationships. *Angew. Chem. Int. Ed.* **1979**, *18* (2), 98–110.
- (12) Karthikeyan, S.; Ramanathan, V.; Mishra, B. K. Influence of the Substituents on the CH... π Interaction: Benzene–Methane Complex. *J. Phys. Chem. A* **2013**, *117* (30), 6687–6694.
- (13) Nishio, M. The CH/ π Hydrogen Bond in Chemistry. Conformation, Supramolecules, Optical Resolution and Interactions Involving Carbohydrates. *Phys. Chem. Chem. Phys.* **2011**, *13* (31), 13873.
- (14) Kamlet, M. J.; Taft, R. W. The Solvatochromic Comparison Method. I. The .Beta.-Scale of Solvent Hydrogen-Bond Acceptor (HBA) Basicities. *J. Am. Chem. Soc.* **1976**, *98* (2), 377–383.
- (15) Kamlet, M. J.; Abboud, J. L.; Taft, R. W. The Solvatochromic Comparison Method. 6. The .Pi.* Scale of Solvent Polarities. *J. Am. Chem. Soc.* **1977**, *99* (18), 6027–6038.
- (16) Taft, R. W.; Kamlet, M. J. The Solvatochromic Comparison Method. 2. The .Alpha.-Scale of Solvent Hydrogen-Bond Donor (HBD) Acidities. *J. Am. Chem. Soc.* **1976**, *98* (10), 2886–2894.
- (17) Catalán, J. Toward a Generalized Treatment of the Solvent Effect Based on Four Empirical Scales: Dipolarity (SdP, a New Scale), Polarizability (SP), Acidity (SA), and Basicity (SB) of the Medium. *J. Phys. Chem. B* **2009**, *113* (17), 5951–5960.
- (18) Laurence, C.; Legros, J.; Chantzis, A.; Planchat, A.; Jacquemin, D. A Database of Dispersion-Induction DI, Electrostatic ES, and Hydrogen Bonding α_1 and β_1 Solvent Parameters and Some Applications to the Multiparameter Correlation Analysis of Solvent Effects. *J. Phys. Chem. B* **2015**, *119* (7), 3174–3184.
- (19) Li, P. Parker, T. M. Hwang, J.; Deng, F. Smith, M. D. Pellechia, P. J. Sherrill, C. D.; Shimizu, K. D. The CH– π Interactions of Methyl Ethers as a Model for Carbohydrate–*N*-Heteroarene Interactions. *Org. Lett.* **2014**, *16* (19), 5064–5067.
- (20) Li, P.; Vik, E. C.; Shimizu, K. D. *N*-Arylimide Molecular Balances: A Comprehensive Platform for Studying Aromatic Interactions in Solution. *Acc. Chem. Res.* **2020**, *53* (11), 2705–2714.
- (21) Zhao, C.; Parrish, R. M.; Smith, M. D.; Pellechia, P. J.; Sherrill, C. D.; Shimizu, K. D. Do Deuteriums Form Stronger CH– π Interactions? *J. Am. Chem. Soc.* **2012**, *134* (35), 14306–14309.
- (22) Yang, L.; Brazier, J. B.; Hubbard, T. A.; Rogers, D. M.; Cockroft, S. L. Can Dispersion Forces Govern Aromatic Stacking in an Organic Solvent? *Angew. Chem. Int. Ed.* **2016**, *55* (3), 912–916.
- (23) Weber, E.; Finge, S.; Csoeregh, I. Modular Design of Hosts Involving a Rigid Succinimide Framework and N-Bonded Lateral Groups. Crystalline Inclusion Properties and Crystal Structures of Inclusion Compounds with Dioxane, Methanol, and DMF. *J. Org. Chem.* **1991**, *56* (26), 7281–7288.
- (24) Srivastav, K.; Verma, A.; Verma, S. Torsional barriers about N-C (aryl) bond and atropisomerism: a ^1H NMR study *Indian J. Chem., Sect. B* **1993**, *32B*, 1143–1148.

- (25) Grossmann, G.; Potrzebowski, M. J.; Olejniczak, S.; Ziółkowska, N. E.; Bujacz, G. D.; Ciesielski, W.; Prezdo, W.; Nazarov, V.; Golovko, V. Structural Studies of N-(2'-Substituted Phenyl)-9,10-Dihydro-9,10-Ethanoanthracene-11,12-Dicarboximides by X-Ray Diffraction and NMR Spectroscopy—Proofs for CH/ π Interactions in Liquid and Solid Phases. *New J. Chem.* **2003**, 27 (7), 1095–1101.
- (26) Raimondi, L.; Benaglia, M.; Cozzi, F. Aliphatic C-H/ π and Heteroatom/ π Interactions in *N*-Aryl-3,4-(9',10'-Dihydroanthracene-9',10'-Diyl)Succinimides: Aliphatic C-H/ π and Heteroatom/ π Interactions. *Eur. J. Org. Chem.* **2014**, (23), 4993–4998.
- (27) Rizzo, V.; Pinciroli, V. Quantitative NMR in Synthetic and Combinatorial Chemistry. *J. Pharm. Biomed. Anal.* **2005**, 38 (5), 851–857.

CHAPTER 4

DEVELOPING SCAFFOLDING MODULES FOR TEACHING
ELECTRONPUSHING FORMALISMS IN UNDERGRADUATE ORGANIC
CHEMISTRY

4.1 Abstract

Teaching modules were developed with guided inquiry exercises on electron movement curved arrow formalisms used in drawing reaction mechanisms. The design of the modules was guided by a survey of exams from underperforming students in a first semester undergraduate organic chemistry, and data from other studies. Students that struggled drawing mechanisms typically have a poor understanding of where curved arrows should begin and end and difficulty assigning formal charges. Therefore, we designed a set of exercises focusing on the placement of the arrows, where predicting formal charges was emphasized. In addition, we developed exercises that requires the interpretation of curved arrows to predict the product of individual mechanism steps in a reaction.

4.2 Introduction

For many undergraduate students, organic chemistry courses are infamous for being extremely difficult, resulting in “weeding out” aspiring scientists, chemical engineers, pharmacists, or physicians. The course has been cited as having up to a 30-50% attrition rate,¹ hampering students' graduation rates and incurring extra financial cost. In particular, many students find electron pushing formalisms (EPF) in reaction mechanisms challenging.²

With this in mind, our goal was to develop learning tools to help struggling students understand reaction mechanisms and EPFs. EPFs were introduced to the field of organic chemistry in 1922 by Kermac and Robinson as an explanatory tool to understand valence electron movements during chemical reactions.³ Understanding the electron movements makes it possible to explain and predict product regioselectivity, stereoselectivity and

reaction rates. However, the importance and utility of EPFs is not obvious to students first learning organic chemistry.⁴

While much criticism is given to having undergraduate students merely memorize organic chemistry concepts, memorizing step-by-step procedures is often the starting point on the way to a deeper understanding of the content. Most students understand that doing well in an organic chemistry course requires a comprehensive understanding of its fundamental concepts. However, the memorization strategy often comes more naturally and initially seems better suited to the rigorous pace of the course.

Scaffolding teaching strategies involve the intervention of an instructor to guide a student toward understanding a concept. The instructor involvement is gradually withdrawn as the student masters the concept.⁵ Typically, scaffolding methodologies involve breaking down a complex task into smaller, more manageable tasks guiding the students to complete the tasks systematically until the overall task is completed.⁶ Guidance can be given as a step-by-step procedure, and/or administered through a series of guiding questions.⁷

Therefore, the goal of this project was to develop scaffolding learning modules for undergraduate students learning EPFs in reaction mechanisms. While there are simple rules and step-by-step procedures for getting the correct answers for other problem types in organic chemistry, it is difficult to find these for mechanism EPFs. One challenge is that understanding mechanisms require mastery of multiple concepts in organic chemistry such as valence electron theory, acid/base chemistry, nucleophilicity and electrophilicity trends, and drawing and interpreting Lewis structures. However, enumerating every single concept


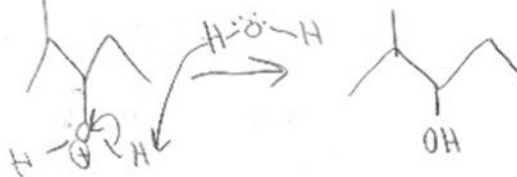


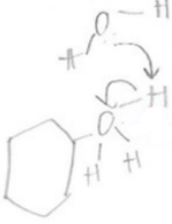
in completing mechanism problems undermines the intention of developing a procedure that is accessible and easily implemented by students.

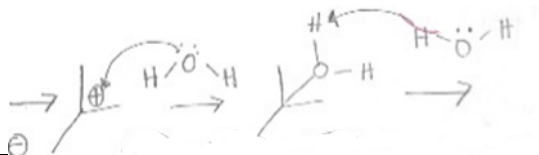
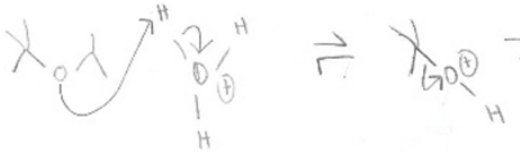

We decided to develop exercises that focus on the most difficult or missed concepts in mechanism EPFs. The modules are not intended as comprehensive solutions to drawing mechanisms, but designed for students to improve performance on exams and give them a foundation for gaining a deeper understanding of the fundamental concepts of mechanisms. These exercises will be integrated into an online learning website designed for undergraduate students (<https://shimizu-uofsc.net/orgo/>).

4.3 Data Collection

In order to ascertain which aspects of drawing mechanisms were the most problematic, we analyzed a sample of exams to see which mistakes were most common for mechanism problems (**Table 4.1**). A total of 34 end-of-course exams from a first semester organic chemistry course (CHEM 333) at the University of South Carolina were selected from > 200 final exams, using the criteria of exams with < 60% of the maximum possible score, i.e. failing grades. The mechanism section was analyzed for the type of errors made by students. The errors were divided into nine categories. If an error was repeated in the same exam, it was still counted only once in the tally.

Table 4.1 Types of errors in the mechanism section of 34 failing grade final exams.

Error Type	Error description and example	Error prevalence
Missing arrows	Arrows necessary to take the reactants or intermediates to the next step of the reaction mechanism were missing. 	44%
Misidentify electron source	A curved arrow begins from the wrong place in the mechanism, but ends in the correct place. 	47%
Misidentify electron sink	A curved arrow begins at the correct place, but ends in the wrong place. 	35%
Arrow direction reversed	Arrow goes in the wrong direction between the correct electron source and sink. 	44%
Product break octet rules	Product or intermediate with an atom that exceeds the maximum valency of an atom. 	32%

Incorrect formal charge	Incorrect formal charge is assigned to an atom in the mechanism. 	53%
Incorrect product	Arrows are correct, but the product is different from what the step would produce. 	41%
Unrecognized radical mechanism	Attempted to do radical mechanisms using full headed arrows, demonstrating the students did not recognize it as a radical mechanism. 	15%
Missing answer	Left at least one mechanism problem blank.	32%

The most common error observed was the inability to identify the formal charges of intermediates. The second most common error was incorrectly identifying where arrows begin and end. Interestingly, problems with radical mechanisms had some of the lowest error rates. One reason for this could be that radical reaction mechanisms are typically presented in a step-by-step scaffolding process of initiation, propagation, and termination and thus easier for students to learn initially and retain.

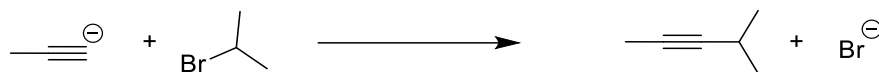
4.4 Structure of Step-by-Step Process for Mechanisms

To address these common errors, a guided inquiry module that breaks down the mechanism EPF problems into a series of questions that focus on accurately drawing the curved arrows was developed. Focusing on the final product as opposed to rationalizing the individual electron movements in a mechanism has been shown to be a major obstacle in learning mechanism EPFs.² Many mistakes come from drawing electron movements to what students think will provide the correct product, without confirming whether the individual curved arrows and intermediate structures are valid in the specific contexts. This is supported by studies showing that students are more likely to draw correct curved arrow formalism when the final product is not shown.⁸

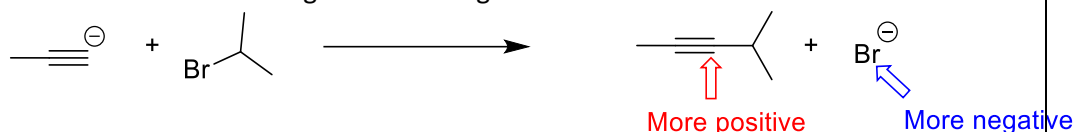
The modules focus on drawing electron movements. Students were provided reactants, reagent, and products for a step of a mechanism and were asked to draw the missing arrows. To guide students, the instructions first asked to identify the covalent bonds that were broken and formed during each step, and only then to draw curved arrows to show the movement of electrons. The curved arrows were classified into three categories: lone pair to bond, bond to bond, and bond to lone pair to help students conceptualize them more easily. Students were then instructed to draw arrows connecting the breaking and forming bonds with electron sources and sinks. This was included since assigning appropriate formal charges is a common error in exams. To aid students in where to start and end with the arrows, they were asked to consider atoms which charges change during the mechanism step. Atoms which became more positive should be considered to be the electron source, whereas atoms which became more negative should be considered electron sinks. Furthermore, students are advised that multiple arrows in a single step

should point in the same direction. In each exercise, a "things to think about" commentary was provided to encourage a deeper understanding of the individual concepts and their application. This was intended to move beyond simple memorization to a more holistic understanding of the topic.

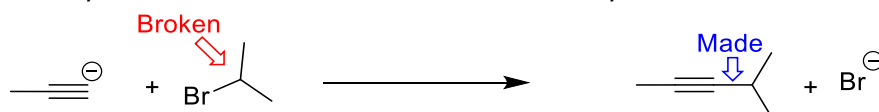
Draw the mechanism arrows for the following mechanism step. Note that this is a one-step S_N2 mechanism.



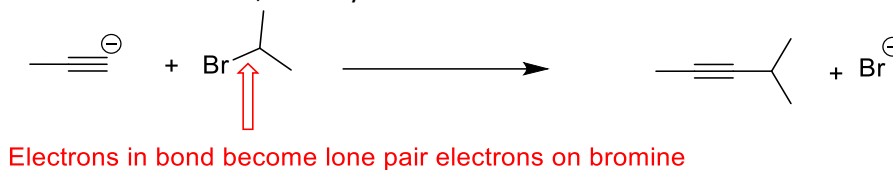
Identify all the atoms which change formal charge.



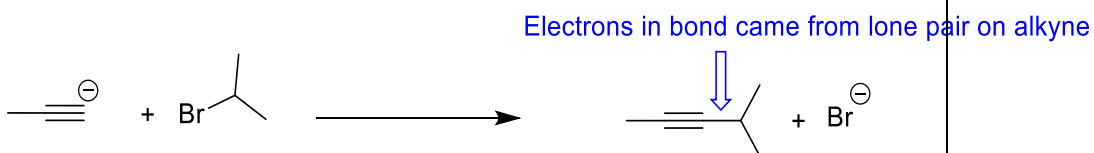
- Identify all the bonds that were broken and identify all the bonds formed.



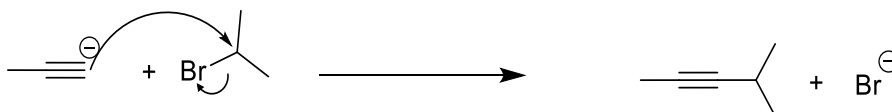
- For each of the broken bonds, identify where their electrons went.



- For each of the new bonds in the products, identify where their electrons came from in the reactants.



- Draw all curved arrows and check that they:
 - Follow a head-to-tail pattern.
 - Start and end at the atoms that change charge.



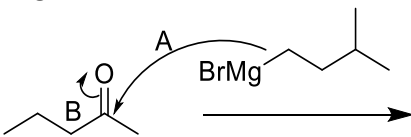
Things to think about:

- 1) What is meant by saying that S_N2 reaction mechanisms are concerted? How is this demonstrated in this problem?
- 2) Which is a more stable base: the acetylide anion or the bromate anion? Hint: if you were to protonate both of them, which one would form the more reactive and unstable acid?
- 3) Which bond is more stable: a C-C bond or a C-Br bond? Hint: which one is longer? How does bond length correlate with bond stability?
- 4) Why does the charge of the atom where the arrows begin in a mechanism step become more positive? Why does the charge of the atom where the arrows end become more negative?

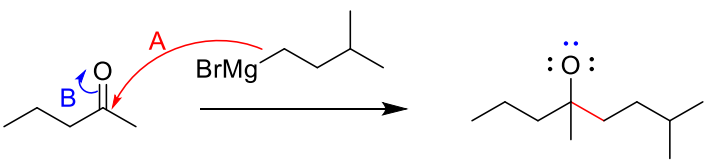
Figure 4.2 Example of mechanism problem where students are asked to draw in formalism arrows.

A complementary set of problems was created in which reactants, reagents, and curved arrows were given, and students were asked to draw the products. These types of problems should be introduced only after students have completed the first module to prevent them from focusing on producing the desired final product. Students are instructed to identify curved arrows corresponding to show bond breaking and then to identify curved arrows that show bond forming. For each arrow, students are guided to identify where the electrons came from and which bonds are going to form lone pairs.

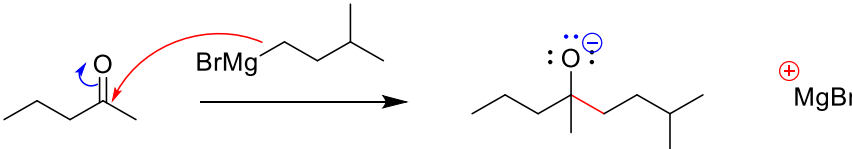
Draw the product given the curved arrows in the mechanism step. This is the first step in a Grignard reaction.



- Does curved arrow A show bond breaking, bond forming, or both?
- Does curved arrow B show bond breaking, bond forming, or both?



- Draw products that show structures with the newly formed and broken bonds.



- Assign formal charges to the atoms at the beginning and end of the flow of arrows. The atom at the beginning should become more positive and the atom at the end should become more negative.

Things to think about:

- 1) What allows the carbon in the Grignard reagent to behave as a nucleophile?
- 2) Describe the stereochemistry of the product. Will there be a single enantiomer or will it be a racemic mixture? Hint: is there anything that would prevent or promote the Grignard reagent attacking from one side of the nucleophile over the other?
- 3) What is the next step in this reaction mechanism? Hint: what can we introduce to help stabilize the negative charge on the oxygen?

Figure 4.3 Example of mechanism problem where students are asked to draw in the products of a mechanism step.

4.6 Conclusions

Step-by-step procedure systems were developed to create systemic frameworks that struggling students can use to perform mechanism EFP problems from which they can then gain a deeper understanding thereof. We plan to release the procedure and practice problems to the public via our teaching website. We will be looking forward to receiving feedback and thus looking for opportunities to improve our system.

4.7 References

- (1) Grove, N. P.; Hershberger, J. W.; Bretz, S. L. Impact of a Spiral Organic Curriculum on Student Attrition and Learning. *Chem. Educ. Res. Pract.* **2008**, 9 (2), 157–162.
- (2) Bhattacharyya, G.; Bodner, G. M. “It Gets Me to the Product”: How Students Propose Organic Mechanisms. *J. Chem. Educ.* **2005**, 82 (9), 1402.
- (3) Kermack, W. O.; Robinson, R. LI.—An Explanation of the Property of Induced Polarity of Atoms and an Interpretation of the Theory of Partial Valencies on an Electronic Basis. *J. Chem. Soc., Trans.* **1922**, 121 (0), 427–440.
- (4) Bodner, G. M.; Domin, D. S. Mental models: The role of representations in problem solving in chemistry. *University Chemistry Education* **2000**, 4 (1), 24–30
- (5) Norman, K. *Thinking Voices: The Work of the National Oracy Project*; Hodder & Stoughton: London, **1992**.
- (6) Burden, P. R.; Byrd, D. M. *Methods for Effective Teaching: Meeting the Needs of All Students*, 8th ed.; Pearson Education, Inc: Hoboken, **2019**.
- (7) *Scaffolding Student Learning: Instructional Approaches and Issues*; Hogan, K., Pressley, M., Eds.; Brookline Books: Cambridge, MA, **1997**.
- (8) Galloway, K. R.; Stoyanovich, C.; Flynn, A. B. Students’ Interpretations of Mechanistic Language in Organic Chemistry before Learning Reactions. *Chem. Educ. Res. Pract.* **2017**, 18 (2), 353–374.

CHAPTER 5

FUTURE RESEARCH

5.1 Abstract

This chapter outlines future research plans pertaining to the hydrophobic and solvophobic catalytic effects on the Diels-Alder reaction, with the goal of developing research projects for undergraduate students. Solvophobic effects will be used to guide the stereoselectivity and regioselectivity of reactions. In addition, future research in using molecular torsional balances to study solvophobic effects will be outlined, that builds on data and lessons learned from earlier generation balance systems.

5.2 Solvophobic Effect Catalysis and Selectivity in Diels-Alder Reactions

Solvophobic and hydrophobic effects typically favor products with smaller surface areas to limit weaker solvent-solute interactions and maximize stronger solvent-solvent interactions. This strategy has been employed to modulate the diastereoselectivity and regioselectivity of various reactions.¹ Due to these attractive characteristics, researchers are interested in utilizing solvophobic effects for reactions to enhance the reaction rates and control product selectivities to synthesize organic sterically strained molecules without the use of extreme reaction conditions or catalysts. Hydrophobic and solvophobic effects can catalyze Diels-Alder reactions by stabilizing diene-dienophile interactions. For instance, the reaction of 3-buten-2-one and 5-methoxy-1,4-naphthoquinone with cyclopentadiene is 290 times and 12,8000 times faster in water than in aprotic solvents (**Figure 5.1**).² The increased reaction rates are attributed to the association of the reactants driven by the hydrophobic effect. Solvophobically accelerated reactions can be advantageous as they are often run under mild conditions without acid, base, or catalysts and enable reactions to be performed at lower temperatures, promoting environmentally

friendly chemistry by reducing the need for additional energy or solvents in the workup to remove catalysts and reactants.

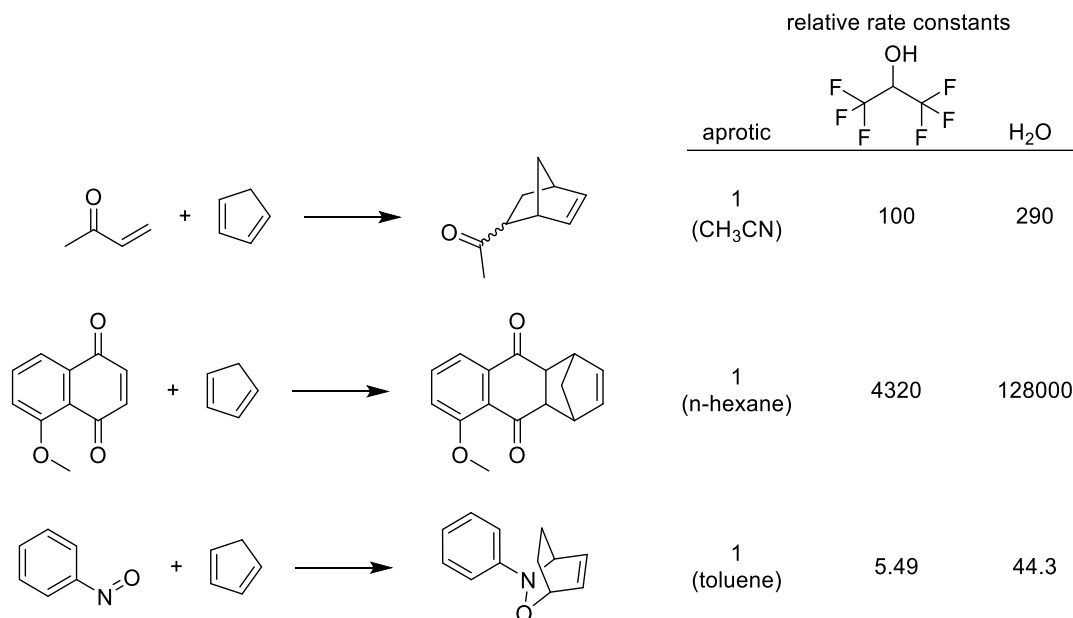


Figure 5.1 Relative Diels-Alder reaction rates in non-polar and polar solvents. Data from Otto et al.²

5.3 Modulating Reactions Using Solvophobic Effects to Form Sterically Strained Groups

5.3.1 Stereoselectivity

We aim to use solvophobic effects to promote the formation of sterically strained products. Bulky substituents such as *t*-butyl groups normally display strong steric effects and thus molecules which have multiple *t*-butyl groups in close proximity are strained and less stable. However, large bulky substrates also form strong solvophobic interactions in polar solvent environments and can exhibit strong dispersion stabilization forces.³⁻⁵ The combination of these forces provides a strategy for synthesizing molecules where these groups are positioned near one another.⁶ This project is designed to provide an educational research experience for undergraduate students through exposure to organic synthesis, molecular characterization, and data analysis. The aim is for the students to present their

findings to the general and scientific communities. The projects were designed to fit into and obtain results within a semester.

A series of reactions were designed to use the solvophobic effect to drive the diastereoselectivity in favor of the less favored, sterically crowded products. The polarity of a solvent has been shown to effect the diastereoselectivity of Diels-Alder reactions.⁷⁻⁹ A maleimide, containing a bulky alkyl group such as ethyl, *t*-butyl, or adamantyl, will be synthesized through the thermal condensation of maleic anhydride and a substituted amine. The maleimide will be utilized as a dienophile in Diels-Alder reactions with 2-*t*-butyl anthracene (**Figure 5.2**). The diastereomeric products were modeled and are confirmed to have ΔS_{ASA} values similar to the balances mentioned in Chapter 3 (**Table 5.1**). The reactions will be performed in solvents of increasing polarity (toluene, *n*-decane, acetonitrile, and DMSO) with the aim of modulating the solvophobic interactions of the reactants. Once the mixture of products is isolated, ¹H NMR NOE experiments will be conducted to assign the diastereomers and measure the *anti*-/*syn*- ratio. As the cohesive energy density of the solvent increases, the expectation is that the diastereoselectivity will shift in favor of the *syn*- product.

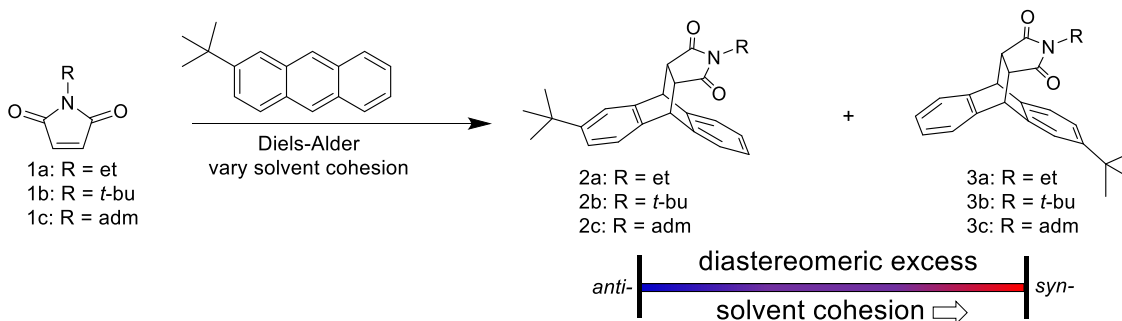


Figure 5.2. Controlling diastereoselectivity to favor *syn*- or *anti*- addition of sterically bulky maleimide substrates by altering solvent environment and solvophobicity.

Table 5.1 Calculated SASA and Δ SASA (\AA^2) of proposed molecule series **2** and **3** (equilibrium geometry optimized by density functional theory, B3LYP-D3, 6-311+G**).

	a	b	c
SASA 2	203	209	229
SASA 3	197	213	224
Δ SASA (2 – 3)	6	4	5

Furthermore, the diastereomeric ratio can be utilized to estimate or measure the strength of the solvophobic interactions. The change in the *syn*- and *anti*- diastereomeric ratio can be used to calculate the solvophobic interaction energy (ΔG) using the Gibbs free energy equation. We expect a strong correlation between the solvophobic interaction energy and the solvent *ced* as seen in other experiments. The diastereoselectivity of the reactions will be compared to a reaction with a control dienophile, 2-methylantracene, containing a smaller methyl group to minimize the solvent accessible surface area. The ΔG from the control reaction can be subtracted from the ΔG of reactants with larger groups to derive a $\Delta\Delta G$ energy, removing any intrinsic or innate biases of the maleimide-anthracene Diels-Alder reaction. Advantages to this approach in measuring the solvophobic interaction are that we can measure the effects of solvophobic interactions on a kinetic process using a simple reaction.

The project is inexpensive, straight-forward, and can be accomplished by one or two undergraduate students over a period of a few months using laboratory equipment and instrumentation commonly found in most undergraduate laboratories. The proposed

reactions do not require a catalyst and the starting materials are commercially available and affordable. Diels-Alder reactions have been performed in a wide range of solvents. If the reaction is slow, the reaction can be performed in a medium-pressure tube vessel to carry out reactions above a solvent's boiling point. Finally, the products can be isolated through precipitation or column chromatography and the diastereomeric ratio can be easily analyzed with ^1H NMR as demonstrated in similar work.

5.3.2 Regioselectivity

The second future research proposal uses solvophobic effects to influence the regioselectivity of Diels-Alder reactions of asymmetrical *p*-benzoquinone derivatives as a cost-effective project for undergraduate researchers. *p*-Benzoquinone features two reactive dienophile sites, which have enhanced reactivity due to the adjacent strong electron donors. Usually, attaching large groups on one alkene shifts the regioselectivity towards the less hindered unfunctionalized alkene.¹⁰⁻¹² Additionally, dicycloaddition products are not formed under mild conditions.¹³

1,3-Cyclohexadiene was chosen as the diene (**Figure 5.3**). It is commercially available and more reactive since the diene is locked in the *cis*- position. The hydrocarbon framework also enhances solvophobicity of the product and transition state structures. The reactions should proceed at room temperature over several days. The reaction mixture will be purified using flash column chromatography, as outlined in previous literature.¹⁴ The reactions will be conducted in solvents of varying polarity, such as toluene, *n*-decane, acetonitrile, and DMSO. The population of the isomers will then be analyzed using ^1H NMR and GC-MS. We expect that solvents with higher solvent cohesion will raise the

overall yields and shift regioselectivities in favor of the more sterically crowded isomers. The possible products have been modeled and were confirmed to have Δ SASA values similar to the balances in Chapter 3 (**Table 5.2**).

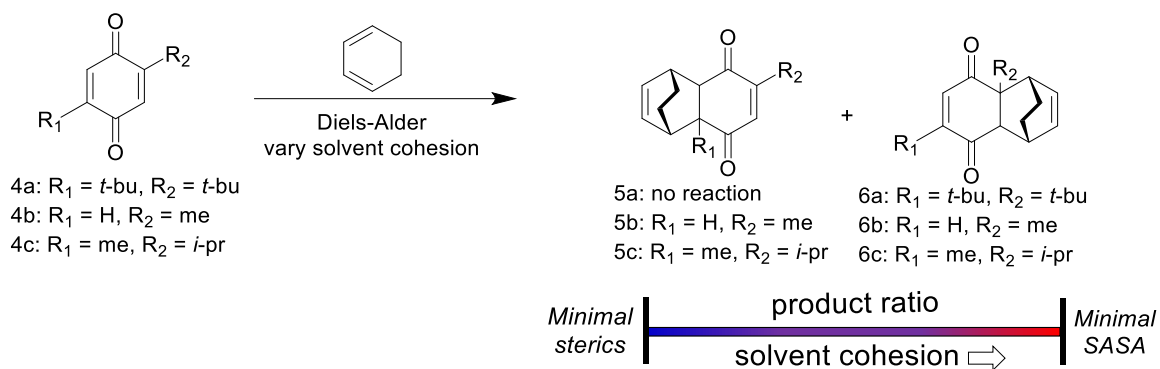


Figure 5.3 Controlling the regioselectivity of Diels-Alder reactions between 1,3-cyclohexadiene and *p*-benzoquinone derivatives using solvophobic effects. Symmetrical compound **4a** is a control designed to form little to no product due to steric strain.

Table 5.2 Calculated SASA and Δ SASA (\AA^2) of proposed molecule series **5** and **6** (equilibrium geometry optimized by density functional theory, B3LYP-D3, 6-311+G**).

	b	c
SASA 5	125	140
SASA 6	118	138
Δ SASA (5 – 6)	7	2

This project serves as an introduction to chemical research for undergraduate students using commercially available, inexpensive compounds. It also employs simple, safe reaction conditions with results attainable within an undergraduate semester.

5.4 Future of Alkyl-Alkyl Interactions with Focus on Past Experiments

During the course of the studies in this dissertation, several research projects were embarked on, but for various reasons, were not completed or realized. The preliminary results from one of these projects will be presented with the purpose that they could be either completed by future research group members or that the results could help guide future research projects.

An issue experienced throughout the experiments in Chapter 2 was the uncertainty in the geometries and orientations of alkyl chains in the *folded* conformation of the balances, particularly with longer alkyl chains. Larger alkyl chains have more flexibility and degrees of freedom that may reduce the probability of forming alkyl-alkyl interactions. Also if the chains are not perfectly parallel, the alkyl groups will have increasing difficulty in maintaining contact as the length of the chains increases.

To address the challenges in measuring the interaction for chains of varying length, particularly with longer alkyl chains, the development of molecular torsional balances with linkers that can template the formation of the weak solvophobic interactions of interest was undertaken. The design incorporated aromatic linker groups for the pendant alkyl chains. We hypothesized that the aromatic linkers would promote the association of attached alkyl chains, via templation by aromatic-aromatic interactions between adjacent linkers.¹⁵⁻¹⁷ This balance system could also be modified to form and measure aromatic-alkyl interactions also.^{18,19} The aromatic linkers were incorporated into the balances through a series of steps. First, the alkyl chain 1-decanol was coupled to 2'-nitro[1,1'-biphenyl]-4-carboxylic acid through a DMAP catalyzed esterification. Next, the nitro group was hydrogenated and the

amine was thermally condensed with maleic anhydride to form a maleimide. A Michael addition of the maleimide with 3-fluoro-4-(sulfanylmethyl)benzoic acid was performed to form a thioether. Finally a second 1-decanol alkyl chain was attached via esterification (**Figure 5.4a**). To synthesize the balances to measure alkyl-aromatic interactions, a Michael addition was performed to attach 1-decanethiol or 1-pentadecanethiol directly to the maleimide (**Figure 5.4b**). The design also allowed for the retention of the fluorine tag on the alkyl and the aromatic-aromatic balances, even though its position had changed.

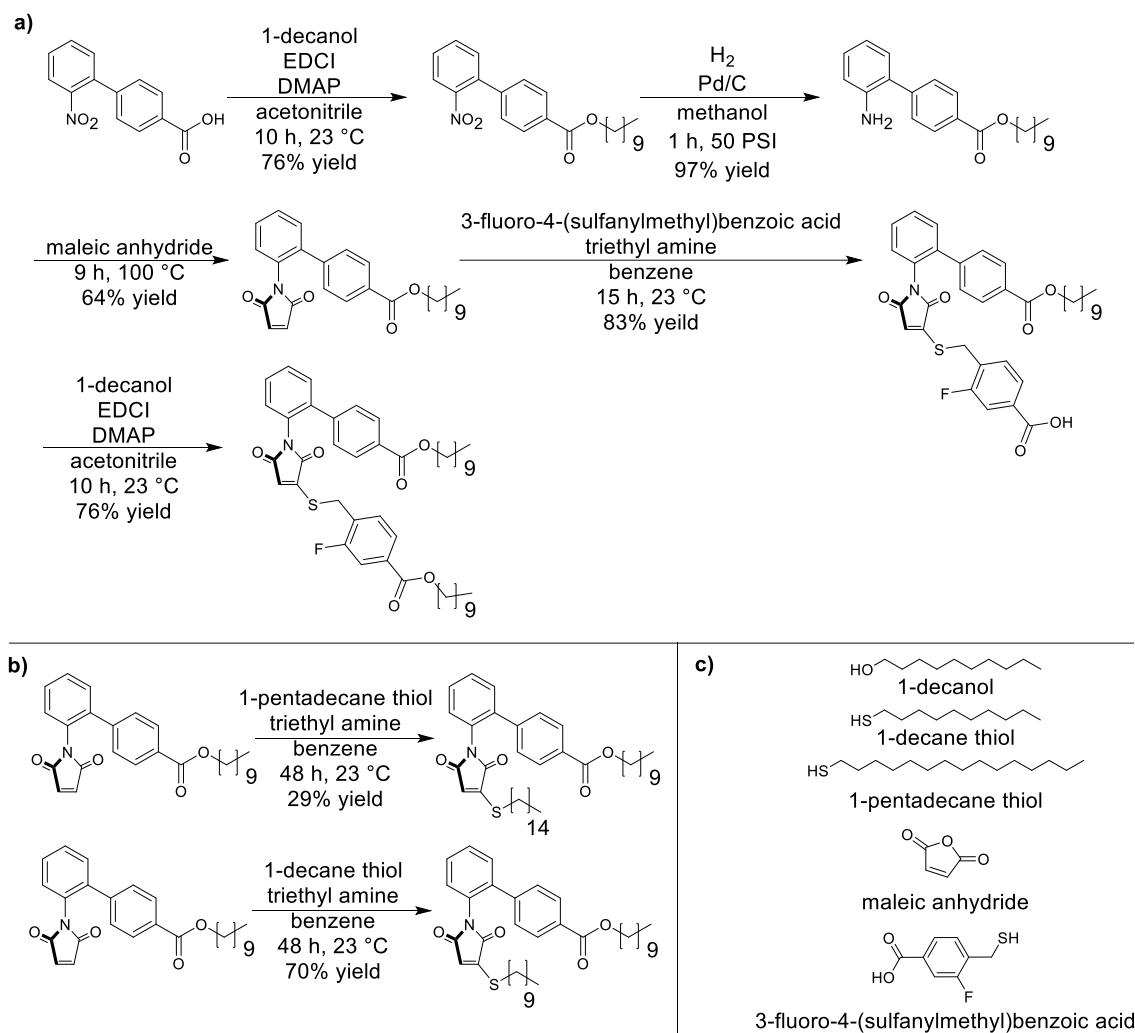


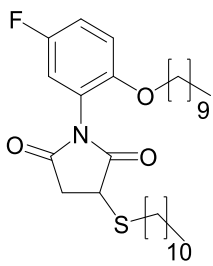
Figure 5.4 Synthesis of aromatic linker balances contain design elements that maybe useful in future systems: a) synthesis of aryl-aryl linker balance, b) formation of alkyl-aryl linker balance starting from maleimide intermediate, c) list of the reaction reagents.

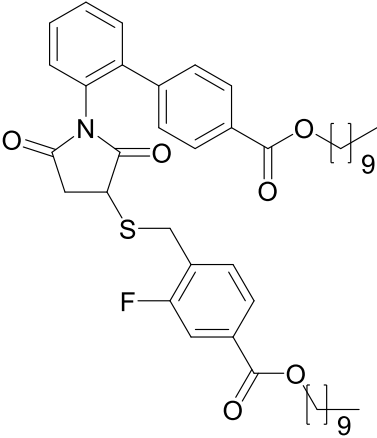
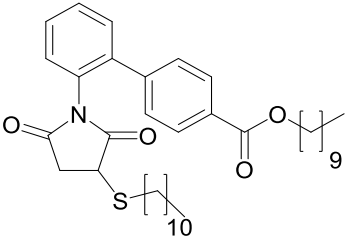
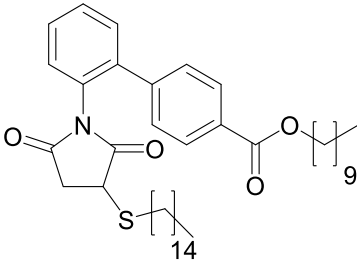
The sensitivity of the fluorine tag positioned on the pendant linker was able to differentiate between the two conformers in the decoupled ^{19}F NMR spectra. However, we could not assign conformation to ^{19}F NMR signals since the study was undertaken before the pre-equilibrium data from Chapter 2 was collected. Additionally, preliminary results from the aromatic linker balances did not show significant changes in folding ratios as was observed for studies of other non-covalent interactions.¹⁹ For example, the folding energies were between -0.06 to -0.21 kcal/mol in chloroform-d and -0.51 to -0.74 kcal/mol in

acetonitrile (**Table 5.3**). This led to the initial conclusion that the balances were not forming a good solvophobic interaction, and as a result, the design was abandoned, and the full characterization of the balances was not undertaken.

In retrospect, the alkyl-alkyl interactions were probably formed in this aromatic linker balance system, and if anything, the interactions were slightly more favorable than in the balances described in Chapter 2. This suggests the strategy of utilizing supporting interactions to promote weaker, non-covalent interactions is viable. Furthermore, the model suggests that it is possible to position the fluorine tag on different parts of molecular torsional balances and still generate consistent accurately measured folding ratios.

Table 5.3 Folding energies of unpublished molecular balances in chloroform-d and acetonitrile-d₃ relative to balance **1a** from Chapter 2.

Balance entry	ΔG in chloroform-d (kcal/mol)	ΔG in acetonitrile-3d (kcal/mol)
 <p>1a (Chapter 2)</p>	-0.14	-0.51

	-0.21	-0.63
	-0.08	-0.71
	-0.06	-0.74

5.5 Conclusions

Two research projects have been developed which utilize the solvophobic effect to influence the diastereoselectivity and regioselectivity of Diels-Alder reactions. The projects are designed to serve as an introduction to chemical research for undergraduate students and can be easily accomplished at mid and small sized universities. Finally, previous unpublished molecular balances prove the merit of using interaction templates to assist in measuring weak interactions.

5.6 Computational Model Coordinates

Table 5.4 Xyz coordinates of the structure of **2a**.

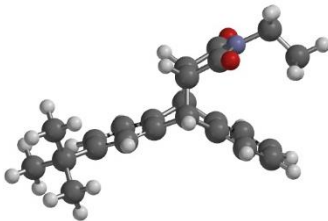
											
H	3.245600	-1.576973	-0.616034	C	-1.477947	3.027852	-0.209831	H	-1.575807	5.354477	-1.935017
C	2.936883	-1.235883	0.366262	C	-0.396833	1.394304	-1.591382	C	-0.287886	3.609312	-3.658157
C	2.109738	-0.404758	2.915066	H	-1.506321	2.616845	1.907647	H	0.220454	2.688551	-3.953075
C	1.642365	-0.773906	0.568127	H	-2.023937	3.952864	-0.082257	H	0.434073	4.236721	-3.129061
C	3.825367	-1.275172	1.442799	H	-0.103050	1.017116	-2.564629	H	-0.587907	4.127597	-4.573985
C	3.414202	-0.862883	2.709493	C	-0.616374	-1.666989	0.037102	C	-0.154881	-3.104977	0.202431
C	1.229526	-0.354834	1.841667	H	-1.430892	-1.643971	-0.688729	C	-0.782419	-2.426636	2.339182
H	4.836964	-1.634413	1.291853	C	-1.055407	-1.221374	1.449858	N	-0.283740	-3.453573	1.541486
H	4.108329	-0.902863	3.541241	H	-2.120634	-0.988713	1.500932	O	0.271149	-3.837387	-0.661860
H	1.779685	-0.103326	3.903059	C	-1.526568	3.331329	-2.777801	O	-0.962902	-2.504749	3.532320
C	0.538138	-0.730121	-0.471295	C	-2.513609	2.432832	-3.561638	C	0.192695	-4.732098	2.070269
H	0.876069	-1.044614	-1.458435	H	-3.411241	2.232605	-2.969979	H	-0.299689	-4.878631	3.031733
C	-0.231979	0.045636	1.893476	H	-2.064299	1.472130	-3.823991	H	-0.136126	-5.510453	1.379018
H	-0.543101	0.376705	2.883820	H	-2.818210	2.925321	-4.490286	C	1.714636	-4.732701	2.211595
C	-0.498673	1.071953	0.806450	C	-2.223101	4.672928	-2.493532	H	2.038852	-3.917821	2.862418
C	-1.114181	2.598478	-1.489632	H	-3.151813	4.540595	-1.931722	H	2.185013	-4.605562	1.235234
C	-0.091246	0.648538	-0.466681	H	-2.482112	5.157990	-3.438382	H	2.053839	-5.678641	2.641021
C	-1.180694	2.271345	0.931832								

Table 5.5 Xyz coordinates of the structure of **3a**.

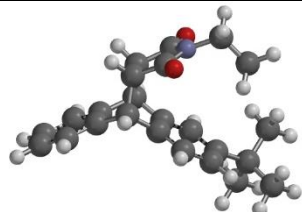
											
H	0.533165	4.337625	-1.737863	C	-1.799778	-1.163921	0.894583	H	-4.106291	-2.502814	-0.161781
C	0.420110	4.283010	-0.660028	C	-0.776981	-0.156724	-1.026353	C	-3.198928	-1.304504	-2.479459
C	0.122650	4.135141	2.124494	H	-1.210776	-0.371303	2.811682	H	-2.570670	-0.660282	-3.098658
C	0.593538	3.074038	-0.000239	H	-2.459240	-1.891321	1.348715	H	-3.941763	-0.674866	-1.982827
C	0.088009	5.424958	0.074790	H	-0.610134	-0.104022	-2.096567	H	-3.723274	-1.995594	-3.146346
C	-0.061386	5.351040	1.458239	C	2.125733	1.195439	1.538154	C	2.408909	-0.262947	1.874636
C	0.447496	2.999953	1.393965	H	2.838965	1.822043	2.075555	C	2.660387	-0.123451	-0.435320
H	-0.059762	6.369425	-0.436687	C	2.289230	1.286225	0.002793	N	2.722728	-0.931457	0.693723
H	-0.325333	6.239267	2.020761	H	3.084645	1.968228	-0.300895	O	2.362389	-0.779218	2.967375
H	0.001822	4.074706	3.200965	C	-2.370344	-2.097816	-1.444145	O	2.856540	-0.507668	-1.566290
C	0.936110	1.742995	-0.644129	C	-1.325162	-2.961481	-2.187185	C	2.974976	-2.370976	0.626069
H	1.030543	1.802307	-1.728044	H	-0.746148	-3.562395	-1.482609	H	3.780954	-2.523575	-0.093941
C	0.665167	1.602217	1.944680	H	-0.626136	-2.350622	-2.762894	H	3.318502	-2.671937	1.616317
H	0.537351	1.540569	3.024857	H	-1.828742	-3.640951	-2.881817	C	1.724234	-3.144544	0.211028
C	-0.247064	0.654570	1.191348	C	-3.325790	-3.048163	-0.699177	H	1.417937	-2.859932	-0.796028
C	-1.649660	-1.122680	-0.494854	H	-2.794570	-3.682725	0.015612	H	0.899131	-2.940030	0.896514
C	-0.095375	0.723038	-0.200494	H	-3.817303	-3.708869	-1.418743	H	1.929019	-4.218252	0.220740
C	-1.099631	-0.291754	1.735779								

Table 5.6 Xyz coordinates of the structure of **2b**.

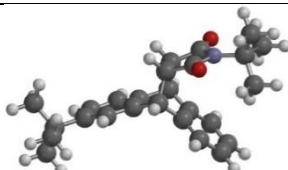
											
C	-0.662197	-0.051356	-2.489160	C	-2.684752	-0.981286	-4.131201	C	-1.472466	-0.303131	-6.256415
C	-0.317197	1.251245	-0.442335	H	-3.485069	-1.356408	-4.758190	C	-0.203198	0.426123	-6.731981
C	-1.749020	-0.729094	-0.415630	C	0.757900	-0.969714	-0.703465	H	0.706679	-0.101561	-6.433395
C	-1.447023	0.653265	0.135028	H	1.323701	-1.613585	-1.378225	H	-0.153655	1.447187	-6.343667
C	-1.804169	-0.627099	-1.923129	C	-0.500128	-1.643118	-0.140303	H	-0.203019	0.486998	-7.823724
C	0.371498	0.359092	-1.458086	H	-0.691586	-2.632764	-0.555454	C	-2.697735	0.469563	-6.797585
H	1.255848	0.822234	-1.894038	C	1.599188	-0.659102	0.523379	H	-3.635678	-0.037119	-6.561068
H	-2.645745	-1.170718	0.018210	C	-0.258935	-1.762599	1.351124	H	-2.635641	0.558917	-7.886578
C	-2.179442	1.325217	1.104271	O	2.684329	-0.123241	0.496581	H	-2.743514	1.476247	-6.373789
H	-3.045038	0.852848	1.556799	O	-0.989685	-2.361114	2.105374	C	-1.465673	-1.726814	-6.859184
C	-1.793679	2.614033	1.482186	N	0.905793	-1.051194	1.678428	H	-2.372575	-2.280205	-6.603817
C	-0.676685	3.212056	0.901287	C	1.327401	-0.588399	3.046397	H	-0.609962	-2.301074	-6.493835
H	-0.383026	4.211815	1.200180	C	0.338619	-1.050792	4.140163	H	-1.402017	-1.675475	-7.950670
C	0.073959	2.525740	-0.056914	H	-0.668196	-0.698840	3.908631	H	1.660312	1.343452	4.002703
H	0.955804	2.979905	-0.495072	H	0.289711	-2.139343	4.171232	H	0.655640	-0.662502	5.114814
C	-2.814620	-1.100013	-2.748737	C	1.337845	0.959006	3.028315	C	2.720858	-1.123571	3.386735
H	-3.700007	-1.561517	-2.323188	H	0.332250	1.314688	2.788304	H	3.443259	-0.757319	2.648350
C	-0.538531	0.060744	-3.870490	H	2.007696	1.320253	2.249040	H	2.705407	-2.219340	3.370369
H	0.359251	0.510110	-4.275495	C	-2.367463	3.149272	2.230206	H	3.011444	-0.777170	4.385124
C	-1.555129	-0.398970	-4.722456								

Table 5.7 Xyz coordinates of the structure of **3b**.

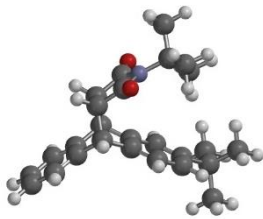
											
C	0.142522	-0.677856	-3.420162	H	-0.698768	-0.930227	-6.695059	H	-3.801496	1.941938	3.047239
C	0.372003	0.597749	-1.339567	C	-1.821264	-1.771885	-5.066046	C	2.550989	-1.125506	-0.500352
C	-0.848201	-1.515704	-1.356550	H	-2.584475	-2.194601	-5.710118	C	0.787001	-2.317567	0.406188
C	-0.693748	-0.118086	-0.786509	C	1.669619	-1.488979	-1.683828	O	3.619552	-0.569620	-0.595765
C	-0.928404	-1.394831	-2.862721	H	2.255994	-2.066607	-2.399366	O	0.129533	-2.925452	1.221284
C	1.137187	-0.186098	-2.388629	C	0.498370	-2.275560	-1.081317	N	1.906906	-1.523171	0.682329
H	1.963924	0.377040	-2.819914	H	0.415775	-3.294309	-1.462147	C	2.304676	-1.183327	2.097318
H	-1.687982	-2.058201	-0.922919	C	-2.165365	2.407277	1.707429	C	1.068571	-0.606190	2.815551
C	-1.491242	0.438152	0.202711	C	-2.921227	3.576899	1.036797	H	0.711194	0.283203	2.292461
H	-2.297598	-0.157758	0.608856	H	-2.231510	4.329095	0.646279	H	1.356271	-0.318076	3.829578
C	-1.258725	1.740985	0.660484	H	-3.584237	4.065408	1.757704	H	0.258564	-1.328939	2.879138
C	-0.181487	2.443551	0.099836	H	-3.527725	3.216363	0.201314	C	3.405775	-0.112265	2.125868
H	0.027113	3.455151	0.426659	C	-1.314927	2.945051	2.878375	H	3.098573	0.785997	1.588549
C	0.635463	1.881958	-0.882889	H	-0.586611	3.689628	2.550606	H	4.341404	-0.460178	1.695409
H	1.466887	2.446691	-1.290630	H	-0.768111	2.133350	3.365229	H	3.574913	0.153125	3.172337
C	-1.906207	-1.945136	-3.681163	H	-1.959472	3.419059	3.624703	H	2.800751	-2.466624	2.780856
H	-2.729359	-2.504882	-3.248796	C	-3.205041	1.430834	2.286981	H	3.673156	-2.865465	2.256462
C	0.230432	-0.513969	-4.796564	H	-2.730908	0.567498	2.761749	H	2.020390	-3.227296	2.803268
H	1.060436	0.034411	-5.229591	H	-3.895390	1.065336	1.521911	H	3.094823	-2.241203	3.809402
C	-0.759286	-1.060182	-5.620256								

Table 5.8 Xyz coordinates of the structure of **2c**.

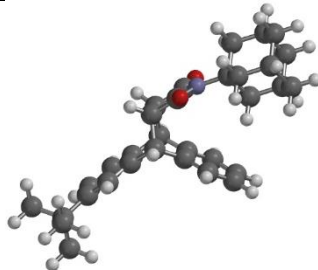
											
C	-0.531179	-2.511680	0.215195	C	-0.069235	-0.173401	1.832803	C	3.197257	5.439347	0.189567
C	-0.476228	-0.394259	-0.984911	H	-0.023112	-0.512872	2.868051	H	4.107445	5.127160	0.713905
C	-1.480913	-0.510182	1.231664	C	1.881005	0.425462	0.519214	H	3.360835	6.465530	-0.158698
C	-1.502147	0.090831	-0.160199	C	0.158083	1.327992	1.774899	C	0.722036	5.845336	0.401053
C	-1.531781	-2.012691	1.056369	O	2.908113	0.329810	-0.109998	H	0.839513	6.882934	0.068855
C	0.397376	-1.438353	-0.313243	O	-0.536057	2.146679	2.334750	H	-0.138918	5.815471	1.077536
H	1.172100	-1.825895	-0.974337	N	1.246237	1.607798	0.935704	C	1.678200	4.984180	-1.760729
H	-2.273328	-0.119935	1.868510	C	1.517837	3.006757	0.450251	H	1.499519	4.348428	-2.635822
C	-2.410748	1.019747	-0.647529	C	0.262783	3.486219	-0.318497	H	1.824044	6.006072	-2.129514
H	-3.199434	1.398679	-0.006809	H	0.078456	2.809098	-1.157180	H	-3.014933	2.174697	-2.360769
C	-2.301240	1.458018	-1.970088	H	-0.611402	3.443064	0.331203	C	-1.467134	-6.249443	0.018532
C	-1.276111	0.983984	-2.786220	C	2.725672	3.063360	-0.511026	C	-0.275189	-6.658693	-0.864398
H	-1.195402	1.331601	-3.810134	H	2.561305	2.402930	-1.363754	H	-0.276756	-6.127051	-1.819755
C	-0.352258	0.058502	-2.291575	H	3.625336	2.710278	-0.005092	H	-0.334314	-7.727720	-1.085646
H	0.448607	-0.312184	-2.922446	C	1.799447	3.939703	1.648312	H	0.681227	-6.475870	-0.367200
C	-2.476509	-2.885351	1.578954	H	2.701321	3.590710	2.163125	C	-1.435107	-7.115122	1.299276
H	-3.264790	-2.517119	2.227732	H	0.972094	3.899497	2.355377	H	-2.299522	-6.928044	1.940613
C	-0.478760	-3.863695	-0.105365	C	0.470881	4.928560	-0.810431	H	-0.532995	-6.916763	1.884620
H	0.305966	-4.207861	-0.767728	H	-0.432655	5.253433	-1.337006	H	-1.443627	-8.177778	1.037303
C	-1.438381	-4.756892	0.393965	C	2.932063	4.509197	-1.005404	C	-2.767851	-6.550444	-0.762205
C	-2.425311	-4.238359	1.244288	H	3.794578	4.518199	-1.679895	H	-2.812531	-5.962214	-1.682739
H	-3.185053	-4.898107	1.646651	C	1.992860	5.384110	1.144390	H	-3.656180	-6.316856	-0.171078
C	1.036617	-0.762570	0.949473	H	2.171142	6.034842	2.007013	H	-2.810894	-7.610575	-1.030893
H	1.668031	-1.490236	1.459167								

Table 5.9 Xyz coordinates of the structure of **3c**.

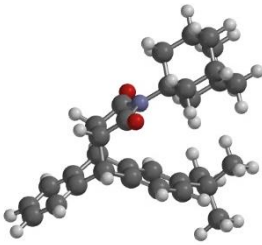
											
C	0.324196	4.312795	0.643164	H	-1.796384	3.151801	1.924314	H	-0.402478	-1.466252	-0.651379
C	0.230621	2.251774	-0.674527	C	-0.004799	1.881279	2.140294	H	0.281753	-1.966490	0.898285
C	1.368527	2.266188	1.471844	H	0.001627	2.193975	3.185362	C	-3.019131	-1.364744	0.057350
C	1.299233	1.724230	0.056742	C	2.702072	-0.884950	-2.415934	H	-2.803643	-0.832201	-0.871744
C	1.389393	3.781955	1.388847	C	3.254241	-0.405039	-3.778227	H	-3.872409	-0.866349	0.516714
C	-0.606724	3.253052	0.092632	H	2.451633	-0.183679	-4.485359	C	-2.136027	-2.053251	2.305464
H	-1.424766	3.657472	-0.502651	H	3.883667	-1.181523	-4.224192	H	-2.983950	-1.553387	2.787367
H	2.199635	1.851918	2.041310	H	3.857713	0.498783	-3.659895	H	-1.288740	-2.012219	2.990351
C	2.104464	0.726616	-0.483951	C	1.815469	-2.130734	-2.643844	C	-0.968601	-3.475746	-0.016358
H	2.906527	0.323520	0.119925	H	0.951706	-1.904371	-3.273250	H	-0.112275	-3.956953	-0.501204
C	1.860715	0.232541	-1.774003	H	1.447191	-2.522281	-1.693755	C	-3.374656	-2.833938	-0.250363
C	0.776557	0.767959	-2.483561	H	2.393598	-2.918820	-3.136179	H	-4.246729	-2.839859	-0.912235
H	0.549236	0.393056	-3.474633	C	3.892168	-1.301477	-1.534686	C	-2.488760	-3.519890	1.991851
C	-0.036665	1.762873	-1.946687	H	3.564491	-1.706252	-0.573236	H	-2.714503	-4.034684	2.931515
H	-0.883154	2.139736	-2.511081	H	4.567271	-0.462436	-1.346007	C	-3.711591	-3.571639	1.058298
C	2.335302	4.628610	1.949878	H	4.464942	-2.082802	-2.041545	H	-4.576824	-3.106306	1.544042
H	3.162076	4.221020	2.522186	C	-2.009550	1.292159	0.900818	H	-3.980816	-4.612688	0.846327
C	0.202899	5.682954	0.461898	C	-0.240564	0.380197	2.089750	C	-1.287054	-4.199142	1.307955
H	-0.621870	6.084602	-0.117609	O	-3.041095	1.392666	0.279693	H	-1.513076	-5.253620	1.113327
C	1.159495	6.534109	1.022138	O	0.465849	-0.444382	2.625600	H	-0.414358	-4.170310	1.969556
H	1.078173	7.605390	0.877113	N	-1.383370	0.106127	1.320352	C	-2.192593	-3.530758	-0.944489
C	2.218685	6.009554	1.760697	C	-1.790185	-1.308243	0.994941	H	-1.966456	-3.029986	-1.892480
H	2.959726	6.674931	2.188817	C	-0.611155	-2.006683	0.276431	H	-2.449648	-4.570341	-1.177630
C	-1.166251	2.480582	1.339545								

Table 5.10 Xyz coordinates of the structure of **5b**.

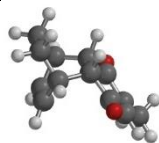
											
C	-0.960479	-0.726717	-1.680582	C	0.635958	1.022481	1.202758	H	-0.548969	3.242887	-0.918024
C	-0.669262	0.308506	0.704515	H	0.740031	0.852101	2.273536	C	0.489085	2.533129	0.886850
C	-0.732175	-2.272668	0.265449	C	0.421966	1.346980	-1.346414	H	1.352550	3.066437	1.289879
C	-0.666867	-1.124861	1.216781	H	0.342911	1.446775	-2.428267	H	-0.396069	2.923448	1.398166
C	-0.873676	-2.056403	-1.055903	C	1.796147	0.473000	0.406983	C	-0.652440	-3.642418	0.866578
C	-0.807257	0.522579	-0.827424	H	2.636636	-0.013375	0.888852	H	0.286119	-3.759226	1.415911
H	-0.941968	-2.886567	-1.753468	C	1.682956	0.637195	-0.914367	H	-0.721699	-4.417299	0.102257
H	-1.510729	0.783289	1.219519	H	2.420510	0.300361	-1.633829	H	-1.451204	-3.781466	1.599960
O	-1.143601	-0.629920	-2.882881	C	0.379827	2.730401	-0.649714	H	-1.702304	1.117176	-1.036525
O	-0.608507	-1.338371	2.414848	H	1.202509	3.342548	-1.025441				

Table 5.11 Xyz coordinates of the structure of **6b**.

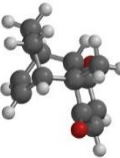
											
C	-0.485803	-1.361852	-1.426134	C	0.916056	0.443509	1.372131	H	-0.596930	2.718606	-0.435997
C	-0.413466	-0.272998	0.946151	H	1.121775	0.206430	2.415794	C	0.686195	1.965438	1.181854
C	-0.382993	-2.834850	0.567910	C	0.441671	0.920908	-1.114661	H	1.577064	2.505932	1.508798
C	-0.416147	-1.689308	1.498186	H	0.269063	1.093158	-2.176198	H	-0.139159	2.287834	1.823736
C	-0.410083	-2.681782	-0.762754	C	2.023418	0.016925	0.439303	H	-1.219660	0.229226	1.490472
C	-0.646897	-0.084601	-0.587751	H	2.930788	-0.448136	0.807281	C	-2.082009	0.411738	-0.862408
H	-0.335942	-3.814670	1.032647	C	1.786324	0.280603	-0.848917	H	-2.284919	1.336674	-0.319370
H	-0.375893	-3.530877	-1.438402	H	2.472558	0.047586	-1.654522	H	-2.817033	-0.330432	-0.535747
O	-0.460404	-1.305110	-2.642576	C	0.380711	2.247360	-0.313218	H	-2.224497	0.587729	-1.930447
O	-0.427748	-1.882057	2.701547	H	1.113957	2.937017	-0.736708				

Table 5.12 Xyz coordinates of the structure of **5c**.

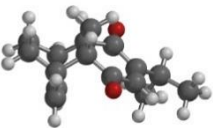
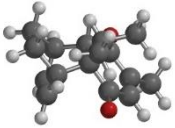
											
C	-0.741101	-0.008788	-1.658498	H	0.459875	2.276962	-2.404563	H	-0.613327	-4.227383	-0.876647
C	-0.340815	0.966796	0.710793	C	2.079587	0.732640	0.057363	H	-2.265559	-3.818155	-0.386789
C	-0.716839	-1.579966	0.288994	H	2.883216	0.067222	0.351345	H	-1.328678	-5.001620	0.534110
C	-0.635226	-0.425894	1.233445	C	1.839042	1.105392	-1.202685	C	0.702366	-3.307459	1.388508
C	-0.779672	-1.340962	-1.033658	H	2.416801	0.772913	-2.056893	H	1.087283	-2.547272	2.070339
C	-0.602780	1.252138	-0.797640	C	0.908556	3.295477	-0.513334	H	1.383548	-3.393639	0.536633
H	-0.877545	-2.150496	-1.749114	H	1.730673	3.852735	-0.966986	H	0.696026	-4.263758	1.918248
H	-0.974288	1.621640	1.315775	H	0.034498	3.949191	-0.543266	C	-1.910217	2.048315	-0.984885
O	-0.835243	0.085313	-2.871657	C	1.252229	2.886102	0.942858	H	-1.878397	2.986072	-0.426951
O	-0.771062	-0.600774	2.432420	H	2.265518	3.194058	1.209455	H	-2.767188	1.474136	-0.619967
C	1.143330	1.342437	1.071691	H	0.571748	3.358374	1.657538	H	-2.070006	2.266119	-2.042222
H	1.351515	1.022129	2.092470	C	-0.723096	-2.960776	0.905282	H	-1.357987	-2.896840	1.794618
C	0.649268	2.026168	-1.361532	C	-1.266055	-4.058543	-0.014597				

Table 5.13 Xyz coordinates of the structure of **6c**.

											
C	1.219947	0.165474	-1.103507	C	-0.181951	2.361404	1.120143	H	3.673346	0.013908	2.680345
C	-0.225441	-0.141187	1.027964	H	0.300035	3.084341	1.768238	H	-0.880178	-0.976369	1.294809
C	2.372597	-0.413383	1.038032	C	-0.239477	2.465631	-0.209720	C	-0.843245	-1.278019	-1.176317
C	1.070198	-0.457428	1.756298	H	0.196418	3.279473	-0.776917	C	0.031332	-2.526041	-0.965474
C	2.402614	-0.126802	-0.275165	C	-2.407316	1.273528	-0.335784	H	0.940092	-2.472986	-1.572378
C	-0.194479	0.001536	-0.530197	H	-2.935140	2.176004	-0.650934	H	-0.513325	-3.424306	-1.266785
H	3.343935	-0.071856	-0.815070	H	-2.948851	0.428543	-0.766571	H	0.331085	-2.653822	0.077528
O	1.385386	0.520562	-2.260249	C	-2.354838	1.173901	1.210896	C	-1.208197	-1.139996	-2.660780
O	1.043054	-0.737092	2.943176	H	-2.849550	2.030205	1.674509	H	-1.954693	-0.361926	-2.830660
C	-0.873035	1.136907	1.668652	H	-2.864824	0.274245	1.568441	H	-1.631823	-2.082899	-3.019258
H	-0.804744	1.057869	2.753253	C	3.599020	-0.694072	1.850399	H	-0.332702	-0.906476	-3.268872
C	-0.962534	1.327223	-0.895693	H	4.501774	-0.633637	1.241426	H	-1.775764	-1.437269	-0.621943
H	-0.959785	1.451446	-1.975724	H	3.531061	-1.686635	2.303889				

5.7 References

- (1) Davis, H. J.; Phipps, R. J. Harnessing Non-Covalent Interactions to Exert Control over Regioselectivity and Site-Selectivity in Catalytic Reactions. *Chem. Sci.* **2017**, 8 (2), 864–877.
- (2) Otto, S.; Engberts, J. B. F. N. Hydrophobic Interactions and Chemical Reactivity. *Org. Biomol. Chem.* **2003**, 1 (16), 2809.
- (3) Grimme, S.; Schreiner, P. R. Steric Crowding Can Stabilize a Labile Molecule: Solving the Hexaphenylethane Riddle. *Angew. Chem. Int. Ed.* **2011**, 50 (52), 12639–12642.
- (4) Maué, D.; Strebert, P. H.; Bernhard, D.; Rösel, S.; Schreiner, P. R.; Gerhards, M. Dispersion-Bound Isolated Dimers in the Gas Phase: Observation of the Shortest Intermolecular CH \cdots H–C Distance via Stimulated Raman Spectroscopy. *Angew. Chem. Int. Ed.* **2021**, 60 (20), 11305–11309.
- (5) Liebman, J. F.; Greenberg, A. A Survey of Strained Organic Molecules. *Chem. Rev.* **1976**, 76 (3), 311–365.
- (6) Geiger, T.; Haupt, A.; Maichle-Mössmer, C.; Schrenk, C.; Schnepf, A.; Bettinger, H. F. Synthesis and Photodimerization of 2- and 2,3-Disubstituted Anthracenes: Influence of Steric Interactions and London Dispersion on Diastereoselectivity. *J. Org. Chem.* **2019**, 84 (16), 10120–10135.
- (7) Pindur, Ulf.; Lutz, Gundula.; Otto, Christian. Acceleration and Selectivity Enhancement of Diels-Alder Reactions by Special and Catalytic Methods. *Chem. Rev.* **1993**, 93 (2), 741–761.
- (8) Tomberg, A.; De Cesco, S.; Huot, M.; Moitessier, N. Solvent Effect in Diastereoselective Intramolecular Diels–Alder Reactions. *Tetrahedron Lett.* **2015**, 56 (49), 6852–6856.
- (9) Macdonald, D. I.; Durst, T. A Highly Stereoselective Synthesis of Podophyllotoxin and Analogues Based on an Intramolecular Diels-Alder Reaction. *J. Org. Chem.* **1988**, 53 (16), 3663–3669.
- (10) Robbins, R. J.; Falvey, D. E. Radical Anion Reactions of Cyclobutane Derivatives; Electron-Transfer Cleavage of Dithymoquinone. *J. Org. Chem.* **1993**, 58 (14), 3616–3618.
- (11) Murahashi, S.-I.; Miyaguchi, N.; Noda, S.; Naota, T.; Fujii, A.; Inubushi, Y.; Komiya, N. Ruthenium-Catalyzed Oxidative Dearomatization of Phenols to 4-(Tert-Butylperoxy)Cyclohexadienones: Synthesis of 2-Substituted Quinones from p-Substituted Phenols. *Eur. J. Org. Chem.* **2011**, 2011 (27), 5355–5365.
- (12) Murahashi, S.-I.; Fujii, A.; Inubushi, Y.; Komiya, N. Synthesis of 2-Substituted Quinones, Vitamin K3, and Vitamin K1 from p-Cresol. BF₃·OEt₂-Catalyzed Methyl Migration of 4-Tert-Butyldioxycyclohexadienones. *Tetrahedron Lett.* **2010**, 51 (17), 2339–2341.
- (13) Donatoni, M. C.; Junior, G. A. B.; de Oliveira, K. T.; Ando, R. A.; Brocksom, T. J.; Dos Santos, A. A. Solvent-Free Diels–Alder Reactions Catalyzed by FeCl₃ on Aerosil® Silica. *Tetrahedron* **2014**, 70 (20), 3231–3238.
- (14) Hwang, J.; Dial, B. E.; Li, P.; Kozik, M. E.; Smith, M. D.; Shimizu, K. D. How Important Are Dispersion Interactions to the Strength of Aromatic Stacking Interactions in Solution? *Chem. Sci.* **2015**, 6 (7), 4358–4364.

- (15) Paliwal, S.; Geib, S.; Wilcox, C. S. Molecular Torsion Balance for Weak Molecular Recognition Forces. Effects of “Tilted-T” Edge-to-Face Aromatic Interactions on Conformational Selection and Solid-State Structure. *J. Am. Chem. Soc.* **1994**, *116* (10), 4497–4498.
- (16) Yamada, M.; Narita, H.; Maeda, Y. A Fullerene-Based Molecular Torsion Balance for Investigating Noncovalent Interactions at the C₆₀ Surface. *Angew. Chem. Int. Ed.* **2020**, *132* (37), 16267–16274.
- (17) Carroll, W. R.; Zhao, C.; Smith, M. D.; Pellechia, P. J.; Shimizu, K. D. A Molecular Balance for Measuring Aliphatic CH– π Interactions. *Org. Lett.* **2011**, *13* (16), 4320–4323.
- (18) Zhao, C.; Parrish, R. M.; Smith, M. D.; Pellechia, P. J.; Sherrill, C. D.; Shimizu, K. D. Do Deuteriums Form Stronger CH– π Interactions? *J. Am. Chem. Soc.* **2012**, *134* (35), 14306–14309.
- (19) Li, P.; Vik, E.C.; Shimizu, K.; Arylimide Molecular Balances: A Comprehensive Platform for Studying Aromatic Interactions in Solution. *Acc. Chem. Res.* **2020** *53* (11), 2705–2714.